

THE CHARACTER AND DISPLACEMENT OF ADIYAMAN FAULT
(SOUTHEAST ANATOLIA): EVIDENCE FROM SUBSURFACE DATA

A THESIS SUBMITTED TO
THE GRADUATE SCHOOL OF NATURAL AND APPLIED SCIENCES
OF
MIDDLE EAST TECHNICAL UNIVERSITY

BY

BAYRAM ALPER DURUKAN

IN PARTIAL FULFILLMENT OF THE REQUIREMENTS
FOR
THE DEGREE OF MASTER OF SCIENCE
IN
GEOLOGICAL ENGINEERING

SEPTEMBER 2019

Approval of the thesis:

**THE CHARACTER AND DISPLACEMENT OF ADIYAMAN FAULT
(SOUTHEAST ANATOLIA): EVIDENCE FROM SUBSURFACE DATA**

submitted by **BAYRAM ALPER DURUKAN** in partial fulfillment of the requirements for the degree of **Master of Science in Geological Engineering Department, Middle East Technical University** by,

Prof. Dr. Halil Kalıpçılar
Dean, Graduate School of **Natural and Applied Sciences** _____

Prof. Dr. Erdin Bozkurt
Head of Department, **Geological Engineering** _____

Prof. Dr. Erdin Bozkurt
Supervisor, **Geological Engineering, METU** _____

Examining Committee Members:

Prof. Dr. Erdinç Yiğitbaş
Geological Engineering, Çanakkale Onsekiz Mart University _____

Prof. Dr. Erdin Bozkurt
Geological Engineering, METU _____

Prof. Dr. Gürol Seyitoğlu
Geological Engineering, Ankara University _____

Assoc. Prof. Dr. Erman Özsayın
Geological Engineering, Hacettepe University _____

Assist. Prof. Dr. Ulaş Avşar
Geological Engineering, METU _____

Date: 13.09.2019

I hereby declare that all information in this document has been obtained and presented in accordance with academic rules and ethical conduct. I also declare that, as required by these rules and conduct, I have fully cited and referenced all material and results that are not original to this work.

Name, Surname: Bayram Alper Durukan

Signature:

ABSTRACT

THE CHARACTER AND DISPLACEMENT OF ADIYAMAN FAULT (SOUTHEAST ANATOLIA): EVIDENCE FROM SUBSURFACE DATA

Durukan, Bayram Alper
Master of Science, Geological Engineering
Supervisor: Prof. Dr. Erdin Bozkurt

September 2019, 134 pages

Structural interpretation of five 2D seismic sections acquired by TPAO is carried out in the Adiyaman region of Southeast Anatolia. The sections are geological calibrated with stratigraphic logs of five boreholes. This study has resulted in the discovery of a previously undefined fault, herein named as Şambayat Fault. The fault is a NW-SE-trending structure that parallels the Bozova Fault and comprises several parallel fault segments. The structural maps of Cretaceous Sayındere and Karababa formations are also prepared and suggest that their sedimentation was controlled by the Şambayat Fault; it is therefore suggested that the Şambayat Fault was active during at least Campanian and because it appears not affecting the Middle Eocene-Oligocene Gaziantep Formation, its activity ceased by then. The segments of the Şambayat Fault is cut and displaced by the Adiyaman Fault. The correlation of these segments on either side of the Adiyaman Fault indicates a total sinistral displacement of about 4400 m. The Şambayat Fault is buried beneath younger sediments and has no surface expression suggesting its activity. Therefore, careful interpretation of seismic sections would be a useful method to identify and map buried structures that may have important implications on the geological evolution of a given region.

Keywords: Şambayat Fault, Adiyaman Fault, Cretaceous geological evolution,
Seismic Interpretation, Southeast Anatolia

ÖZ

ADİYAMAN FAYININ KARAKTERİ VE ATIM MİKTARI (GÜNEYDOĞU ANADOLU): YERALTI VERİLERİ KULLANILARAK

Durukan, Bayram Alper
Yüksek Lisans, Jeoloji Mühendisliği
Tez Danışmanı: Prof. Dr. Erdin Bozkurt

Eylül 2019, 134 sayfa

Güneydoğu Anadolu Adıyaman bölgesinde TPAO tarafından atılan 5 adet 2B sismik kesitin yapısal yorumu yapılmıştır. Bu kesitler 5 adet kuyunun stratigrafik logları ile kalibre edilmiştir. Bu çalışma, daha önce tanımlanmamış bir fayın keşfedilmesine neden olmuştur, bu faya Şambayat Fayı adı verilmiştir. Bu fay, Bozova Fayı ve bölgedeki bir kaç fay ile paralel, kuzeybatı-güneydoğu doğrultulu yapılarıdır. Kretase yaşlı Sayındere ve Karababa Formasyonlarının yapısal haritaları çizilmiş ve çökelimlerinin Şambayat Fayı ile kontrol edildiği görülmüştür. Bu nedenle, Şambayat Fayının Kampaniyen'de etkin olduğu, Orta Eosen-Oligosen'de etkisinin durduğu önerilmiştir. Şambayat Fayı'nın bölümleri Adıyaman Fayı tarafından kesilip ötelenmiştir. Bu bölümleri Adıyaman Fayının her iki yanında eşleştirdiğimizde, Adıyaman Fayının, atım miktarı 4400m. olan, sol atımlı bir fay olduğu ortaya çıkmaktadır. Şambayat Fayı genç sedimanlar tarafından örtülmektedir ve yüzeyde herhangi bir aktivitesi gözlenilmemektedir.

Bu nedenle, dikkatli bir şekilde yapılmış sismik yorum, haritada görülemeyen fakat bölgedeki jeolojik evriminde önemli etkileri olabilen gömülü yapıları tanımlayan kullanışlı bir metoddur.

Anahtar Kelimeler: Şambayat Fayı, Adıyaman Fayı, Kretase jeoloji evrimi, Sismik Yorum, Güneydoğu Anadolu

To my family; Ilknur, Begüm Zeynep ve Kaan Faruk DURUKAN

ACKNOWLEDGEMENTS

I would like to express my appreciation to my supervisor Prof. Dr. Erdin Bozkurt, for monitoring each step of this thesis with a great concern and supporting the progress of the work with his valuable advices. I am especially grateful for his clear guidance and his endless help during the study. It was a great chance for me to have utilized his profound knowledge on this study. Whenever I was discouraged he motivated me with a wise and affectionate manner and gave me the strength to continue my work.

I would like to express my deepest gratitude to my committee members; Prof. Dr. Erdiñ Yiđitbař, Prof. Dr. Grol Seyitođlu, Assoc. Prof. Dr. Erman zsayın, Assist. Prof. Dr. Ulař Avřar for their scientific support, encouragement and valuable advices during this study.

I would like to thank Ali lmez for his motivation, understanding approach, encouragements and valuable recommendations during my studies.

I would like to express my gratitude to my colleague Mahmut Utmanođulları for his contributions throughout this study.

I would like to thank to Gkhan Hacımehmetođlu, Zbeyir Kk, Yaser Fatih zbay for their help and support.

I would also like to thank to my parents řaheste and Rıza Durukan and my brother Aydın Durukan for their endless support.

Finally, I must express my very profound gratitude to my beloved wife Ilknur Durukan and my children Begm Zeynep Durukan and Kaan Faruk Durukan to for providing me with unfailing support and continuous encouragement throughout my years of study and through the process of researching and writing this thesis. This accomplishment would not have been possible without them. Thank you.

This study was supported by The Turkish Petroleum Incorporated (TPAO). All data were supplied by TPAO and include laboratory analysis on core and cutting samples, drilling results and well logs which are Gamma Ray, Sonic and Density.

TABLE OF CONTENTS

ABSTRACT	v
ÖZ	vii
ACKNOWLEDGEMENTS.....	x
TABLE OF CONTENTS	xii
LIST OF TABLES.....	xv
LIST OF FIGURES	xvi
CHAPTERS	
1. INTRODUCTION.....	1
1.1. General Information.....	1
1.2. Geographic Location: The Study Area	5
1.3. Adiyaman Fault.....	5
1.4. Purpose and Scope	12
2. STRATIGRAPHY.....	23
2.1. General Stratigraphy	23
2.2. Allochthonous Units	27
2.2.1. Koçali Complex.....	27
2.2.2. Karadut Complex	28
2.3. Autochthonous Units.....	28
2.3.1. Precambrian-Paleozoic Units	28
2.3.1.1. Telbesmi Formation.....	29
2.3.1.2. Sadan Formation.....	29
2.3.1.3. Koruk Formation	30

2.3.1.4. Sosink Formation	30
2.3.2. Cretaceous Rock Units.....	30
2.3.2.1. Mardin Group.....	31
2.3.2.2. Adiyaman Group.....	33
2.3.2.3. Şırnak Group	35
2.3.3. Paleogene Rock Units.....	39
2.3.3.1. Midyat Group.....	39
2.3.3.2. Silvan Group	41
2.3.4. Neogene Units.....	43
2.3.4.1. Şelmo Formation.....	43
3. Methodology.....	45
3.1. General	45
3.2. Seismic Interpretation.....	47
3.2.1. Horizon Interpretation: Check-shot Data and Synthetic Seismograms	49
3.2.1. Fault and Seismic Horizon Interpretation.....	51
3.2.2. Structural Maps.....	57
3.3. Ground Truthing.....	58
4. Interpretation of the subsurface data.....	61
4.1. Seismic Fault Interpretation Results.....	61
4.2. Seismic Line AD-03-229.....	62
4.3. Seismic Line AV-00-113.....	67
4.4. Seismic Line AD-00-202.....	67
4.5. Seismic Line DD-6071	69
4.6. Seismic Line AV-00-110.....	77

4.7. Seismic Horizon Interpretation	81
4.7. Ground Truthing	92
5. Discussion and Conclusion	99
REFERENCES	103
APPENDICES	
A. Materials.....	121
B. Checkshot Geometries of the Three Wellbores.....	126
C. Checkshot Values for Wellbores	128
D. Calculated Formation Velocities in Each Well.....	131

LIST OF TABLES

TABLES

Table 3.1. Formation top values of wells B-1, B-2, BA-1, D.B-1, and D.B-2 used calculate the velocity values of formations using a simple spreadsheet menu.	55
Table 3.2. Checkshot velocities for different formations calculated from checkshot values.....	57
Table C.1. Checkshot values of well B-2.	128
Table C.2. Checkshot values of well D.B-1.....	129
Table C.3. Checkshot values of well D.B-2.....	130
Table D.1. Calculated check shot velocity values of well D.B-1.	131
Table D.2. Calculated check shot velocity values of well D.B-2.	132
Table D.3. Calculated check shot velocity values of well B-2.	133
Table D.4. Calculated check shot velocity values of well BA-1.	134

LIST OF FIGURES

FIGURES

Figure 1.1. Overall tectonic sketch map of the Middle East (from Cawazza et al., 2018). AT- Anatolide-Tauride terrane; IZ- İstanbul Zone; SkZ- Sakarya Zone; KM- Kırşehir Massif; NAF- North Anatolian Fault; EAF- Eastern Anatolian Fault; EP- Eastern Pontides; IAESZ- İzmir-Ankara-Erzincan Suture Zone; SASZ- Sevan-Akera Suture Zone; GC- Greater Caucasus; LC- Lesser Caucasus; DSF- Dead Sea Fault. Arrows indicates GPS vectors 2

Figure 1.2. Structural map of eastern Turkey showing the African, Arabian, Anatolian and Eurasian plates and major active faults (thick black lines). The Adıyaman Fault is shown in thick red line. Red and blue arrows indicate GPS velocities with respect to a fixed Arabian lithospheric plate, and blue and red circles indicate GPS measurement errors, according to Reilinger et al. (2006) and Aktuğ et al. (2016), respectively. The inset map and box with white dashed lines show the location of the figure. EF- Ecemiş Fault; KTJ- Karlıova Triple Junction; MTJ- Maraş Triple Junction; OF- Ovacık Fault; SF- Savrun Fault. Figure is taken from Khalifa et al. (2019). 3

Figure 1.3. *"I gpgt cıktı gf " vgevppke" o cr " qh' uqwj gcıwgt p" Cpcvırk0' Eqo r kğf " İt qo " Rgt k p ± g m l g v' c r 0 * 3 ; : 9 + * 3 go gp * 3 ; ; 2 + * Rgt k p ± g m l c p f * 3 go gp * 3 ; ; 2 - 0 V j g ' l j t q w i j / i q l p i " f q w g f ' İ k p g ' o c t m u ' l j g ' p q t v j g t p ' d q w p f c t { " q h ' l j g ' r g c f k p i ' g f i g ' q h ' l j g ' E t g x c e g q w u ' l j t w u u " * o q f k k g f ' İ t q o ' Rgt k p ± g m l c p f * 3 go gp . ' 3 ; ; 3 - 0 V j g ' İ k i w t g ' k u ' v c n g p ' İ t q o ' D g g t " * 4 2 3 : ... 6*

Figure 1.4. Structural map of the Adıyaman area, showing major faults in and around study area. The rectangle shows study area (from Tatar et al., 2019). 7

Figure 1.5. Structural map of Adıyaman and Gaziantep region (from Şahbaz and Seyitoğlu, 2018). The rectangle shows the location of the study area. EAFZ- East Anatolian Fault Zone; AF- Adıyaman Fault; HF- Halfeti Fault; BF- Bozova Fault; HRF- Harmancık Fault; ÇBT- Çakırhüyük blind thrust, ABT- Araban blind thrust, YBT- Yavuzeli blind thrust; GKBT- Gemrik-Karababa blind thrust; FA- Faldağı

anticline; SA- Suvarlı anticline, KA- Karadağ anticline. The rectangle shows location of the study area.	8
Figure 1.6. Google Earth™ image showing the geographic location of the study area.	9
Figure 1.7. Adıyaman Fault and major structural features around Diyarbakır, Erzincan and Şanlıurfa (Perinçek et al., 1987).....	11
Figure 1.8. (a) Simplified map showing major plates and their boundary faults in the Eastern Mediterranean region and location of the study area; (b) simplified neotectonic map showing major fault zones and strike-slip basins comprising the East Anatolian Fault System (EAFS) in the Lake Hazar and Bingöl region (from Aksoy et al., 2007).	13
Figure 1.9. Neotectonic map of the East Anatolian Fault Zone in the Lake Hazar region, showing several parallel faults in the region (from Aksoy et al., 2007).....	14
Figure 1.10. Geological map of the Adıyaman area, showing Adıyaman Fault and major structural features (Aksu et al., 2014). Pzmzg-Pütürge Metamorphics ; Pzmz Malatya Metamorphics- ; Km-Mardin Group ; Ks- Sayındere Formation; Kska- Kastel Formation; Jkk- Koçali Allocthonous; Kka-Karadut Allocthonous; Ktsg- Germav Formation; Tg- Gercüş Formation; Tmh- Hoya Formation; Tg- Gercüş Formation; Tmga2- Gaziantep Formation (Marn Member); Tmga1- Gaziantep Formation (Limestone Member); Tf- Fırat Formation ; Tli- Lice Formation; Tş- Şelmo Formation; PIQ- Plio-Quaternary sediments; Qb- Yavuzeli basalts; Qal- Quaternary Alluvium.	15
Figure 1.11. Google Earth™ image illustrating a well-developed fault scarp at the expense of Hoya Formation limestone to the east of Kutluca village at Faldağı location. Tmh- Hoya Formation (Eocene Limestone), Tş- Şelmo Formation (terrestrial sediments), PIQ- Plio- Quaternary loose sediments.....	16
Figure 1.12. Google Earth™ image illustrating a well-developed fault valley (Ziyaret riverlet valley), to the south of Adıyaman city. KTsg- Germav Formation (Marl), Tmh- Hoya Formation (Eosen limestone), Tş- Şelmo Formation (terrestrial sediments), PIQ- Quaternary loose sediments.	17

Figure 1.13. Google Earth™ image illustrating a well-developed Alidağı push-up to the south-east of Kutluca village. At the Top of push-up area, Hoya Formation is exposed. Germav Formation occurs at the edge of push-up area. Şelmo Formation covers the Hoya Formation at the south of push-up area. KTsg- Germav Formation (marl), Tmh- Hoya Formation (Eosen limestone), Tş- Şelmo Formation (terrestrial sediments), PIQ- Quaternary loose sediments. 18

Figure 1.14. Shaded relief image showing the trace of the Adıyaman Fault indicated by yellow arrows (from Khalifa et al., 2019). 19

Figure 1.15. Detailed map of the Alidağ flower structure (from Aksu and Durukan, 2014). The a-a' line shows the location of sketch cross-section in Figure 1.16. Ktsg: Germav Formation, Tmh: Hoya Formation, Tş: Şelmo Formation, and PIQ: Plio-Quaternary sediments. 19

Figure 1.16. Sketch cross-section illustrating the structural elements of the Alidağ positive flower structure (from Aksu and Mülayim, 2015). See Figure 1.15 for location of sketch cross-section (a-a' line). Ktsg- Germav Formation, Tmh- Hoya Formation, Tş- Şelmo Formation, and PIQ- Plio-Quaternary sediments. 20

Figure 1.17. A field view from the Alidağı, view from west (from Aksu and Mülayim, 2015). 20

Figure 2.1. General tectono-stratigraphic section of Southeast Anatolia (Yalçın, 1976; Yılmaz, 1993) 24

Figure 2.2. Geology map of study area (Çemen et al., 1991). The rectangle shows location of the study area. Ktsg– Germav Formation; Tmh–Hoya Formation; Tmga2–Gaziantep Formation (marl member); Tmga1– Gaziantep Formation (limestone member); Tş– Şelmo Formation; PIQ– Plio- Quaternary sediments; Qal– Quaternary alluvials..... 25

Figure 2.3. Simplified columnar section of the autochthonous rock units in and around the study area (Güven et al., 1991). 26

Figure 3.1. A Google Earth™ image showing location of boreholes and 2D seismic sections. 46

Figure 3.2. The synthetic seismogram calculated by using check shot data and sonic log for the well D.B-2. TVD- True vertical depth; TWT- Two Way Time; RHOB- Sonic log; RC- Reflection coefficient. The formation contacts have been identified by using both cutting samples and well log information gathered from well.	50
Figure 3.3. The synthetic seismogram calculated by using check shot data and sonic log for the well BA-1. TVD- True vertical depth; TWT- Two Way Time; RHOB- Sonic log; RC- Reflection coefficient. The formation contacts have been identified by using both cutting samples and well log information gathered from well.	51
Figure 3.4. Horizon picks based on synthetic seismogram calibrated by sonic log and check-shot data on well D.B-2 in seismic section line AD-03-229. Top of the Karababa Formation (third black stripe from the top) is calibrated with well-log information to interpret the key horizon level.....	52
Figure 3.5. Horizon picks based on synthetic seismogram calibrated by sonic log and check-shot data on well BA-1 in seismic section line AV-00-113. Top of the Karababa Formation (third black stripe from the top) is calibrated with well-log information to interpret the key horizon level.....	53
Figure 3.6. Horizon picks based on synthetic seismogram calibrated by sonic log and check-shot data on well BA-1 on seismic section line AV-00-113. Formation tops are calibrated with well-log information to interpret key horizon levels of top of the Gaziantep, Germav, Kastel, Sayindere, Karaboğaz, Karababa, Derdere and other older formations (see Table 3.1 for more information).....	53
Figure 3.7. Horizon picks based on synthetic seismogram calibrated by sonic log and check-shot data on well D.B-2 on seismic section line AD-03-229. Formation tops are calibrated with well-log information to interpret key horizon levels of top of the Gaziantep, Germav, Kastel, Sayindere, Karaboğaz, Karababa, Derdere and other older formations (see Table 3.1 for more information).....	54
Figure 3.8. Seismic synthetic menu that is used in well-tying, that is conversion of the well-log measurements from depth to the time domain.....	56
Figure 3.9. Fault interpretation on seismic line AD-03-229	59

Figure 3.10. Top of the Karababa (red) and Sayindere (green) formations, and Fault interpretation on seismic line AD-03-229	60
Figure 4.1. Uninterpreted seismic section AD-03-229 (migration). See Figure 3.1 for location.	63
Figure 4.2. Horizon picks based on synthetic seismogram calibrated by sonic log and check-shot data on well D.B-2 on seismic section line AD-03-229. Formation tops are calibrated with well-log information to interpret key horizon levels of top of Gaziantep, Germav, Kastel, Sayindere, Karaboğaz, Karababa, Derdere and other older formations (see Table 3.1 for more information).	64
Figure 4.3. Fault interpretation on seismic line AD-03-229.....	65
Figure 4.4. Top of the Karababa (red) and Sayindere (green) formations, and Fault interpretation on seismic line AD-03-229	66
Figure 4.5. Uninterpreted seismic section AV-00-113 (migration). See Figure 3.1 for location.	68
Figure 4.6. Horizon picks based on synthetic seismogram calibrated by sonic log and check-shot data on well D.B-2 on seismic section line AV-00-113. Formation tops are calibrated with well-log information to interpret key horizon levels of top of Gaziantep, Germav, Kastel, Sayindere, Karaboğaz, Karababa, Derdere and other older formations (see Table 3.1 for more information). Fault Interpretation is also performed.....	70
Figure 4.7. Top of the Karababa (red) and Sayindere (green) formations, and fault interpretation on seismic line AV-00-113.	71
Figure 4.8. Uninterpreted seismic section AD-00-202 (migration). See Figure 3.1 for location.	72
Figure 4.9. Fault interpretation on seismic line AD-00-202.....	73
Figure 4.10. Top of the Karababa (red) and Sayindere (green) formations, and fault interpretation on seismic line AD-00-202.	74
Figure 4.11. Uninterpreted seismic section D-6071 (migration). See Figure 3.1 for location.	75

Figure 4.12. Horizon picks based on synthetic seismogram calibrated by sonic log and check-shot data on well D.B-2 on seismic section line D-6071. Formation tops are calibrated with well-log information to interpret key horizon levels of top of Gaziantep, Germav, Kastel, Sayındere, Karaboğaz, Karababa, Derdere and other older formations (see Table 3.1 for more information). The fault interpretation of the section is also performed.	76
Figure 4.13. Top of the Karababa (red) and Sayındere (green) formations, and fault interpretation on seismic line D-6071	78
Figure 4.14. Uninterpreted seismic section AV-00-110 (migration). See Figure 3.1 for location.	79
Figure 4.15. Fault interpretation on seismic line AV-00-110.	80
Figure 4.16. Top of the Karababa (red) and Sayındere (green) formations, and Fault interpretation on seismic line AV-00-110.	82
Figure 4.17. 2D image of the fault planes interpreted in five seismic sections. The correlation of the fault segments (blue and green planes) indicates that the Adıyaman Fault (red) forms a domain boundary between the fault segments. The relative position of the segments is consistent with a sinistral displacement along the Adıyaman Fault.	83
<i>Hki wt g'6Ø</i> : 02D image of the fault planes on Google Earth™ image. See Figure 4.20 for explanation.	83
Figure 4.19. The interpretation and correlation of seismic sections analyzed during this research.	84
Figure 4.20. Two Way Time (TWT) map of the Karababa Formation. Contour interval is 100 m. The white lines show fault planes. Faults 1 and 2 represent the Şambayat Fault, 3 the Adıyaman Fault. Note that the Adıyaman Fault marks a sudden break in TWT contours. Note also that fault segments 1 and 2 in the northwestern block of the Adıyaman Fault bounds an area of low true vertical depths that is interpreted as a push-up structure. The sudden break in TWT contours across the fault segments 1 and 2 of the northwestern block of the Adıyaman Fault is more pronounced, whereas they are	

not evident in the southeastern block. The fault segment to the east of the Adıyaman Fault may be an artifact of poor seismic resolution..... 86

Figure 4.21. Two Way Time (TWT) map of the Sayındere Formation. See Figure 4.23 for more information..... 86

Figure 4.22. 3D view of the Sayındere Formation with seismic sections AV-00-202 and D-6071. See Figure 4.23 for labelling of faults. 87

Figure 4.23. 3D view of the Karababa Formation with seismic sections AV-00-202 and D-6071. See Figure 4.23 for labelling of faults. 87

Figure 4.24. Velocity map of the Karababa Formation. 88

Figure 4.25. Velocity map of the Sayındere Formation. 88

Figure 4.26. Structure map of the Karababa Formation. See Figure 4.23 for labelling of faults. 90

Figure 4.27. Structure map of the Sayındere Formation. See Figure 4.23 for labelling of faults 90

Figure 4.28. Structure map of Karababa Formation, showing vertical displacements. See Figure 4.23 for labelling of faults. The vertical displacement amount is varying from 320–340 at northern part of Şambayat Fault and it is varying from 320–360 at Southern part of Şambayat Fault at the man of the top of Karababa Formation. 91

Figure 4.29. "Structure contour map of top of Sayındere Formation. The vertical displacement amount at the northern part of Şambayat Fault is about 460m. The displacement amount at the Southern part of Şambayat Fault is 430 m. the difference between Karababa Formation and Sayındere Formation vertical amounts is caused by the distance between Seismic sections that is called seismic resolution. If Seismic is 3D the results could be more similar to each other. 91

Figure 4.30. These sections, which are at the opposite side of Adıyaman Fault, shows that the Sayındere Formation is syntectonic. The formation is thicker in the North and South of the Şambayat Fault. This proves that they are the same fault. 93

Figure 4.31. **(a)** Relief map showing the surface expression of the Adıyaman Fault. Note the pronounced linear trace of the fault; **(b)** the interpretation of the DEM map;

the red lines represent the Adiyaman Fault. Blue rectangle indicates location of the study area.	94
Figure 4.32. Geology map of the study area (from Aksu et al., 2012). The faults are modified during this fieldwork. The trace of the Şambayat Fault is placed according to field observations and seismic interpretation. Qal– Quaternary alluvials, PIQ– Plio–Quaternary loose sediments.....	95
Figure 4.33. A Google Earth image showing Şambayat Fault (green), Adiyaman Fault (red), Halfeti Fault (blue) and Bozova Fault (purple).....	96
Figure A.1. Lithology log of well D.B-1	121
Figure A.2. Lithology log of well D.B-2.	122
Figure A.3. Lithology log of well BA-1	123
Figure A.4. Lithology log of well B-1.	124
Figure A.5. Lithology log of well D.B-2.	125
Figure B.1. Checkshot geometry of well DB-1.	126
Figure B.2. Checkshot geometry of well DB-2	126
Figure B.3. Checkshot geometry of well B-2.	127

CHAPTER 1

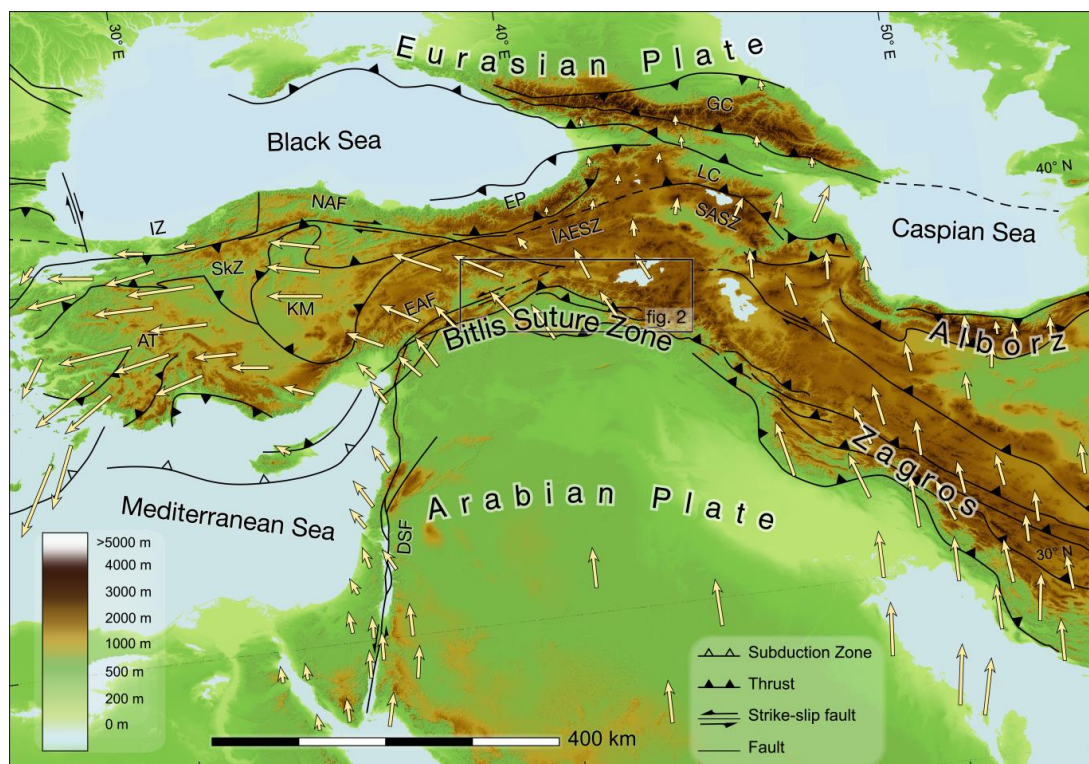
INTRODUCTION

1.1. General Information

The study area, Adıyaman region, is the principal oil-producing region in southeast Turkey. It is located within the collisional zone of southeast Turkey that marks the final closure of the southern Neotethys across the Bitlis Suture Zone (BSZ); the BSZ 'ku'c "dgn'ql'j ki j 'wt ckp"cpf 't crlf "wr rlv'dgvy ggp" Ct cdkcp'Rrc vlt o "vq"vj g'uqwj "cpf "c" eqmxi g"ql'eqpvkp gpcn"lt ci o gvu "kucpf "ct eu."cpf "qr j kqrk"e"o 2rcpi g"vq"vj g"pqt vj " (quoted from Hempton 1985)' (Figure 1.1). The 500-km-long arcuate belt of suture therefore marks continent collision between Arabian Plate in the south and Eurasian Plate in the north (e.g., Şengör and Kidd, 1979; Şengör and Yılmaz, 1981; Hempton, 1985; Dewey et al., 1986; Yılmaz, 1991, 1993; Yılmaz et al., 1993; Yiğitbaş and Yılmaz, 1993). The Adıyaman region therefore lies within the foreland area of the suture.

The geology and evolution of the suture zone have been the subject of several researchers (e.g., Hall, 1976; Yazgan et al., 1983; Çağlayan et al., 1984; Göncüoğlu and Turhan, 1984; Hempton, 1985; Okay et al., 1985; Perinçek, 1990; Yılmaz, 1993; Robertson, 1998, 2000; Jolivet and Faccenna, 2000; Bilgiç, 2002; Günay and Şenel, 2002; Şenel and Ercan, 2002; Tarhan, 2002; Barazangi et al., 2006; Robertson et al., 2007; Allen and Armstrong, 2008; Okay, 2008; Oberhänsli et al., 2010, 2012, 2013; Yılmaz et al., 2010; Karaoğlu et al., 2013; Seyitoğlu et al., 2017; Cawaza et al., 2018; Bakkal et al., 2019 and references therein). Although several papers have been published, the age of the continental collision has always been debated with proposed ages range widely from the Late Cretaceous to the Pliocene (Hall, 1976; Berberian and King, 1981; Şengör et al., 1985; Yılmaz, 1993; Alavi, 1994; Jolivet and Faccenna,

2000; Agard et al., 2005; Robertson et al., 2007; Allen and Armstrong, 2008; Okay et al., 2010; Rolland et al., 2012; McQuarrie and van Hinsbergen, 2013). Recently, Cawazza et al. (2018) concluded that continental collision has started in the mid-Miocene.



Overall tectonic sketch map of the Middle East (from Cawazza et al., 2018). AT- Anatolide-Tauride terrane; IZ- İstanbul Zone; SkZ- Sakarya Zone; KM- Kırşehir Massif; NAF- North Anatolian Fault; EAF- Eastern Anatolian Fault; EP- Eastern Pontides; IAESZ- İzmir-Ankara-Erzincan Suture Zone; SASZ- Sevan-Akera Suture Zone; GC- Greater Caucasus; LC- Lesser Caucasus; DSF- Dead Sea Fault. Arrows indicates GPS vectors

The BSZ is also named as Southeast Anatolian orogenic belt, which is described as a geological mosaic formed as a result of progressive amalgamation of varying, roughly east–west-trending tectonostratigraphic units, separated from one another by thrusts (Yılmaz, 1990, 1991, 1993; Yiğitbaş et al., 1992; Yılmaz et al., 1993; Yiğitbaş and Yılmaz, 1993); from the south to the north, these are ‘*y g' C t c d k p' R r v q t o ø*’, ‘*y g' | q p g' q h' k o d t k e c v k p'*’, and ‘*y g' p c r r g' | q p g'*’. The geology of the belt is attributed to the

Alpine orogeny which has developed in two major stages during Late Cretaceous and Middle Eocene–Miocene (Yılmaz, 1990, 1991, 1993; Yılmaz et al., 1993; Yiğitbaş and Yılmaz, 1993).

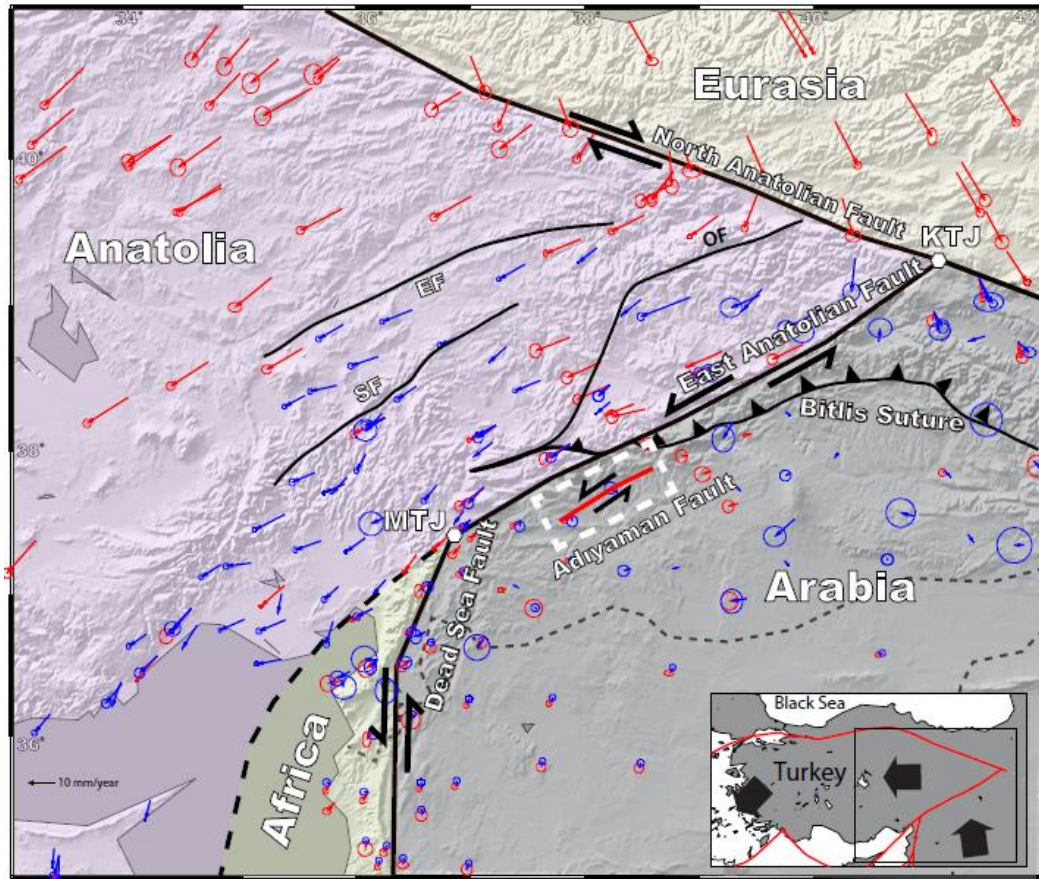


Figure 30 Structural map of eastern Turkey showing the African, Arabian, Anatolian and Eurasian plates and major active faults (thick black lines). The Adiyaman Fault is shown in thick red line. Red and blue arrows indicate GPS velocities with respect to a fixed Arabian lithospheric plate, and blue and red circles indicate GPS measurement errors, according to Reilinger et al. (2006) and Aktuğ et al. (2016), respectively. The inset map and box with white dashed lines show the location of the figure.

EF- Ecemiş Fault; KTJ- Karlova Triple Junction; MTJ- Maraş Triple Junction; OF- Ovacık Fault; SF- Savrun Fault. Figure is taken from Khalifa et al. (2019).

The southeast Turkey is located on the northern margin of the Arabian Platform, which is represented by an autochthonous Lower Paleozoic–Middle Miocene sedimentary succession of largely marine origin (Yılmaz, 1984; Yılmaz et al., 1993; Sungurlu 1974; Perinçek 1990; Perinçek et al., 1991); remnants of ophiolite nappes emplaced

onto the platform during the Late Cretaceous and Eocene periods also occur in the region (Yiğitbaş et al., 1992; Yılmaz et al., 1993). The region was structurally uplifted in the Middle Jurassic (Perinçek et al., 1991) or Late Jurassic–Early Cretaceous (Sungurlu, 1974; Ala and Moss, 1979), and is associated with a series of Paleozoic highs, which extend from northern Saudi Arabia via western Iraq and Syria to Turkey (Beydoun, 1989; Best et al., 1993).

The Arabian Plate is bounded by a narrow (up to 5 km in width) imbricated zone, made up of allochthonous units (e.g., Yılmaz et al., 1987; Yılmaz, 1993). The nappe zone occurs to the north of the zone of imbrication and is composed essentially of two nappes: *wrrgt "pcrrg* of metamorphic rocks (Bitlis and Pötürge massifs) and *nqy gt "* *pcrrg* of metamorphosed ophiolitic associations.

The study area is located within the Arabian Platform, near southwest of the city of Adıyaman. The Şambayat oil field and Besni district also lie within or near west of the study area.

East Anatolian Fault Zone (EAFZ), a plate boundary between the Arabian and Anatolian plates, forms the major structural element in the region and runs through northwest of the Adıyaman area (Seyitoğlu et al., 2018)(Figures 1.2 and 1.3). Other major structural elements in the area include NW–SE-trending right-lateral and NE–SW-trending left-lateral strike-slip faults (e.g., Adıyaman Fault, Bozova Fault, Çalğan Fault, Samsat Fault, Lice Fault, Halfeti Fault, and Harmancık Fault; Figures 1.4 and 1.5) (e.g., Şahbaz and Seyitoğlu, 2018; Khalifa et al., 2019; Tatar et al., 2019). The region is also characterized by a ~E–W-trending blind thrust system (e.g., Çakırhüyük blind thrust, Araban blind thrust, Yavuzeli blind thrust and Gemrik-Karababa blind thrust) and associated asymmetric ridges, interpreted as asymmetric anticlines (e.g., Faldağı anticline, Suvarlı anticline, Karadağ anticline; Figure 1.5); these anticlines are attributed to surface expression of the blind thrusts (Şahbaz and Seyitoğlu, 2018). Strike-slip faults appear to cut and displace these anticlines, attesting their ages.

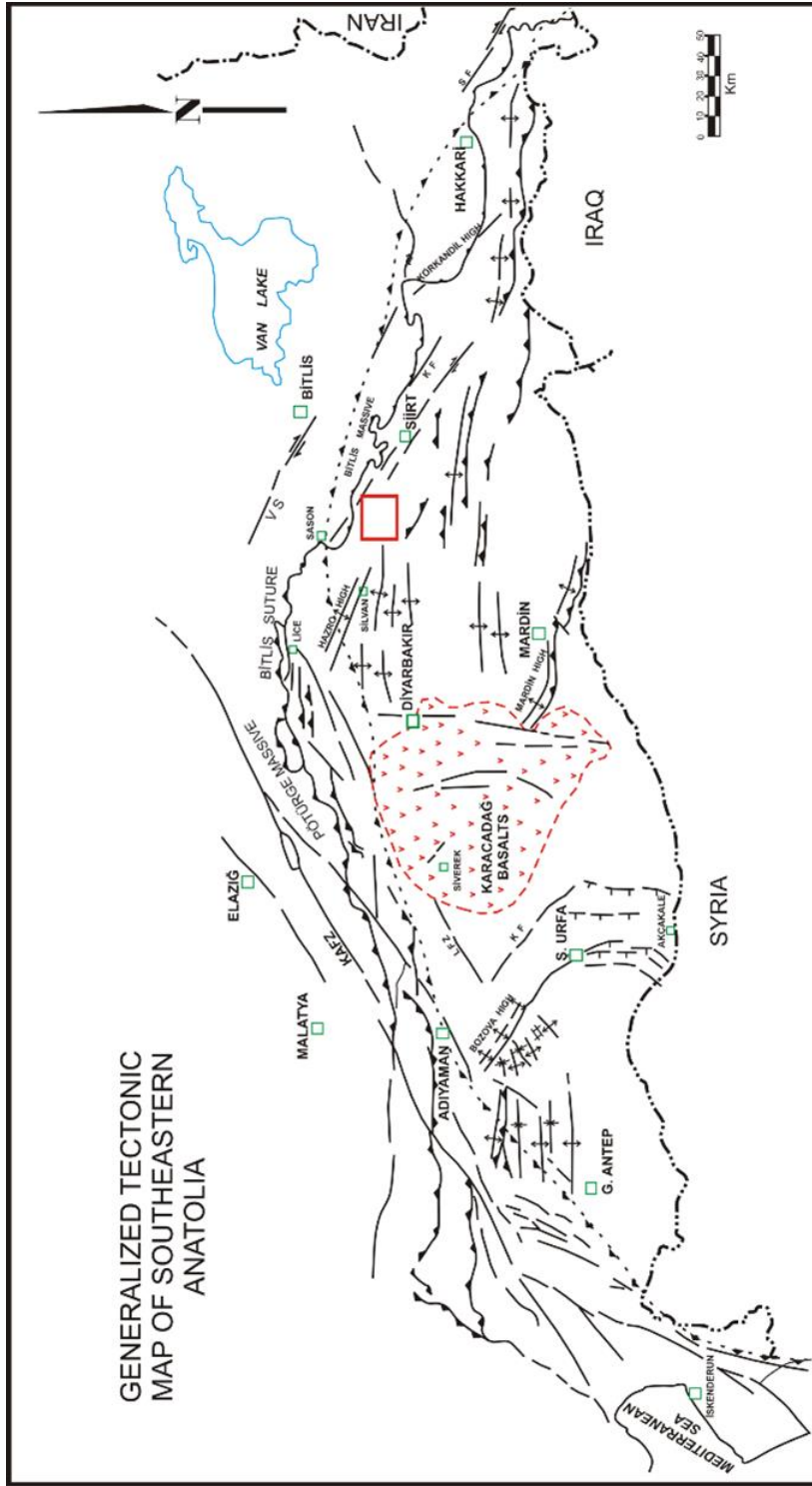
The present study aims to provide evidence that bears on the age and offset of the Adıyaman Fault.

1.2. Geographic Location: The Study Area

The study area is geographically located in the Adıyaman province of the southeast Turkey. It lies between the Besni district in the west and the city of Adıyaman in the southwest. It covers an area of 310 km² in the 1/25000 topographic sheets of M39-c2, M40-d1, M40-d2, M40-d3 and M40-d4 (Figure 1.6). Atatürk Dam lies to the southeast of the study area.

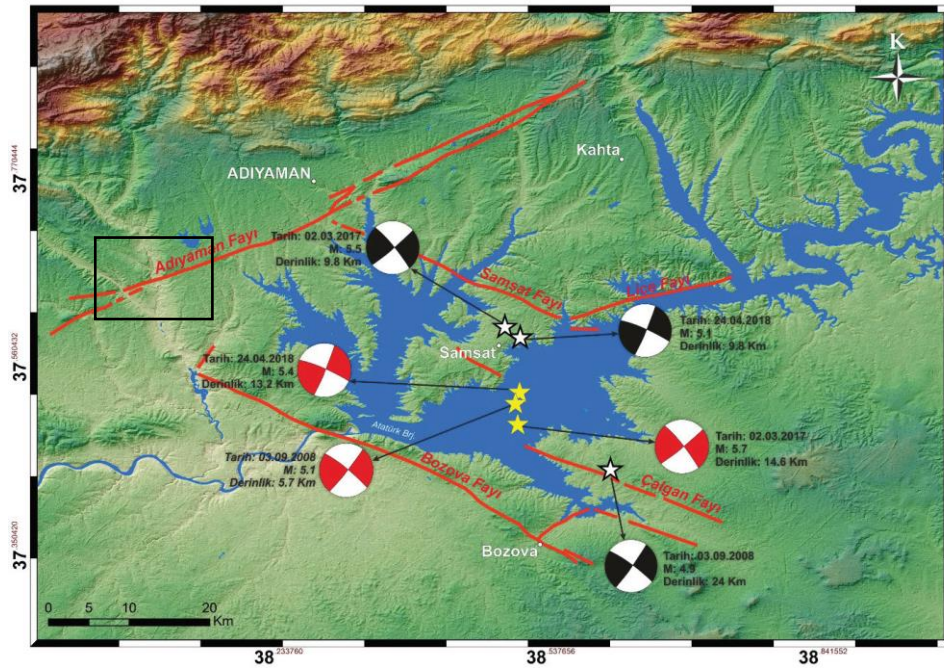
1.3. Adıyaman Fault

The East Anatolian Fault Zone (EAFZ) is one of the most important active neotectonic structures of the Eastern Mediterranean region and is interpreted as a transform boundary between the Anatolian and Eurasian, and the African and Arabian lithospheric plates (e.g., Arpat and Şaroğlu, 1972, 1975; Hempton et al., 1981; Şengör et al., 1985; Dewey et al., 1986; Hempton, 1987; Şaroğlu et al., 1987, 1992a, b; Muehlberger and Gordon, 1987; Barka and Kadinsky-Cade, 1988; Yürür and Chorowicz, 1998; Perinçek and Çemen, 1990; Herece and Akay, 1992; Westaway, 1994, 2004; Westaway and Arger, 2001; Çetin et al., 2003; Herece, 2003, 2008; Reilinger et al., 2006; Aksoy et al., 2007; Karabacak et al., 2011; Duman and Emre, 2013; Mahmoud et al., 2013; Öner et al., 2013; Aktuğ et al., 2016). Timing of initiation of the EAFZ is highly debated and claims range from Late Miocene to Late Pliocene (Arpat and Şaroğlu, 1972; Şengör et al., 1985); a Late Pliocene age is well accepted among researchers (Şaroglu et al., 1987, 1992; Yürür and Chorowicz, 1998; Westaway and Arger, 2001; Westaway, 2004).



Generalized tectonic map of southeastern Anatolia. Compiled from Perinçek et al. (1987), Çemen (1990), Perinçek and Çemen (1990). The through-going dotted line marks the northern boundary of the leading edge of the Cretaceous thrusts (modified from Perinçek and Çemen, 1991). The figure is taken from Beşer (2018).

In addition to East Anatolian Fault Zone, there are a number of secondary faults that run (sub)parallel or oblique to the main trend of the EAFZ (Figures 1.2., 1.7 and 1.8) (e.g., Hempton, 1987; Şaroğlu et al., 1992; Şengör et al., 1985; Taymaz et al., 1991; Westaway, 1994; Aksoy et al., 2007; İmamoğlu and Çetin, 2007; İnceöz and Zengin, 2014; Khalifa et al., 2018, 2019 and references therein). Adıyaman Fault is one of those structures. It is first described as branch of the a branch of East Anatolian Fault Zone (Perinçek et al., 1987). Adıyaman Fault is described as NE–SW-trending sinistral strike-slip fault that runs in the area between southwest of Adıyaman and west of Palu where it branches off the EAF (Figure 1.7). The linear valleys around Palu to the south of Lake Hazar forms the morphological evidence of the Adıyaman Fault.



Hki wt g'300 Structural map of the Adıyaman area, showing major faults in and around study area. The rectangle shows study area (from Tatar et al., 2019).

Near the west of Hazar Lake, the continuum of the fault is difficult to trace as it is running through the Pütürge metamorphics. The trace is obvious in the area between north of Kahta and south of Besni (Perinçek et al., 1987). It cuts and displaces Miocene units and Fırat river valley around Çüngüş. Coşkun (2004) stated that Adıyaman Fault

shares similar subsurface tectonic style with, and therefore is the northern continuity of, the Dead Sea Fault.

The Adiyaman Fault is also studied by İmamoglu and Çetin (2007). The fault branches off the East Anatolian Fault Zone around west of Palu, runs southwest through Helindir and Hazar settlements to the south of Lake Hazar. It is about 210-km-long left-lateral fault. The Adiyaman Fault cuts and displaces river Euraptues valley, and the runs through Adiyaman province. In the area south of Besni, the Adiyaman Fault appear to terminate where it branches into several segments imitating a horse-tail pattern. The Adiyaman Fault is interpreted as R fracture of East Anatolian Fault Zone.

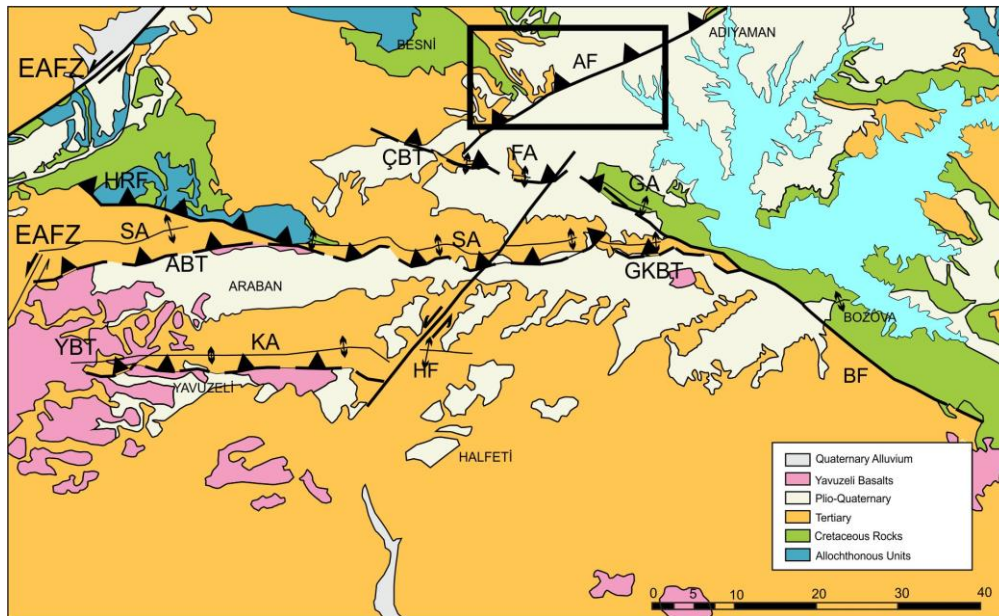


Figure 3.10 Structural map of Adiyaman and Gaziantep region (from Şahbaz and Seyitoğlu, 2018). The rectangle shows the location of the study area. EAFZ- East Anatolian Fault Zone; AF- Adiyaman Fault; HF- Halfeti Fault; BF- Bozova Fault; HRF- Harmancık Fault; ÇBT- Çakırhüyük blind thrust, ABT- Araban blind thrust, YBT- Yavuzeli blind thrust; GKBT- Gemrik-Karababa blind thrust; FA- Faldağı anticline; SA- Suvarlı anticline, KA- Karadağ anticline. The rectangle shows location of the study area."

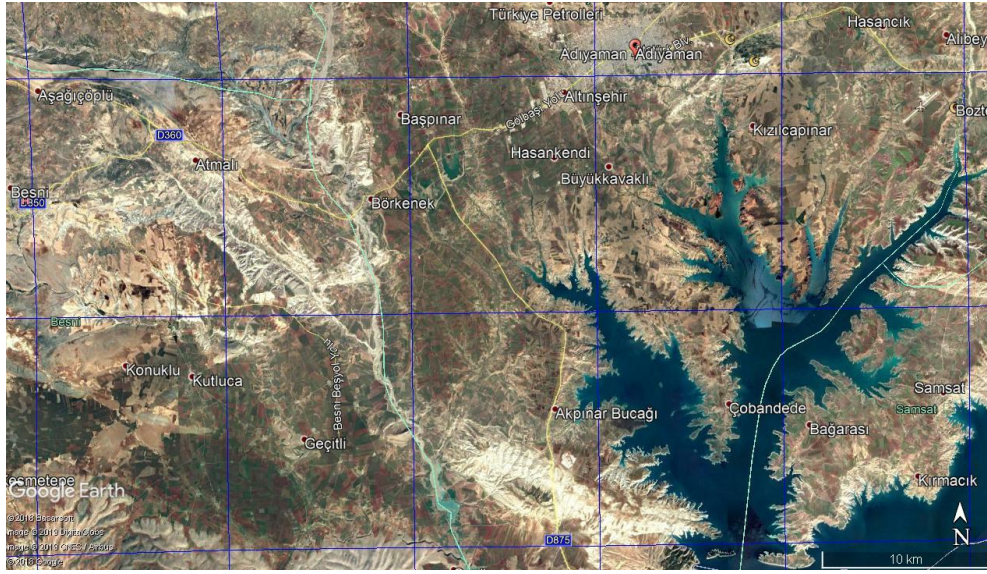


Figure 1. Google Earth™ image showing the geographic location of the study area.

Yazar (2009) stated that Adiyaman Fault appears on seismic section with weak reflections. The fault is interpreted to induce fractures and small faults in Adiyaman, Çemberlitaş, Çukurtaş and Cendere petroleum oil fields. The age of the fault is Miocene.

Adiyaman Fault is also mapped by Aksoy et al. (2007) in detail where it is described as an active left-lateral strike-slip fault (Figures 1.2., 1.8 and 1.9). The fault is seismically active and capable of producing low to moderate frequency of relatively small to moderate magnitude ($M_w = 3.0-5.5$) earthquakes (Khalifa et al., 2019). The March 2, 2017 Adiyaman-Samsat earthquake ($M_w = 5.5$) is the largest recorded on the fault. Quantitative geomorphic indices along the Adiyaman Fault provide evidence that the entire is a moderately to highly active structure and that it reflects a moderate to high seismic risk (Khalifa et al., 2019). The Adiyaman Fault is of secondary importance compared to the EAF in accommodating the relative motion between the Arabian and Anatolian lithospheric plates (Khalifa et al., 2019).

Northeastern part of the Adiyaman Fault is mapped by İnceöz and Zengin (2014); five left-lateral fault segments and fault set are described. The authors have named these structures as NNW–SSW-trending ($N10^\circ-20^\circ E$) Işıktepe Fault set, Başkaynak Fault

set, E–W-trending Üçdeğirmenler Fault, Çakıroğlu Fault, and ENE–WSE-trending (N70°E) Gökçepelit Fault. The interaction between different fault segments/sets result in formation of pull-apart basins. Elongated hills, linear valleys, offset river courses, and pull-part basins of variable sizes are mapped. The paleostress data is interpreted to suggest five deformational phases: (i) early Eocene extensional phase, (ii) Oligocene compressional phase, (iii) early Miocene extensional phase, (iv) middle–late Miocene compressional phase and finally (v) Plio–Quaternary strike-slip faulting. The last phase has resulted in anticlockwise rotation of fault-bounded blocks within the East Anatolian Fault Zone. The authors have considered the Adıyaman Fault within the East Anatolian Fault Zone. The age of the fault is suggested as late Pliocene (ca. 1.5 Ma). The observed offsets of river courses along the fault are variable and reported as: 9 km offset of Caru Çayı, 5 km offset of Euraptus river and 1.5 km offset of Maden Çayı.

Sunkar and Karataş (2015) stated that Adıyaman Fault comprises several parallel to sub-parallel fault segments in the area between Palu (Elazığ) and Besni (Adıyaman) where it disappears. The width of the fault zone reaches up to 3 km and it is about 210-km long. The Adıyaman Fault is interpreted as R-shear of the East Anatolian Fault Zone.

The paper by Tatar et al. (2019) documents evidence, based on Synthetic Aperture Radar Interferometry (InSAR) method and detailed field observations made immediately after the earthquake, about surface deformations that has occurred during 2 March 2017 Samsat earthquake ($M_w= 5.5$). There is no surface rupture occurred but surface deformations in the form of local and discontinuous fissures developed in some areas. Samsat Fault, a N40°–50°W-trending right-lateral structure, is interpreted as the major structure that produced this earthquake.

Adıyaman Fault is ~210-km-long active left-lateral strike-slip fault segment trending in ~065°N direction. The fault starts in the area to the northeast of Kahta and runs in WSW direction through south of Adıyaman near Büyükkavaklı village and finally

terminates around Kutluca to the SSE of Besni (Figure 1.10). Major rock types along the Adiyaman Fault include Upper Cretaceous ophiolitic mélange, Middle–Upper Miocene continental clastic rocks, and Plio–Quaternary undifferentiated continental clastic and carbonate rocks (see next section for more details).

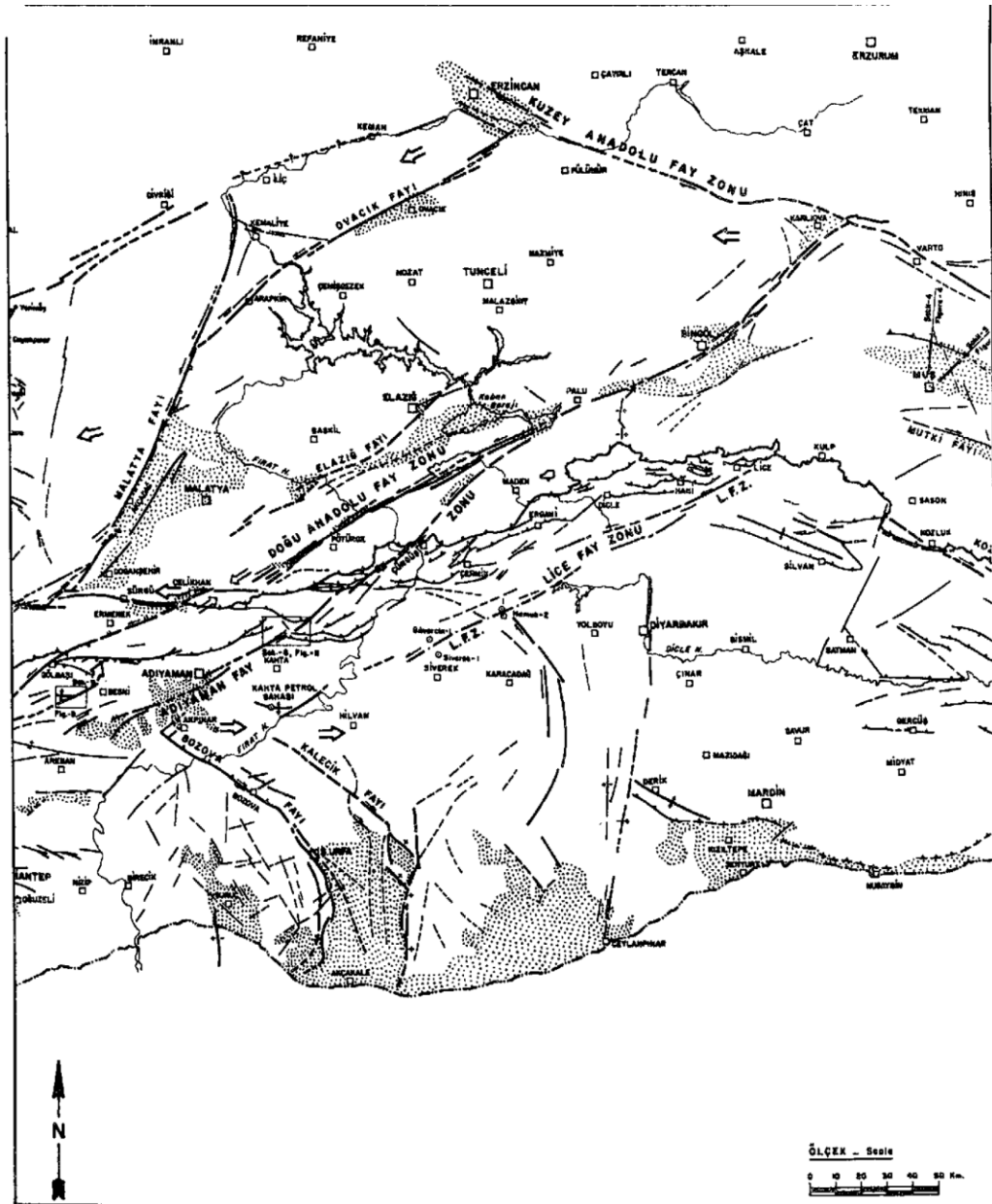


Figure 1.10 Adiyaman Fault and major structural features around Diyarbakır, Erzincan and Şanlıurfa (Perinçek et al., 1987)

In many places along strike, the fault is covered by unconsolidated sandy silty units that make it difficult to follow the fault trace in the field (Figure 1.10). In places, the fault is marked by typical topographic relief (scarps) (Figure 1.11), linear valleys (Figure 1.12), and push-up structures (Figure 1.13). Nevertheless, in areas of younger loose sediments, it is still possible to trace the fault on DEM or shaded relief images (Figure 1.14).

Another well-developed structure in the area is named as Alidağ flower structure (Aksu et al., Durukan, 2014; Aksu and Mülayim, 2015) and it is well reflected in seismic sections (Figures 1.13 and 1.15–1.17; see also Chapter 4 more information). Alidağ is located about 8 km southeast of Adıyaman city. Middle Maastrichtian–upper Paleocene Germav Formation, lower Eocene–lower Oligocene Hoya Formation, and upper Miocene–lower Pliocene Şelmo Formation occur within this positive flower structure; these units are tilted towards northwest up to 40°. Because the Plio–Quaternary Lahti Formation is not affected by the faults, the formation of the flower structure is attributed to the activity of the Adıyaman Fault during late Miocene time (Aksu and Mülayim, 2015).

1.4. Purpose and Scope

Despite of its geological importance, little is known about the Adıyaman Fault (AF) and its tectonic activity. The age of the fault is also poorly constrained; it is suggested that the fault might have been initiated during the Late Miocene to Early Pliocene time interval, at the same time as the EAFZ (Şengör et al., 1985; Dewey et al., 1986; Aksoy et al., 2007; İmamoğlu and Çetin, 2007; İnceöz and Zengin 2014).

The total displacement of the Adıyaman Fault is also poorly documented; the reported offset amounts are variable (between 1.5 km to 9 km) and appear to be contrasting. In particular, there is no offset geological feature/structure to comment on the total displacement of the Adıyaman Fault.

Adıyaman region is generally overlain by loose terrestrial sediments that fill mostly depression areas. These units generally cover the Adıyaman Fault and its second-order

structures; that is why, the Adıyaman Fault is difficult to follow in the study area and occurs mostly as structure buried beneath loose sediments. Since overlying units are loose sediments, it fills the depressions and overburden fault structures. Displacement amount of the Adıyaman Fault can therefore not be realized by fieldwork. There are several seismic sections across the Adıyaman Fault shot by TPAO and this work therefore choose to interpret these sections to address the main issue(s) outline above.

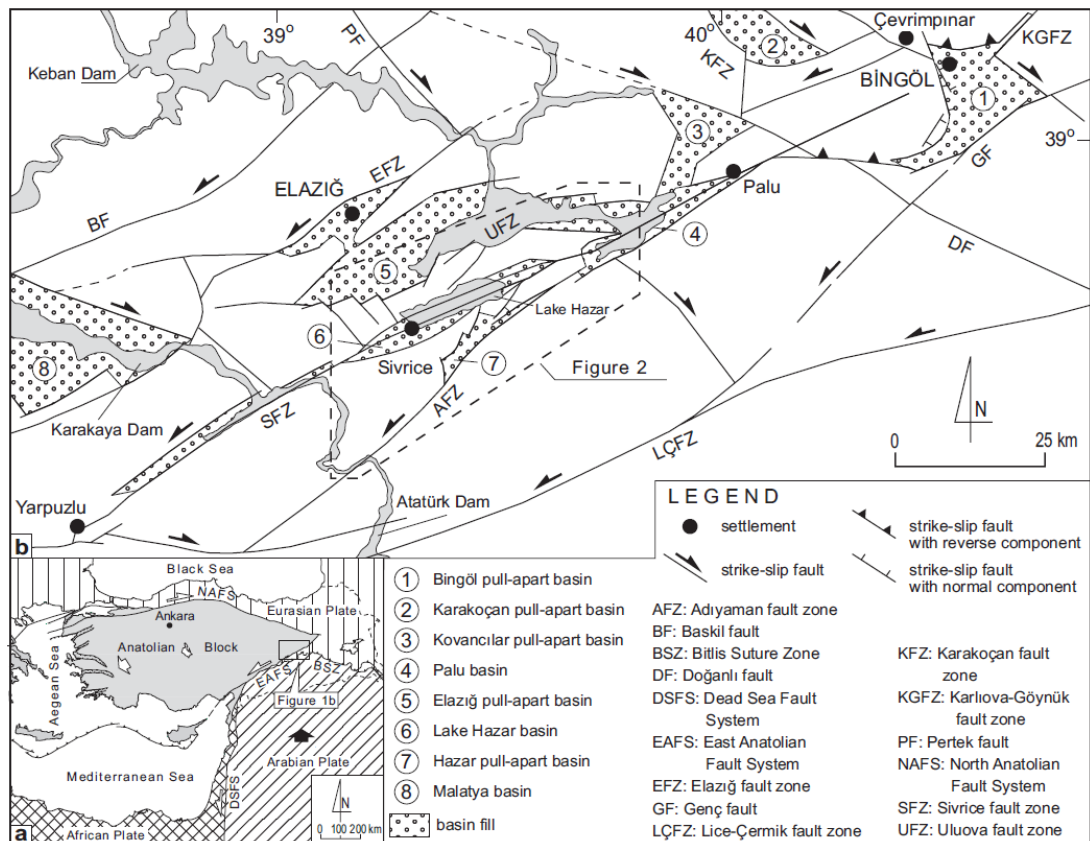
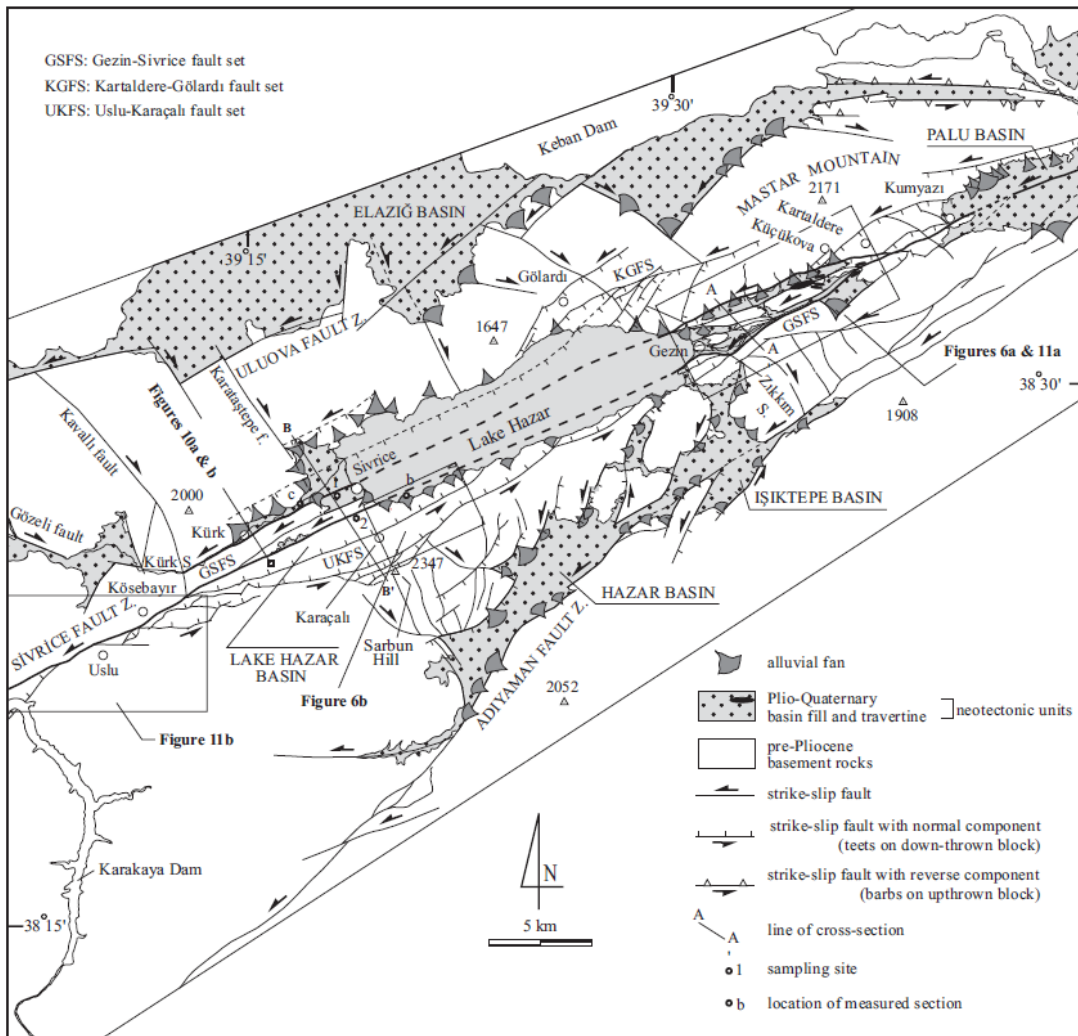


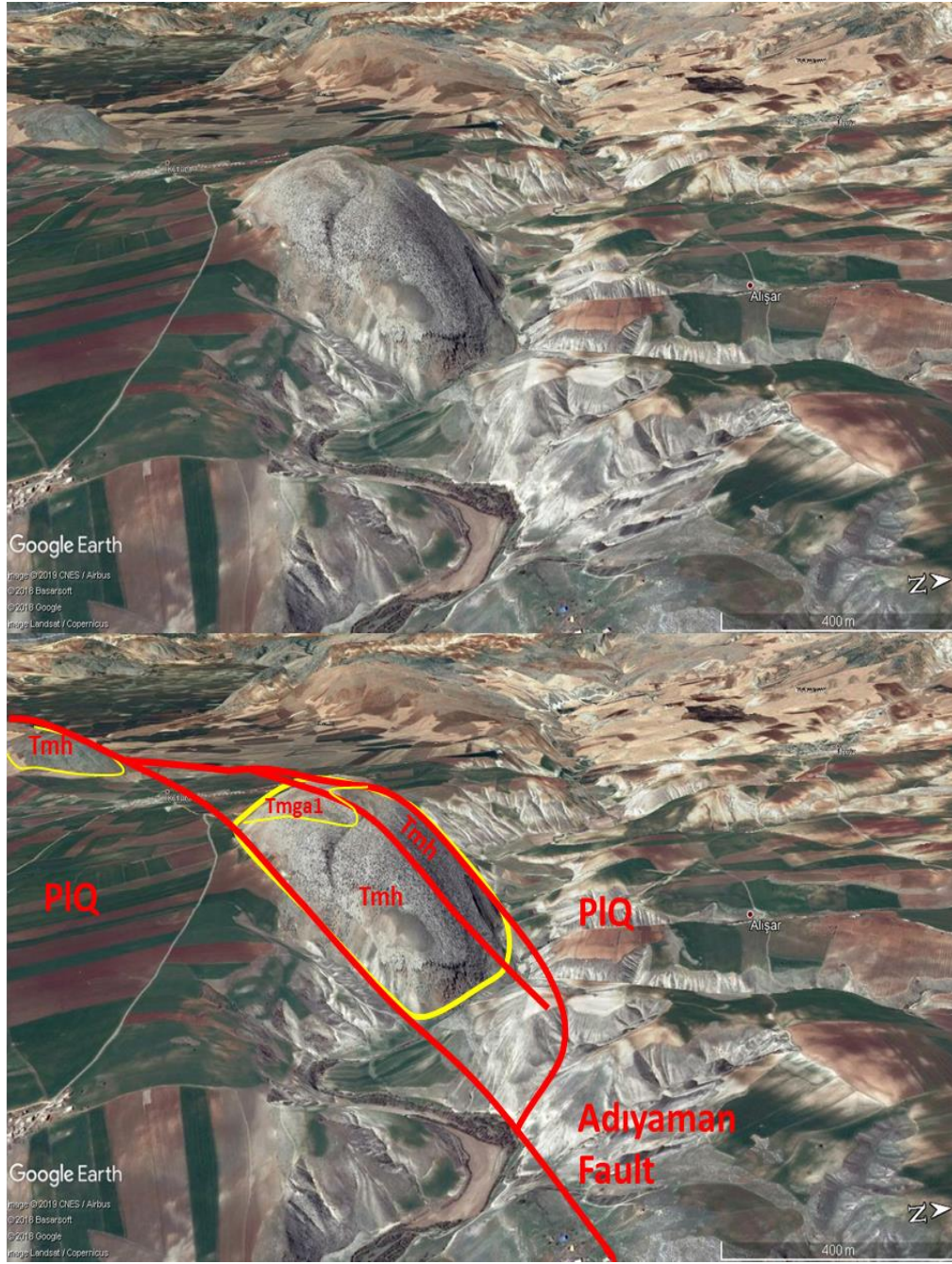
Figure 2 (a) Simplified map showing major plates and their boundary faults in the Eastern Mediterranean region and location of the study area; (b) simplified neotectonic map showing major fault zones and strike-slip basins comprising the East Anatolian Fault System (EAFS) in the Lake Hazar and Bingöl region (from Aksoy et al., 2007).

Preliminary study of the seismic sections in the early stages of this research has shown that the Adıyaman Fault cuts and displaces an unknown (?) fault(s); and this relationship may therefore form firm geological evidence about the offset amount along the Adıyaman Fault.

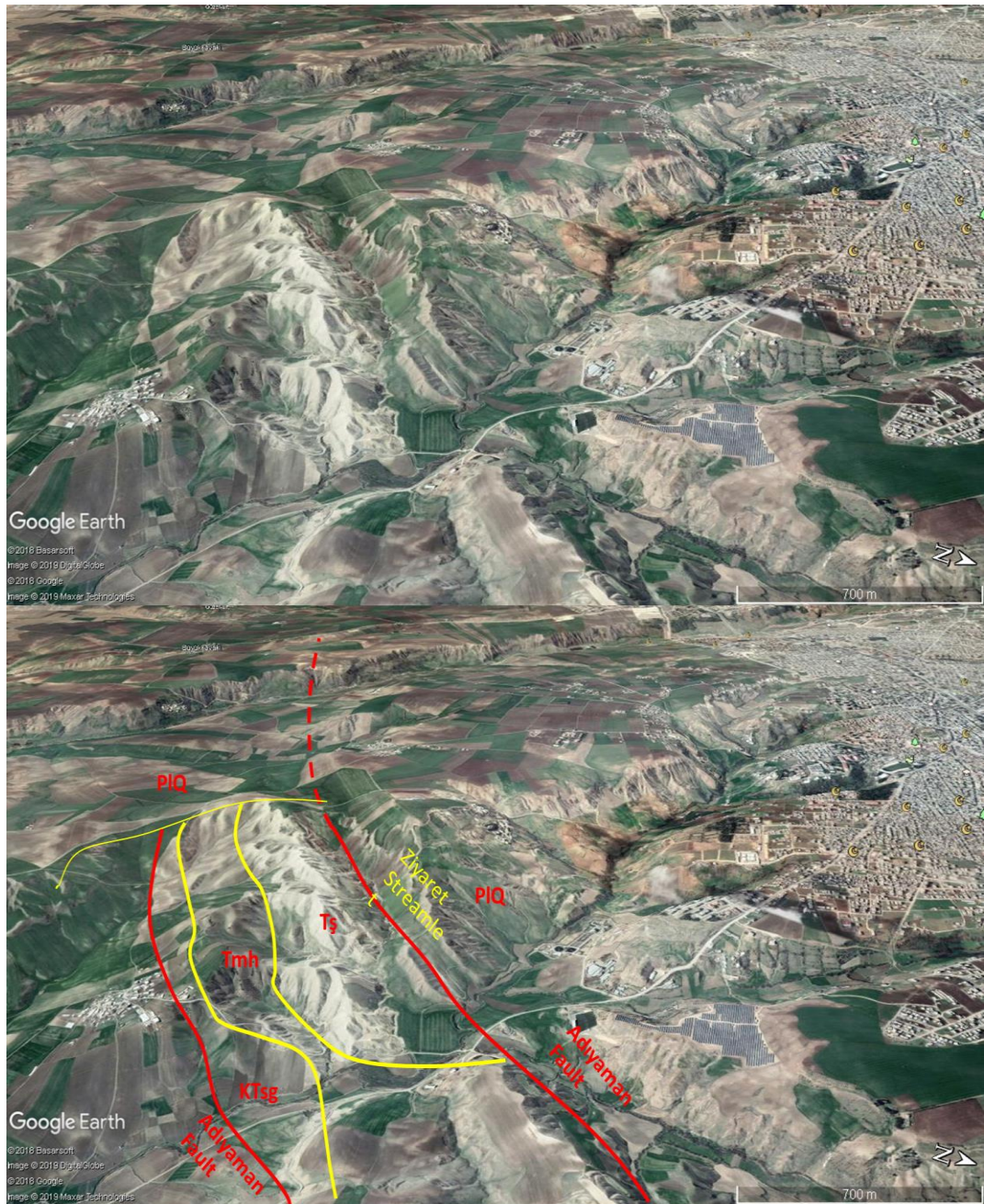


Hikmet Aksoy Neotectonic map of the East Anatolian Fault Zone in the Lake Hazar region, showing several parallel faults in the region (from Aksoy et al., 2007).

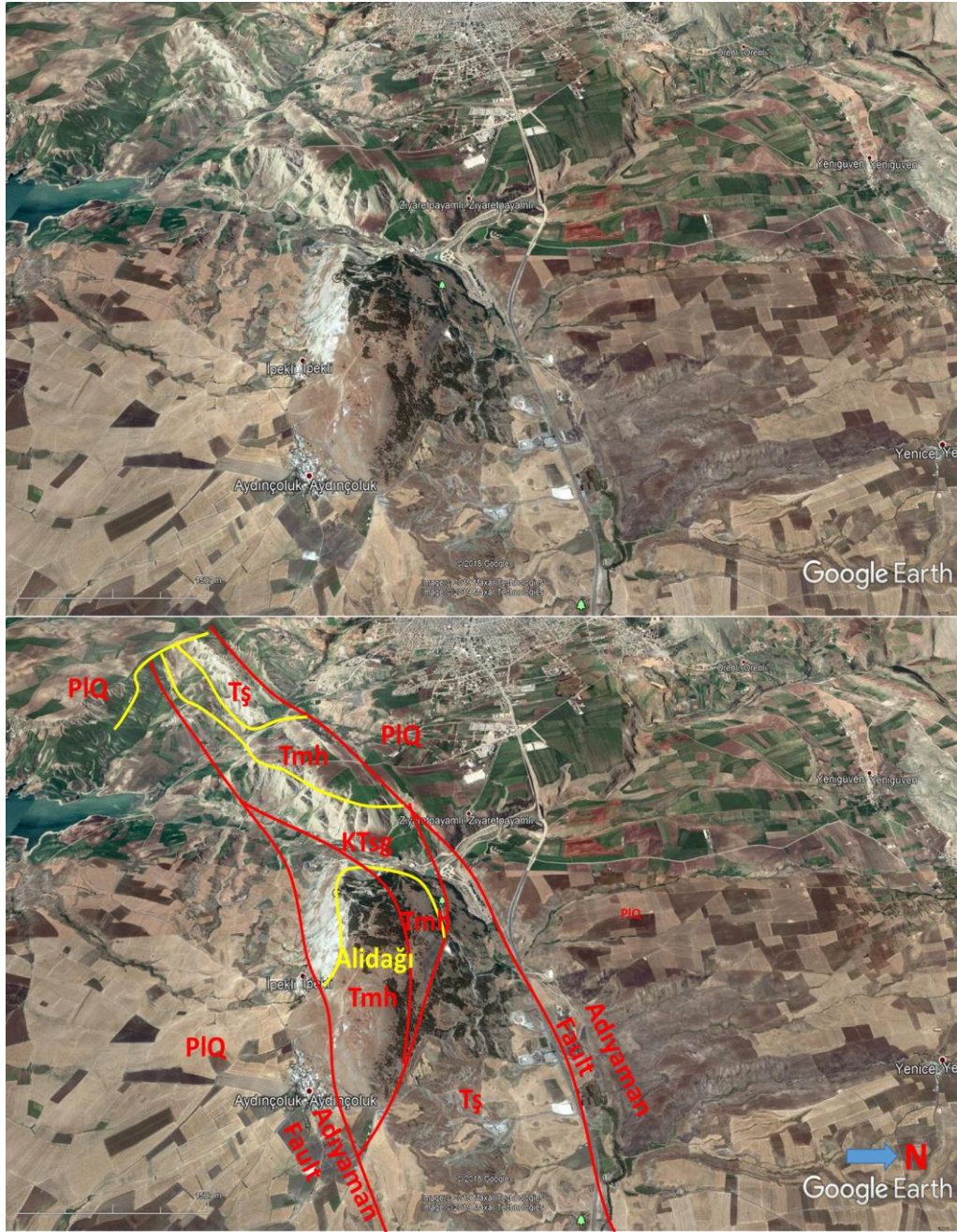
The results of the present study has more regional and economical implications because the Şambayat oil field lies within the Adıyaman Fault area; the recognition of, and amount of displacement along, the Adıyaman Fault therefore becomes crucial as the structure may have important role in the formation of (fractured) reservoir. The determination of total offset may also lead us to trace the location of new oil field(s) in the other block of the Adıyaman Fault. One of the scopes of this study is therefore to obtain evidence that bears on the total displacement amount of the Adıyaman Fault.



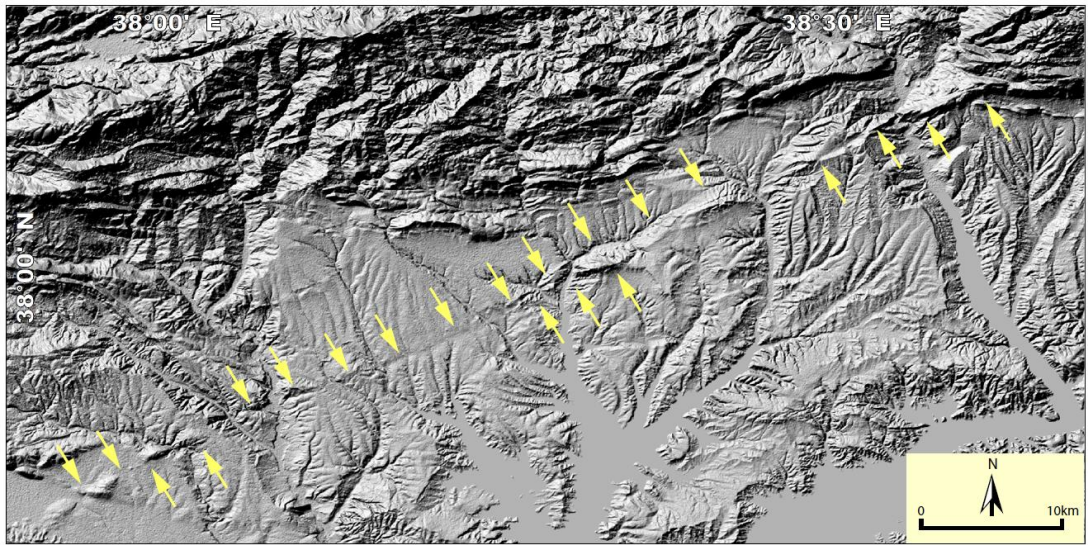
Hli wt g'3030 Google Earth™ image illustrating a well-developed fault scarp at the expense of Hoya Formation limestone to the east of Kutluca village at Faldağı location. Tmh- Hoya Formation (Eocene Limestone), Tş- Şelmo Formation (terrestrial sediments), PIQ- Plio- Quaternary loose sediments.



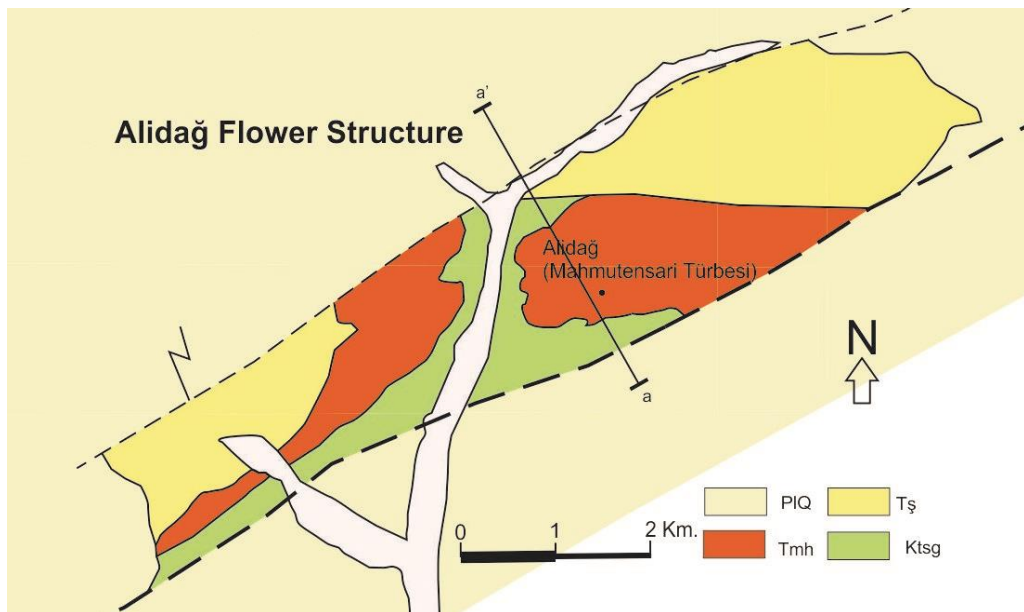
Hki wt g'30840 Google Earth™ image illustrating a well-developed fault valley (Ziyaret riverlet valley), to the south of Adiyaman city. KTsg- Germav Formation (Marl), Tmh- Hoya Formation (Eosen limestone), Tş- Şelmo Formation (terrestrial sediments), PIQ- Quaternary loose sediments.



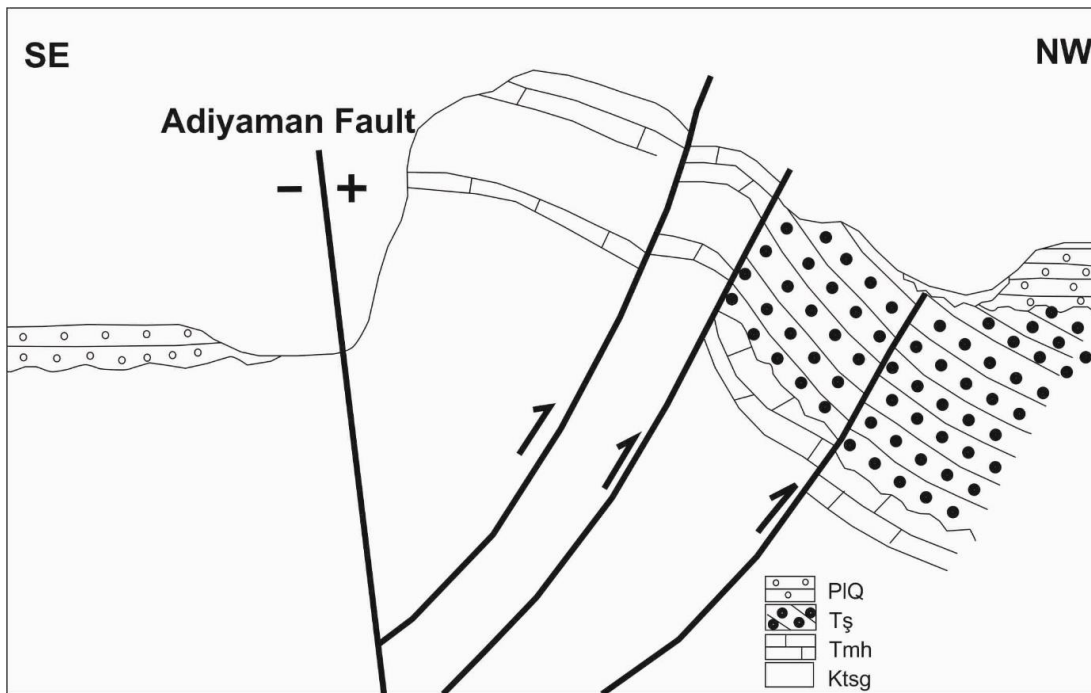
Hki wt g'3050 Google Earth™ image illustrating a well-developed Alıdağı push-up to the south-east of Kutluca village. At the Top of push-up area, Hoya Formation is exposed. Germav Formation occurs at the edge of push-up area. Şelmo Formation covers the Hoya Formation at the south of push-up area. KTsg- Germav Formation (marl), Tmh- Hoya Formation (Eosen limestone), Tş- Şelmo Formation (terrestrial sediments), PIQ- Quaternary loose sediments.



Hki wt g'3Ø60 Shaded relief image showing the trace of the Adıyaman Fault indicated by yellow arrows (from Khalifa et al., 2019).



Hki wt g'3Ø70 Detailed map of the Alıdağ flower structure (from Aksu and Durukan, 2014). The a-a' line shows the location of sketch cross-section in Figure 1.16. Ktsg: Germav Formation, Tmh: Hoya Formation, Tş: Şelmo Formation, and PIQ: Plio-Quaternary sediments."



Hki wt g'30880 Sketch cross-section illustrating the structural elements of the Alidağ positive flower structure (from Aksu and Mülayim, 2015). See Figure 1.15 for location of sketch cross-section (a-a' line). Ktsg- Germav Formation, Tmh- Hoya Formation, Tş- Şelmo Formation, and PIQ- Plio-Quaternary sediments.



Hki wt g'30890A field view from the Alidağı, view from west (from Aksu and Mülayim, 2015)."

Apart from the Adıyaman Fault, the preliminary interpretation of the seismic sections indicate the presence of a unknown NW–SE-trending fault(s) within the study area; this structure is named here as Şambayat Fault zone (ŞFZ) and considered to form one of the major structural elements of the Adıyaman region. It is not mapped previously and will be described during this study. The preliminary data also suggest that the ŞFZ is cut and displaced by the Adıyaman Fault; this may also be used, if well documented, as firm evidence to comment on the total offset amount along the Adıyaman Fault. The present study therefore also aims to provide evidence for the existence and age of the ŞFZ, define and map the structure, and finally investigate its relation to the Adıyaman Fault that may lead us to calculate the total offset of the AF.

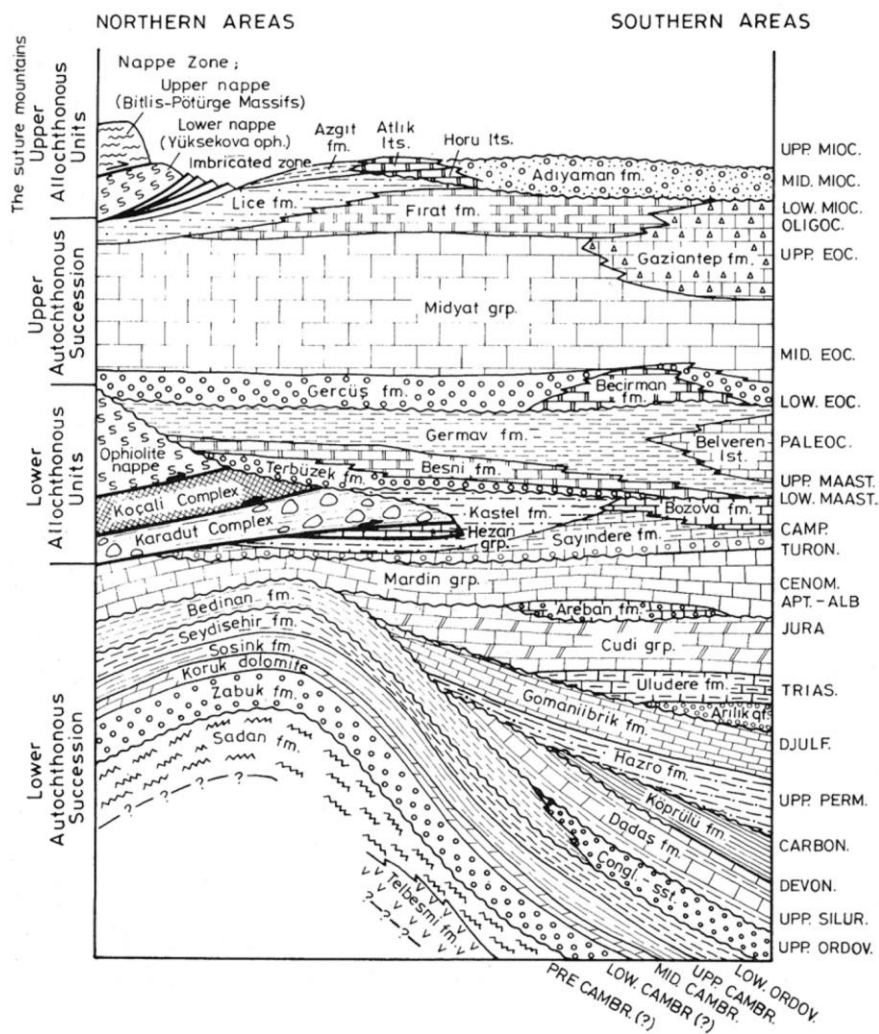
CHAPTER 2

STRATIGRAPHY

2.1. General Stratigraphy

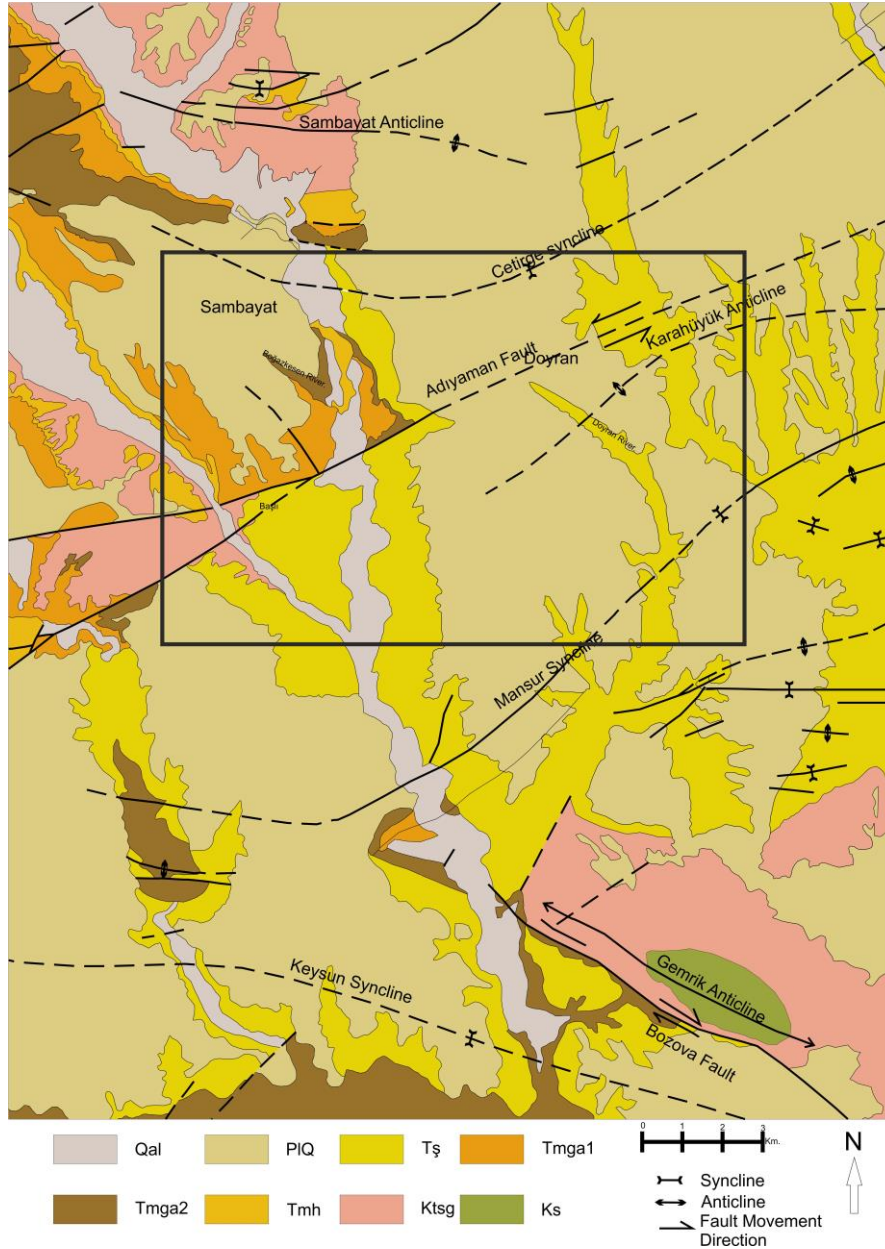
The stratigraphy of the study area and its nearby surroundings is represented by bi-partite rock association: allochthonous and autochthonous units (Figures 1.10, 2.1–2.3). The stratigraphy of the rock units in the Adıyaman region commences with Precambrian and Lower Paleozoic shallow-marine sedimentary rocks (Figures 2.1 and 2.3) deformed during Late Paleozoic orogenesis (e.g., Ketin, 1966; Dean, 1975, 1980; Bozdoğan et al., 1987; Husseini, 1989; and Cater and Tunbridge, 1992; Dean et al., 1997). The Adıyaman region was emergent between the end of the Ordovician and the beginning of the Aptian, and no sediments were deposited during this time interval; Mardin-Kahta uplift (Early Cretaceous) forms the evidence of this time interval. The largely Paleozoic sequence therefore is unconformably overlain by Aptian–early Campanian carbonates (limestones and dolomites) of the Mardin Group, deposited on the southern passive margin (shelf and intrashelf basins) of the Neotethys Ocean (e.g., Horstink, 1971; Sungurlu, 1974; Görür et al., 1987; Uygur and Aydemir, 1988; Çelikdemir et al. 1991; Tardu, 1991). The Mardin Group comprises unconformity-bound thri-partite lithologic association (Figure 2.3): (i) the Areban and Sabunsuyu formations; (ii) the Derdere Formation; and (iii) the Karababa Formation. The Mardin Group is unconformably overlain by anoxic deep-marine organic-rich pelagic limestones of the Adıyaman Group (Karaboğaz and Sayındere formations) as product of regional marine transgression during the Campanian. The carbonate rocks of the Mardin and Adıyaman groups, particularly that of Derdere, Karababa, Karaboğaz and Sayındere formations are considered as the most important source rocks of the Adıyaman oilfields, particularly the Şambayat (Duman and Bozcu, 2019). The southward advance of the nappes/thrust sheets is marked by deposition of sandstone-

shale alternation with olistostromes deposited in the rapidly subsiding Kastel Basin during Campanian to Early Maastrichtian. The regional transgression continued with the deposition of siliciclastics and reefal carbonates of the Terbüzek and Besni formations of the Şırnak Group. Then, the deeper-water basinal conditions have prevailed with the deposition of the clastic and carbonate rocks of the middle Maastrichtian–Paleocene Germav and Sinan formations. The Eocene–Oligocene Midyat Group (Gercüş, Hoya and Gaziantep formations) was deposited in a restricted shallow-marine shelf and slope to relatively deep-marine setting.



Hikmet 4080 General tectono-stratigraphic section of Southeast Anatolia (Yalçın, 1976; Yılmaz, 1993)

The early Miocene is marked by the deposition of Silvan Group (Kapıkaya, Fırat and Lice formations) in a rather fluvial to shallow-marine environment to reefal to submarine fan. The area was emergent as marked by continental deposits of the Şelmo Formation.



*Hki wt g'400*Geology map of study area (Çemen et al., 1991). The rectangle shows location of the study area. Ktsg– Germav Formation; Tmh–Hoya Formation; Tmga2–Gaziantep Formation (marl member); Tmga1– Gaziantep Formation (limestone member); Tş– Şelmo Formation; PIQ– Plio-Quaternary sediments; Qal– Quaternary alluvials.

AGE		ROCK UNITS		LITHOLOGY	THICKNESS (m)	ENVIRONMENT	
		GROUP	FORMATION				
PLIO-QUATERNARY			ALLUVION		50-100		
TERTIARY	MIOCENE	LATE	ŞELMO (T ₉)		200-800	TERRESTRIAL	
		EARLY	SILVAN (Ts)	LİCE (Tt)		300-800	OPEN SHELF SLOPE
				FIRAT (Tf)		100-200	SHALLOW PLATFORM
	OLIGOCENE	MİDYAT (Tm)	GERMİK (T _{mp})		200-1200	CAMPANIAN PLATFORM	
	EOCENE		HOVA (T _h)				
	PALEOCENE	MARDİN (Km)	ŞİRİNAK (K _ş)	GERMİK (T _{mp})		500-1000	DEEP MARINE-SLOPE
			ALT GERMAY (K _{ag})	GERMİK (T _{mp})			
	CRETACEOUS	LATE	MAASTRICHTIAN	ŞİRİNAK (K _ş)	GERMİK (T _{mp})	500-1500	DEEP MARINE-SLOPE
				ŞİRİNAK (K _ş)	GERMİK (T _{mp})		
		CAMPANIAN	MARDİN (Km)	ŞİRİNAK (K _ş)	GERMİK (T _{mp})	500-1500	DEEP MARINE-SLOPE
ŞİRİNAK (K _ş)				GERMİK (T _{mp})			
SANTONIAN CONIACIAN		MARDİN (Km)	ŞİRİNAK (K _ş)	GERMİK (T _{mp})	500-1500	DEEP MARINE-SLOPE	
			ŞİRİNAK (K _ş)	GERMİK (T _{mp})			
TURONIAN		MARDİN (Km)	ŞİRİNAK (K _ş)	GERMİK (T _{mp})	500-1500	DEEP MARINE-SLOPE	
			ŞİRİNAK (K _ş)	GERMİK (T _{mp})			
ALBIAN		MARDİN (Km)	ŞİRİNAK (K _ş)	GERMİK (T _{mp})	500-1500	DEEP MARINE-SLOPE	
			ŞİRİNAK (K _ş)	GERMİK (T _{mp})			
APTIAN	MARDİN (Km)	ŞİRİNAK (K _ş)	GERMİK (T _{mp})	500-1500	DEEP MARINE-SLOPE		
		ŞİRİNAK (K _ş)	GERMİK (T _{mp})				
ORDOVICIAN	HABUR (Oh)	BEDİNAN (Ob)		500-1500	SHALLOW LAGOON		
		SEYDİŞEHİR (Os)		500-1000	SHALLOW/MARINE		
CAMBRIAN	LATE	DERİK (Ed)	SOSİNK (Edso)		100-300	SHALLOW/MARINE	
			KORUK (Edk)		50-200	TIDAL FLAT	
	EARLY	DERİK (Ed)	SADAN (Eds)		200-500	TERRESTRIAL SHALLOW/MARINE	
			TELBEŞMİ (Edt)		500+?	VOLCANIC VOLCANIC	
PRECAMBRIAN		TELBEŞMİ (Edt)		500+?	VOLCANIC VOLCANIC		

Hki wt g'400 Simplified columnar section of the autochthonous rock units in and around the study area (Güven et al., 1991).

Basic characteristics of these rock units will be summarized, based on the available literature and field observations, in the following subsections.

2.2. Allochthonous Units

The allochthonous units are composed of rock units that represent elements of subduction accretionary complexes during the Late Cretaceous closure of the Neotethyan Ocean. They possess distinctive lithological associations as chaotic mixture of many rock types that may locally retain primary features, metamorphosed in places, and contain tectonic slices of oceanic crust. Two rock units, namely Koçali and Karadut complexes occur in the region; they display thrust contact relationships where the former overlies structurally the latter.

2.2.1. Koçali Complex

Koçali Complex is composed of tectonically imbricated slices of radiolarian cherts, cherty limestones, platform carbonates, pelagic limestones, silicified shales, dolomitic limestone, dolomites, ultrabasic rocks, basic volcanics and serpentinites (Sungurlu, 1973; Perinçek, 1979a, b, 1990). It also comprises massive limestone blocks. It was first described and named by Ozan Sungurlu (1973) in the Adıyaman region where three lithological associations are identified: volcanics, sedimentary units and ultrabasics. The alternation of limestones and volcanic rocks is common feature of the complex. The age of the complex, based on the fossil assemblages (radiolarites, benthonic foraminifera and calpionellids) is Late Jura–Early Cretaceous (Sungurlu, 1973; Tuna, 1973). Recently it is claimed, based on the radiolarian content, that the depositional age of the volcano-sedimentary sequences of the Koçali Complex is mainly the Late Triassic (Middle Carnian to Rhaetian) (Uzunçimen et al., 2011). The Koçali Complex is thrust over the Karadut Complex. It is unconformably overlain by younger autochthonous rock units. Ophiolites of the Kocali Complex originate from the Tethyan ocean floor (Şengör and Yılmaz, 1981) and thrust southwards over the

Arabian Shelf in the Late Cretaceous (Perinçek and Özkaya, 1981). The unit is not exposed within the study area but is penetrated as grey, light grey, stiff, clayey, marl at BA-1 and D.B-2 boreholes.

2.2.2. Karadut Complex

Karadut Complex consists of silicified limestones, cherty limestones, siliceous shales, shales, bedded cherts, conglomeratic fossiliferous limestones, conglomerate, turbiditic sandstone, silicified siltstones and marl (Yoldemir 1987). It is first described by geologists of Turkish Gulf Oil in Kevan-1 well as Karadut Formation (1962). Later, Sungurlu (1973) described the unit as Karadut group in the Adiyaman region. The complex terminology is first assigned by Perinçek (1978). The age of the unit, based on fossils from limestones and siltstones, is Cenomanian–Lower Turonian (İmamoğlu, 1993). It is tectonically overlain by the Koçali Complex and/or unconformably by younger autochthonous rock units.

2.3. Autochthonous Units

Autochthonous units are represented by quintet rock association: Precambrian–Paleozoic rock units, Cretaceous rock units, Tertiary rock units and Quaternary alluvials (Figures 2.1–2.3).

2.3.1. Precambrian-Paleozoic Units

There are six formations defined in the Precambrian–Paleozoic successions in southeast Anatolia (Figure 2.3). Among them, only four – Telbesmi, Sadan, Koruk and Sosink formations – are exposed in Tut (Adiyaman) region. The characteristics of these formations are described below.

2.3.1.1. Telbesmi Formation

Vgndguo k'Hqt o cvkqp (Kellogg, 1960) represents the oldest rock unit in the region and forms the basement to the autochthonous succession. It is composed of unfossiliferous clastic sediments that crop out in Tut province. The formation comprises, from bottom to top, black shale, glauconitic sandstone and greywacke, dark green siltstone-shale alternation, red-wine red quartz sandstone-shale alternation; an about 10-m-thick sill lies at the top of the sequence (Ketin, 1966; Dean et al., 1997). The base of the unit is not exposed. It is unconformably overlain by the coarse-grained quartz sandstone and pebbly sandstones of the Sadan Formation. The unit is initially named as Meryemüşağı Formation (Ketin 1966), and is correlated with the Telbesmi Formation (Kellogg 1960) or Derik Formation (Schmidt, 1965) exposed in the Derik province. The age of the unit is accepted as Precambrian–early Cambrian (Ketin, 1966; Dean et al., 1997).

2.3.1.2. Sadan Formation

Ufcp"Hqt o cvkqp, red or purple siliciclastic unit, is described in the Derik region (Schmidt 1965), then defined in the Tut (Adiyaman) province as Kaplandere Formation (Ketin 1966). It is represented by a quartzite–sandstone sequence of cross-bedded conglomerate and sandstone; there is a diabase sill (?), 25-m-thick, at the top of the formation. The different lithologies include quartzite-shale alternation, red-purple thick- and cross-bedded, pebbly sandstone-quartzite alternation, and thin-bedded quartzitic sandstone. The formation overlies the Telbesmi Formation with angular unconformity and is overlain conformably by dolomites of the Koruk Formation (Dean et al., 1997). The age of the formation is accepted as late Early Cambrian although there is no fossils reported (Dean et al., 1997).

2.3.1.3. Koruk Formation

Mqtwm'Hqt o cvkqp, a limestone/dolomite unit, was introduced by Schmidt (1965) in Derik area and is named as '*f qnqo kg''hqt o cvkqp*' in Tut area (Ketin 1966). It is represented by a carbonate sequence in-between conformable quartzites of the Sadan Formation and siltstone-shale alternation of the overlying Sosink Formation. It consists of thick–medium-bedded grey dolomite with stromatolites, red nodular limestone, and red shale with silty mudstone intercalations. According to the trilobite fragments and macrofossils, the age of the formation is assigned as Middle Cambrian.

2.3.1.4. Sosink Formation

Uqkpm'Hqt o cvkqp, siltstone–sandstone succession, was described by Kellogg (1960) in the Sosink area, near Derik. The unit is named as Yerlikaç Formation in Tut area (Ketin, 1966). The formation is composed, from bottom to the top, of grey silty shales, grey mudstone with thin beds of limestone, light brown thin-bedded siltstone and shale alternation with thin limestone interbeds, medium–thick-bedded sandstone and cross-bedded quartzites (Monod and Dean, 1980; Bozdoğan, 1982; Ketin, 1966; Dean et al., 1997). Light brown weathering is characteristic. The age of the unit, based on fossil assemblages, is late Cambrian (Dean et al., 1997). The unit overlies conformably the Koruk dolomites and is overlain unconformably by upper Cretaceous Areban Formation. It is not exposed in the study area but is penetrated in D.B-2 and D.B-1 wells where medium- to coarse-grained, medium sorted, pinkish sandstone with semi-rounded quartz grains represents the formation.

2.3.2. Cretaceous Rock Units

The Cretaceous rocks unconformably overlie the Paleozoic rocks of the Adıyaman region that commences with pebbly sandstones of the Areban Formation. Different lithological associations are described in three groups (Mardin, Adıyaman and Şırnak)

and they display either lateral-vertical passages and/or display unconformable relationships (Figures 2.1–2.3). Several formations are described in each group; basic characteristics of these units, based on personal field observations and available literature, will be described in detail below.

2.3.2.1. Mardin Group

Mardin Group (Schmidt, 1961), a transgressive succession of mostly shallow-marine clastic and carbonate rocks rich in organic matter, consists of sandstone, shale, limestone, dolomite and marl that were deposited in beach to shallow sea to shelf and intrashelf basins (even reefal environments) along the northern passive margin of the Arabian Plate (Schmidt, 1961; Horstink, 1971; Tuna, 1973; Sungurlu, 1972; Erenler 1989; Çelikdemir and Dülger, 1990; Duran and Araş 1990; Çoruh, 1991; Duran, 1991; Araç and Yılmaz, 1991; Çelikdemir et al., 1987, 1991; Uygur and Aydemir, 1988; Perinçek et al., 1991; Demirel and Güneri, 2000; Sonel et al., 2002). The group comprises four distinct formations; these, from the oldest to the youngest, are Areban, Sabunsuyu, Derdere and Karababa formations (Figure 2.1). The age of the formation is Aptian–early Santonian–(?)early Campanian (Erenler, 1989; Çoruh, 1991).

2.3.2.1.1. Areban Formation

Areban Formation is named by Schmidt (1961). It represents the basal clastics of the Mardin group. The unit is composed of mostly sandstone and brownish-yellowish sandstone, siltstone, marl, shale and sandstone-marl alteration. It was deposited in beach-shallow sea (restricted lagoonal to tidal-flat) environment. The age of the formation is assigned as Aptian (Tuna, 1974; Sinanoğlu and Erkmen, 1980; Erenler, 1989). The formation is not exposed in the study area. It is penetrated in D.B-1 and D.B-2 wells; the Areban Formation is represented by fine- to coarse-grained, poorly sorted, yellowish sandstone, with semi-rounded quartz grains and dolomite cement.

2.3.2.1.2. Sabunsuyu Formation

Areban Formation is conformably overlain by the carbonates of the Sabunsuyu Formation. The unit is named by Wilson and Krummenacher (1959). It is composed of shallow-sea dark thin-bedded (laminated in upper levels) grey dolomites, dolomitic limestone-marl alternation and grey limestones with shell fragments and cherts in places; this lithological association is ascribed to a restricted to semi-restricted shallow-marine and tidal-flat to subtidal carbonate platform deposit (Perinçek et al., 1991). The age of the formation, based on fossil assemblages, is Albian–Cenomanian (Köylüoğlu, 1986; Erenler, 1989). The formation is not exposed in the study area. It is penetrated in D.B-1 and D.B-2 wells; the Sabunsuyu Formation is represented by grey-white-brownish grey-dark grey micro-crystalline dolomitic limestone.

2.3.2.1.3. Derdere Formation

Derdere Formation is named by Handfield et al. (1959) and comprises three members as thick-bedded, cream-red-light brown microcrystalline dolomites in lower levels, dolomitic limestones in the middle and creamy-grey-red-brown clayey bioclastic massive limestones (locally with cherts) in the upper horizons (Mülayim et al., 2016). Carbonate mudstone and fossiliferous mudstone occur in the uppermost levels. These organic-rich carbonates are deposited in deep marine environment which was later shallowing to a lagoonal to tidal-flat setting (Erdoğan, 1975; Perinçek, 1979, 1980, 1989, 1990; Aksu, 1980; Pasin et al., 1982; Güven et al., 1988; Perinçek et al., 1991; Sonel et al., 2002). The formation unconformably overlies the underlying Sabunsuyu Formation whereas the Karababa Formation is unconformable above. The age of the unit, based on fossil assemblage, is Cenomanian–Turonian (Erenler, 1989; Çoruh, 1992; Ertuğ, 1991; Sonel et al., 2002). The formation is not exposed in the study area. It is penetrated in B-2, BA-1, D.B-1 and D.B-2 wells; the Derdere Formation is represented by white-creamy white-beige micro-crystalline dolomitic limestone.

2.3.2.1.4. Karababa Formation

Karababa Formation forms the youngest unit of the Mardin Group and overlies unconformably the Derdere Formation. It is named by Gossage (1956) and is composed of fossil-bearing and organic-rich limestones and dolomites. The formation also contains quartz, glauconite, phosphate, pyrite and chert nodules. These carbonates are deposited in shallow-marine and restricted to semi-restricted lagoonal conditions (Çelikdemir et al., 1991; Sonel et al., 2002). It overlies unconformably the Derdere Formation and is unconformably overlain by the Karaboğaz and Sayındere formations. The formation is divided into three members: (i) Karababa A is composed dark brown phosphatic, organic matter-rich fossiliferous microcrystalline limestones (with chert nodules) deposited in restricted shelf lagoon and shelf environment; (ii) Karababa B consists of creamy beige-grey-brownish cherty fossiliferous limestones and black cherts, deposited in a shallow-sea environment to intrashelf basins or depressions and (iii) Karababa C is represented by shallow-marine creamy beige bioclastic limestones and partly dolomites (Perinçek, 1980; Çoruh, 1983; Wagner and Pehlivanlı, 1985; Şengündüz and Aras, 1986; Erenler, 1989; Çelikdemir and Dülger, 1990; Duran, 1991; Araç and Yılmaz, 1991; Çelikdemir et al., 1991; Sonel et al., 2002; Mülayim et al., 2016). Late Coniacian–Santonian age is, based on fossil assemblages, assigned to the formation (Erenler, 1989; Çoruh, 1991). The formation is not exposed in the study area. It is penetrated in B-2, BA-1, D.B-1 and D.B-2 wells; the Karababa Formation is represented by white-creamy white limestones and very hard light to dark brown smoky chert.

2.3.2.2. Adıyaman Group

Adıyaman Group (Gossage, 1956) consists of Campanian carbonates deposited in a deep-shallow marine environment (Çoruh, 1991; Güven et al., 1991; Perinçek and Çemen, 1991). The group is named by Gossage (1956). The group is represented by a conformable sequence of four distinct formations; these are, from bottom to the top,

middle Campanian Karaboğaz Formation, middle Campanian Ortabağ Formation, upper Campanian Sayındere Formation and upper Campanian–early Maastrichtian Beloka Formation (Figures 2.1 – 2.4). Among these formations, Karaboğaz and Sayındere formations are exposed in the study area. The unit displays conformable relationships with the underlying Karababa Formation and overlying Şırnak Group.

2.3.2.2.1. Karaboğaz Formation

Karaboğaz Formation is named by Fournier (1958) and Handfield et al. (1959) to describe organic-rich pelagic carbonates with phosphate and glauconite nodules. The unit is composed of thin–thick bedded, organic matter-rich, grey-dark grey-dark beige coloured, fossiliferous microcrystalline clayey limestones with chert intercalations, nodules and lenses; glauconite and phosphate nodules are also reported (Turner, 1958; Handfield et al., 1959; Braynt, 1960; Tuna, 1973; Sungurlu, 1973; Soytürk and Erdoğan, 1974; Erdoğan, 1975; Günay, 1984; Dellaloğlu and Pasin, 1984; Görür et al., 1987; Güven et al., 1988, 1991). It passes upward into the Sayındere Formation. The formation is interpreted as one of the source rock for hydrocarbon around Adıyaman region. An anoxic deep-marine environment to platform shelf environment is suggested for the Formation (Şengündüz and Aras, 1986; Görür et al., 1987; Wagner and Tuna, 1988; Uygur and Aydemir, 1988; Duran, 1991; Güven et al., 1991; Duran, 1991; Sayılı and Duran, 1994). The age of the formation, based on planktonic and benthic foraminifer assemblages, is assigned as Middle Campanian (Tuna, 1973; Güven et al., 1991; Çoruh, 1991; Ertuğ, 1991). The formation is not exposed in the study area. It is penetrated in B-2, BA-1, D.B-1 and D.B-2 wells; the Karaboğaz Formation is represented by beige-dark beige-brownish beige-dark brown coloured clayey limestone with dark brown to smoky black brown chert bands and nodules.

2.3.2.2. Sayındere Formation

Sayındere Formation is named by Gossage (1959) to describe thin-medium bedded, clayey limestone. The limestones are dirty yellow-grey-dark-grey-bluish grey-creamy beige coloured, thin to medium bedded, glauconitic-phosphatic-cherty, fossiliferous and micritic (Gossage, 1959; Ketin, 1964; Tuna, 1973; Sungurlu, 1973, 1974; Ahmed, 1975; Proctor and Özkaya, 1975; Özkaya, 1978; Perinçek, 1979, 1980, 1989, 1990; Perinçek and Özkaya, 1981; Dellaoğlu and Pasin, 1984; Günay, 1984; Günay ve Sarıdaş, 1984; Sarıdaş, 1987; Demirkol, 1988; Güven et al., 1988, 1991; Önalın, 1989-1990; Çoruh, 1991). A deep marine environment is suggested for the deposition (Güven et al., 1991). The age of the formation, based on planktonic and benthic foraminifer assemblages, is assigned as late Campanian (Çoruh, 1991; Güven et al., 1991). The formation is not exposed in the study area. It is penetrated in B-2, BA-1, D.B-1 and D.B-2 wells; the Sayındere Formation is represented by beige-dark beige-creamy white, microcrystalline limestone.

2.3.2.3. Şırnak Group

The upper Campanian–Paleocene continental to marine sediments exposed in Şırnak area is named as Şırnak Group (Perinçek et al., 1991). The terminology was first used by Tromp (1940). The group is represented by a sequence of several formations; these are, from bottom to the top, Kastel, Bozova, Kıradağ, Terbüzek, Besni, Haydarlı, Garzan, Germav, Üçkiraz, Sinan, Antak, Kayaköy, Belveren and Becirman formations (Figures 2.1 – 2.4) (Çoruh, 1991; Güven et al., 1991; Perinçek et al., 1991). Among these formations, Kastel, Terbüzek, Besni, Germav and Sinan formations are exposed in the study area.

2.3.2.3.1. Kastel Formation

Kastel Formation is the oldest unit of the Şırnak Group and is named by Tuna (1973). It commences with marls, grades into sandstone-shale alternation, and ends with shale-marl alternation. It shows gradation contact relationship with the underlying Sayındere and overlying Terbüzek formations; allochthonous units structurally overlie the formation (Ketin, 1964; Tuna, 1973; Sungurlu, 1973, 1974; Erdoğan, 1975; Yalçın, 1978; Baştuğ, 1980; Perinçek and Özkaya, 1981; Günay, 1984; Thomas et al., 1986; Yoldemir, 1987; Güven et al., 1988, 1991; Perinçek, 1989, 1990; Önalın, 1989-1990; Günay, 1990). The formation represents clastic sedimentation in the rapidly-subsiding relatively narrow depression (Kastel Basin) developing in front of the southward advancing nappes during Campanian to Early Maastrichtian time interval and it is therefore composed of debris (sandstones and shales, together with olistostromal materials) derived from allochthonous units (Rigo de Righi and Cortesini, 1964; Sungurlu, 1974; Perinçek, 1979; Ala and Moss, 1979). The formation is interpreted to deposit in a continental shelf to deep marine environment (Güven et al., 1991). The age of the formation, based on planktonic foraminifer assemblages, is assigned as is late Campanian–middle Maastrichtian (Çoruh, 1991; Güven et al., 1991). The formation is not exposed in the study area. It is penetrated in B-2, BA-1, D.B-1 and D.B-2 wells; the Kastel Formation is represented by variably coloured, fine- to coarse-grained, poorly sorted, poorly carbonate cemented polygenic sandstone, light brown-brown-brownish grey shale and light grey-light brownish grey marn.

2.3.2.3.2. Terbüzek Formation

Terbüzek Formation is named by Bryant (1960) to describe siliciclastic rocks (conglomerate, sandstone and siltstone) exposed in the Adıyaman area. It commences unconformably above the allochthonous units (Koçali veya Karadut complexes) and represents a polygenetic basal conglomerate (Sungurlu, 1974; Perinçek, 1979; Günay,

1984; Meriç et al., 1987; Güven et al., 1988; Çoruh, 1991; Sarıdaş, 1991; Özer, 1992). It displays concordant relationships with the underlying Kastel and overlying Germav formations (Günay, 1984; Meriç et al., 1987; Güven et al., 1988; Sarıdaş, 1991; Özer, 1992). Whereas Besni Formation is unconformable with the underlying Terbüzek Formation. The main lithology of the formation is red-claret red-grey-yellow coloured, poorly sorted, very thick-bedded to massive, large-scale cross-bedded polygenetic conglomerates; they are locally lense-shaped or display wedge-shaped geometries. The semi-rounded to semi-angular fragments are mostly derived from the allochthonous Koçali veya Karadut complexes. Turbiditic sandstone and limy shales occur as intercalations (Tuna, 1973; Sungurlu, 1973, 1974; Yaçın 1977, 1978; Perinçek, 1979; Günay, 1984; Günay and Sarıdaş, 1984; Meriç et al., 1985; Thomas et al., 1986; Güven et al., 1988, 1991; Çoruh, 1991; Sarıdaş, 1991). The depositional environment is suggested as alluvial fan, fluvial and flood plain (Güven et al., 1991). Age of the formation is, based on the stratigraphic position, is early–middle Maastrichtian (Güven et al., 1991). In the study area, the formation is represented by red-claret red-grey-yellow-greenish grey-yellowish brown, poorly sorted, semi-rounded to rounded, thick-bedded to massive and cross-bedded polygenic (source is generally allochthonous units) channel-fill conglomerates (Tuna 1973, Sungurlu 1973, Yalçın, 1977). The unit is not penetrated in the boreholes.

2.3.2.3.3. Besni Formation

Besni Formation is named by Periam and Krummennacher (1958) to describe fossiliferous reefal limestones. The Formation displays sharp conformable contact relationships with the overlying Germav and gradational contact with the underlying Terbüzek formations. Where exposed, the formation unconformably overlies the Koçali and Karadut complexes. In places, it displays unconformable relationship with the Kastel Formation. The formation commences with yellow coloured, altered sandstones and beige coloured sandy-pebbly (ophiolitic clasts) limestones, continues with grey-yellow-dirty white medium-thick bedded fossiliferous (larger benthic

foraminifers –Loftusia, mollusks, ruddists, algea, corals and shell fragments) limestones (Bolgi, 1964; İlker, 1972; Tuna, 1973; Sungurlu, 1973, 1974; Erdoğan, 1975; Meriç, 1978; Yalçın, 1978; Perinçek, 1979; Günay, 1984; Meriç et al., 1987; Güven et al., 1988, 1991; Çoruh, 1991; Sarıdaş, 1991; Özer, 1992). The depositional environment is suggested as shallow marine (Bryant, 1960; Güven et al., 1988, 1991). Age of the formation is, based on the fossil content, is middle–late Maastrichtian (Bryant, 1960; Saltık ve Saka 1971; Tuna 1973; Güven et al., 1988, 1991). In the study area, the formation is represented by dirty creamy-grey coloured, thick-bedded karstic fossiliferous limestones (Güven et al., 1988). The unit is not penetrated in the boreholes.

The siliciclastics and reefal carbonates of the Terbüzek and Besni formations are considered to deposit during the late Maastrichtian regional transgression.

2.3.2.3.4. Germav Formation

Germav Formation is named by Maxson (1936) to describe a clastic sequence of shale, siltstone, sandstone, and marls. The unit overlies the Besni Formation conformably and is unconformably overlain by the Belveren, Fırat and Becirman formations whereas it displays conformable contact relationships with the Midyat Group (Gercüş and Hoya formations) (Altınlı, 1952; Türküenal, 1955; Badgley, 1957; Bolgi and Sezgin, 1960; Bolgi, 1961; Tolun et al., 1962; Tuna, 1973; Yalçın, 1978; Perinçek, 1979, 1990; Açıkbash et al., 1981; Günay, 1984; Meriç et al., 1987; Yoldemir, 1987; Güven et al., 1988; Duran et al., 1989; Çoruh, 1991). The formation commences with alternation of greenish grey-beige-dark grey silty marl, dark grey-greenish siltstone, greenish grey-brownish sandstone and creamy beige marl. The unit continues with greenish shale-dark grey shale with sandstone intercalations, beige grey-greenish sandstone and greenish grey siltstone, and ends with creamy marls. The depositional environment is suggested as deeper sea and abyssal fan (Güven et al., 1991). Age of the formation is, based on the fossil content (benthic foraminifers), is middle

Maastrichtian–late Paleocene (Güven et al., 1991; Çoruh, 1991). In the study area, the formation is represented by dark grey-blueish grey-brownish dark grey coloured shale and marl alteration). It is also penetrated in BA-1 and D.B-2 wells; the formation is composed of grey-light grey clayey marl (Güven et al., 1988).

2.3.2.3.5. Sinan Formation

Sinan Formation is named by Blakslée et al. (1960) to describe a carbonate sequence of limestone, dolomitic limestone and dolomite. It is divided into two members as lower Sinan of late Maastrichtian age and upper Sinan of early–middle Paleocene age. Lower Sinan member commences with clayey limestones, continues with dolomites and limestones, and ends with bioclastic limestones; it is deposited in a shallow-marine platform. Upper Sinan member is composed mainly of bioclastic limestones, dolomitized limestones and dolomites with rare gypsum, marl and shale. The unit is deposited in a terrestrial, tidal flat, shelf lagoon, semi-restricted shelf and shallow carbonate platform environment (Meriç, 1978; Güven et al., 1991).

2.3.3. Paleogene Rock Units

2.3.3.1. Midyat Group

Midyat Group is named by Maxson (1936) to describe Eocene–Oligocene carbonates exposed in Mardin area. The stratigraphy of the group is described by Açıkbash et al. (1979) where it is represented by a sequence of several formations; these are, from bottom to the top, Gercüş, Kavalköy, Hoya, Gaziantep, Havillati and Germik formations (Figures 2.1–2.3) (Açıkbash et al., 1979; Duran et al., 1988, 1989; Yılmaz and Duran, 1997). Among these formations, Gercüş, Hoya and Gaziantep formations are exposed in and around the study area. The group is deposited in a fluvial, alluvial fan, shallow marine, shelf and deep marine environments during Eocene–Oligocene time interval (Duran et al., 1988, 1989)

2.3.3.1.1. Gercüş Formation

Gercüş Formation is named by Maxson (1936); it is described as the basal clastic sediments of the Midyat Group in the Southeastern Turkey (Aksu et al., 2014). The formation unconformably overlies the allochthonous units and Şırnak Group (Besni, Germav and Sinan formations) while it is unconformable with the overlying Hoya Formation (Altınlı, 1952; Türkünel, 1955; Bolgi and Sezgin, 1960; Bolgi and Kırathioğlu, 1962; Sungurlu, 1973; Perinçek, 1979; Açıkbash et al., 1981; Günay, 1984; Yoldemir, 1985, 1987; Duran et al., 1988, 1989; Güven et al., 1988; Pasin, 1989; Sarıdaş, 1991). The formation is easy to recognize in the field with its characteristic color and physical properties. It comprises conglomerate, sandstone, siltstone, marl, shale, clayey limestone and limestone (Tolun, 1948, 1954; Altınlı, 1952; Badgley, 1957; Bolgi and Sezgin, 1960; Bolgi, 1961; Tolun et al., 1962; Bolgi and Kırathioğlu, 1962; Kırathioğlu, 1964; Önem, 1967, 1968; Akarsu, 1968; Dağdelen, 1970; İlker, 1972; Sungurlu, 1973; Yalçın, 1978; Açıkbash et al., 1981; Günay, 1984, 1986; Thomas et al., 1986; Güven et al., 1988, 1991; Duran et al., 1988, 1989; Pasin, 1989; Sarıdaş, 1991). The depositional environment is interpreted as lacustrine, lagoon, fluvial, flood plain, braided river and alluvial fan (Güven et al., 1991). Age of the formation is, based on the fossil content, early Eocene (Duran et al., 1988; İmamoğlu 1993).

2.3.3.1.2. Hoya Formation

Hoya Formation is named by Perinçek (1978) to describe a thin–thick bedded to massive carbonate unit. It conformably overlies the Germav Formation and is unconformably overlain by reefal limestones of the Fırat Formation. It is mainly composed of limestones and dolomites that shows a weak to well-developed reservoir characteristics (Bolgi, 1961; Tuna, 1973; Sungurlu, 1973, 1974; Açıkbash and Baştuğ, 1975; Perinçek, 1979, 1981, 1989, 1990; Açıkbash et al., 1981; Yılmaz, 1982; Görür and Akkök, 1982, 1984; Günay, 1984; Amoco, 1985; Yoldemir, 1985, 1987; Duran et

al., 1988, 1989; Sarıdaş, 1991). The formation display conformable relationship with the underlying Gercüş Formation while it is unconformably overlain by Kapıkaya and Fırat formations (of the Silvan Group). The depositional environment is suggested as restricted shallow-marine shelf (Duran et al., 1988, 1989). Age of the formation is, based on the fossil content (benthic and planktonic foraminifers), is early Eocene–early Oligocene (Duran et al., 1988, 1989). It is also penetrated in BALABAN-1 well.

2.3.3.1.3. Gaziantep Formation

Gaziantep Formation is named by Kreusert et al. (1958); it is composed of mainly white carbonates. The formation mostly forms a soft topography of clayey limestone, and chalky limestones. At different horizons, grey-beige-yellowish grey colored, thick–medium-bedded, locally very thick-bedded, fossiliferous (mostly benthic, occasionally algae and corals) microcrystalline limestones also occur as characteristic lithology. Clayey limestones are whitish-grey-cream-dirty yellow colored, thin–medium bedded and contain rare chert nodules. It conformably overlies the Hoya Formation whereas Fırat Formation lies unconformably (angular unconformity) above. The clayey limestones and chalky limestones were deposited in slope to relatively deep-marine environment, limestones to turbulent shallow water and reefal environments (Duran et al., 1989). It is late Eocene (Priabonian) – late Oligocene (Chattian) (Duran et al., 1989; Terlemez et al., 1997)

2.3.3.2. Silvan Group

Silvan Group is first named by Duran et al. (1988) and comprises three formations, Kapıkaya, Fırat and Lice formations. These formations are interpreted as syn-tectonic with respect to the Miocene (Aquitainian–Burdigalian) tectonics in the region. Since Miocene nappes are far away from the study area, the rock units of the group are not exposed in and around the study area.

2.3.3.2.1. Kapıkaya Formation

Kapıkaya Formation is named by Perinçek (1980); it is composed of conglomerate, shale, siltstone, sandstone and evaporites. Reddish-brownish and grey conglomerate-sandstone alternation and siltstone-mudstone alternation form the most dominant lithological associations. Also, typically white evaporates (gypsum) (Derge evaporate member) occur at the lower levels while lacustrine limestones (Zokayit limestone) at the upper horizons. Reddish shale, grey-green shale and reddish mudstone also occur at different levels of the formation. The topmost lithology is composed of reddish thick-bedded sandstones. The formation unconformably overlies the Hoya Formation, and is transitional with the overlying Fırat Formation. The contact with the overlying Şelmo Formation is an unconformity. The Kapıkaya Formation is deposited in a fluvial, flood plain, shallow-sea environment (Duran et al., 1988). The age of the formation is Early Miocene (Duran et al., 1988).

2.3.3.2.2. Fırat Formation

Fırat Formation is named by Krauset (1958), then by Peksü (1969); it is composed of fossiliferous limestones with limestone pebbles. The formation commences with cream-whitish-dirty yellow colored, medium-thick-bedded (locally massive) limestones, and continues with dirty yellow colored, medium-thick-bedded, cherty (nodular) fossiliferous (shell fragments) limestones. At the top, the formation is represented by creamy-dirty white colored, thick-very thick-bedded, cherty (nodular but few) fossiliferous (echinoids, ostrea, gastropoda and lamella branches) bioclastic limestones (Wilson and Krummenacher, 1957; Krauset, 1958; Peksü, 1969; Tuna, 1973; Duran et al., 1989; Ulu et al., 1991; Şafak and Meriç, 1996). The contact relationships with the underlying Gaziantep Formation and overlying Şelmo Formation are represented by unconformity surfaces (İmamoğlu, 1993). The overlying Lice Formation displays conformable relationship. The limestones of the formation were deposited in turbulent shallow water, shelf edge-bank and reefal environments

(Duran et al., 1989). Age of the formation is, based on the fossil content of the limestones, latest Oligocene–early Miocene (Aquitania–Burdigalian) (Duran et al., 1988; Erdoğan and Yavuz, 2002; Terlemez et al., 1997).

2.3.3.2.3. Lice Formation

Lice Formation is named by Koaster (1963) and Stratum (1963) to describe a lithological association of sandstone, marl, siltstone and limestone. It commences with claret red-red to greyish yellow-green colored, medium–thick-bedded to cross-bedded (locally pebbly) sandstones, continues with pinkish colored, thin-bedded, gypsiferous turbiditic shale and ends with sandstone-conglomerate and medium–thick-bedded sandy fossiliferous limestone. Shale forms the dominant lithology; it appears as massive and is characterized by fractures filled with gypsum. The gypsum-bearing lithologies are interpreted to form in a flood plain to sabkha environment whereas limestone, shelf to slope, turbiditic sediments, submarine fan environment (Duran et al., 1988). The age of the formation is Aquitania–Burdigalian (Early Miocene) (Duran et al., 1988; İmamoğlu, 1993).

2.3.4. Neogene Units

2.3.4.1. Şelmo Formation

Şelmo Formation is named by Bolgi (1961) to describe a clastic sedimentary sequence of conglomerate, sandstone, siltstone, and shale. It is unconformably overlain by the younger units whereas it overlies the Mardin Group with an angular unconformity (Tuna, 1973; Açıkbay and Baştuğ, 1975; Perinçek, 1979, 1989, 1990; Savcı and Dülger, 1980; Biçer, 1981; Yılmaz, 1982; Günay, 1990). The formation is composed of dirty yellow-pinkish-wine red-yellowish grey-reddish-brownish coloured, thick bedded, weak-moderately carbonate cemented, poorly sorted, coarse-grained polygenetic conglomerate with gypsum interbeds; dirty yellow-claret red siltstone;

and alternation of light grey-white shale and yellowish grey-light grey-brownish marl (Bolgi, 1961; Kıratlıoğlu and Bolgi, 1961; Saltık, 1970; İlker, 1972; Tuna, 1973; Açıkbay and Başbuğ, 1975; Perinçek, 1979, 1980, 1989, 1990; Savcı and Dülger, 1980; Açıkbay et al., 1981; Yılmaz, 1982; Pasin, 1989). The depositional environment is suggested as beach sand, tidal flat, playa and fluvial (Çemen et al., 1990). Age of the formation is, based on its stratigraphic position, is late Miocene–early Pliocene (Çemen et al., 1990). In the study area, the formation is represented by greyish green, pinkish, brownish purple coloured, thick- to cross-bedded sandstone, shale, sandy siltstone; these lithologies are porous, poorly sorted and carbonate cemented. It is also penetrated in BA-1 well; the formation is composed of variably coloured, polygenetic gravel, light brown silty-sandy-marly claystone and greenish grey silt-sandy marl (Bolgi, 1961).

All of these lithologies are unconformably overlain by Quaternary alluvials. They are composed river and alluvial fan deposits.

CHAPTER 3

METHODOLOGY

3.1. General

The study area is located more specifically from east of Besni and southwest of Adiyaman (Figure 1.6). The idea of this research has arisen when a team of TPAO field geologists (including the author) was working in the Adiyaman area to revise the geological maps and the stratigraphy of the region (Figure 1.10). This part lies outside the scope of the thesis.

In order to address the main objectives of this research, the completion of the previous works in and around the study area is carried out and the literature is carefully reviewed. A special emphasis is given to structural works about the Adiyaman Fault. Preliminary field observations confirmed that the recognition of the Adiyaman Fault and its relationship with other possible structures need to be studied largely by structural interpretation of the available 2D seismic lines because the Adiyaman Fault area is largely covered by loose sediments along its most trace. The logs of five boreholes (D.B-1, D.B-2, BA-1, B-1, B-2) are also available; these logs are carefully examined and evaluated. The checkshot values of each borehole are studied and integrated. There are five 2D seismic sections interpreted during this study: three of them are oriented almost parallel (AD-03-229, AD-00-202, and AV-00-110), one is oblique (DD-6071), and the last is almost orthogonal (AV-00-113), to the general trend of the Adiyaman Fault (Figure 3.1). The borehole logs and checkshot values are presented in Appendix A. The aim of this study is therefore to develop a structural and stratigraphic model of the subsurface data by using seismic reflection, well data and field observations.

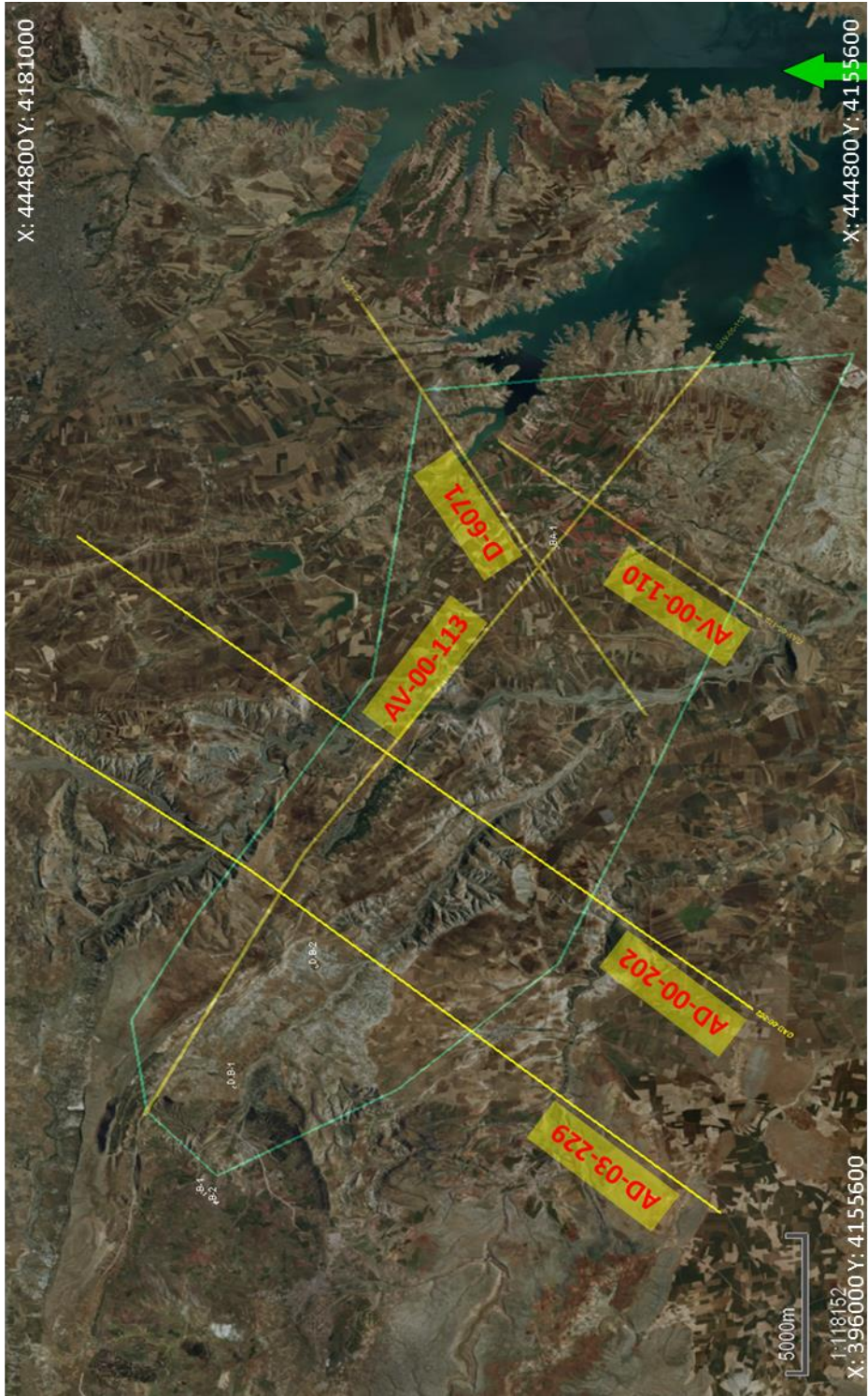


Figure 3.1. A Google Earth image showing location of boreholes and 2D seismic sections.

The 2D seismic sections are geologically calibrated with wellbore logs; stratigraphic horizons (Karababa and Sayındere formations) are picked based on synthetic seismograms calibrated by sonic log and checkshot data; and finally, faults are interpreted with Schlumberger's Petrel™ version 2016. Picked horizons are interpolated and converted to surface models; two-way-time (TWT) of the Karababa and Sayındere formations are calculated; accordingly, TWT maps, 3D views and structural maps of these formations are prepared. Faults are picked manually as discontinuities on vertical planes (inlines/crosslines) in 2D seismic sections and fault model(s) are generated. Three dimensional surfaces of the horizons (maps of the two formations) are created by interpretation and interpolation methods implemented in Petrel™ software. They are integrated with faults; structural models are prepared to calculate vertical displacements along these fault segments. At the end of the research, the study area was visited for ground truthing of what has been interpreted on the seismic sections. Finally, a structural and stratigraphic (only the Karababa and Sayındere formations) model of the subsurface data is developed by using seismic reflection, well data and field observations. The detail information about the different methods employed will be provided in the following subsections.

3.2. Seismic Interpretation

While seismic waves travel within the earth, they pass through different media. A change in the media causes an acoustic impedance change; seismic waves are therefore reflected, refracted and returned to earth. A seismic wave is the transfer of energy through elastic earth materials by way of particle oscillation/vibration. When they reach to surface, seismic waves are recorded by geophones via seismic recorder. The depth and velocity parameters are determined by using travel time of seismic waves. Some physical parameters are determined by 'Velocity = distance/time' formula. Seismic methods, used to determine the position of subsurface geological layers, are based on physical principles that explain the spreading of elastic waves through earth (Snell Law, Fermat Law, Huygens Law). The recorded data from

geophones gathered with complicated programs. It is called as 'rtqegulkpi'. Then it is loaded to seismic interpretation program with their geometry in space.

The seismic data gives an opportunity to visualize underground. The geological calibration of 2D seismic sections is therefore very important and this is done by logs of wells in the target area. Well coordinates, formation tops, logs and checkshot values are all loaded to system. The sonic well logs are used to determine velocity of formation. It must however be considered that fluid in the wells and well diameter can change the measured velocity. Checkshot values of the wells are also used to determine velocity of formation contacts and then to calibrate sonic logs. Reliable convert time seismic sections to the depth images are needed for reservoir calculations. Measurements are used to determine average velocity versus depth, such as from an acoustic log or check-shot survey. Acquiring a velocity survey is also known as 'uj qqkpi "c'y gni'. The recorded data gives lots of opportunities. The target formation is investigated with acoustic measurements. The measurement of depth is more accurate. Also, it has a depth control. The data validation should be carried out. Relationship to the geology in the subsurface should be observed and calibrated in seismic sections.

Providing accurate time/depth correlation from check-shot surveys gives a confirmation of where you are in both time and depth, regardless of borehole geometry. Thus, anyone could take an informed drilling decision by positioning drilling in the seismic section. Average, Interval and RMS velocity data, provides the essential information for acoustic log calibration and improves correlation of log-derived synthetic seismogram to surface seismic.

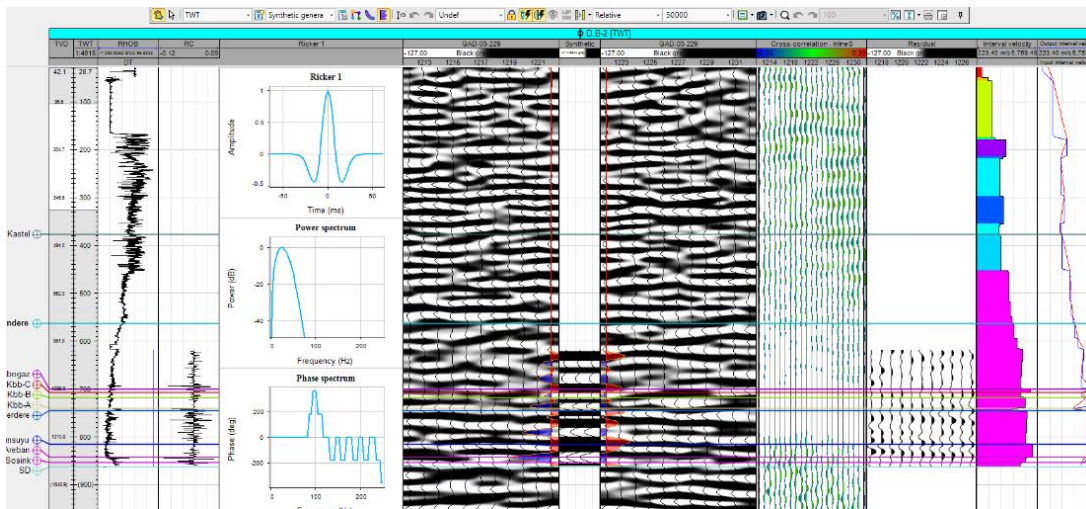
The depth of formation is gathered from well data. Also, time value can be gathered from checkshot value of the well. If these two are combined, velocity value will appear. Using these values, the top of Formation could be picked at seismic section which passes through the well. After that, anyone can continue to pick that level as

top of the formation. This interpretation gives faults and Two-way-time (TWT) map of the formation. The displacement amount of a fault can be calculated by using this map. Also, if the fault cuts the ground level, the displacement amount can be calculated with the lines that created from the intersection of fault surface and ground.

Seismic interpretation process is composed of five steps: (1) determination of lithological changes and identification of key stratigraphic horizons by using logs of available wells; (ii) tying of wells D.B-1, D.B-2, BA-1, B-1, B-2 checkshot values and synthetic seismic data to seismic cubes; (iii) picking of identified horizons (Karababa and Sayindere formations) throughout the seismic data; (iv) calculation of variance cubes for each seismic reflection data, and (v) fault interpretation by using generated seismic and variance cubes (slightly revised from Beşer, 2018).

3.2.1. Horizon Interpretation: Check-shot Data and Synthetic Seismograms

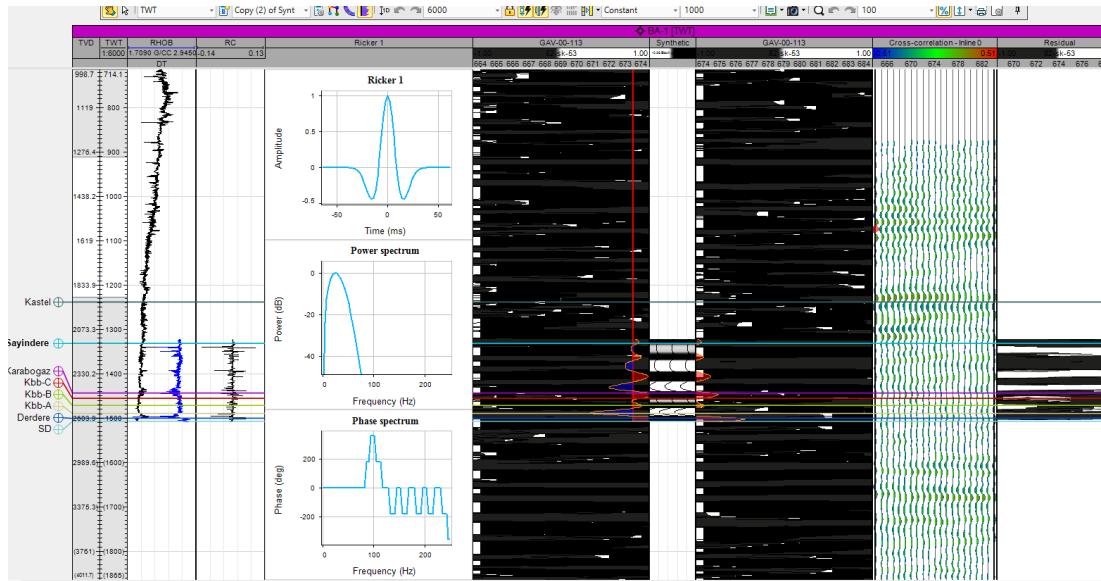
In seismic exploration, well-log measurements are commonly used to verify and calibrate seismic data at several stages during processing and interpretation. The well-log information should be aligned with the seismic data before the well-log information is used for interpretations. This process is called *well-tying*, and includes the conversion of the well-log measurements from depth to the time domain (Figures 3.2 and 3.3). Subsurface discontinuities form reflections in seismic attribute data and these surfaces can be interpreted as structural and stratigraphic markers as they create interfaces with impedance contrasts. Two different levels – top of the upper Coniacian–Santonian Karababa Formation and top of the upper Campanian Sayindere Formation – have been picked and mapped by using Schlumberger product Petrel™ version 2016 (Figures 3.4 and 3.5). Similarly, subsurface discontinuities form reflections in seismic attribute data and these surfaces can be interpreted as structural and stratigraphic markers because they create interfaces with impedance contrasts (Figures 3.6 and 3.7).



Hikmet g'5040 The synthetic seismogram calculated by using check shot data and sonic log for the well D.B-2. TVD- True vertical depth; TWT- Two Way Time; RHOB- Sonic log; RC- Reflection coefficient. The formation contacts have been identified by using both cutting samples and well log information gathered from well.

The study area wells are loaded to seismic interpretation software with their coordinates, Kelly bushing and total depth. formation tops (Figure 3.9 and Table 3.1) are loaded in to well data. Thus, we know the depth of formations. The synthetic log of wells are generated from sonic and density logs. These logs show the well tops on seismic sections. Since the velocity of formations can be calculated by seismic synthetic, the formation well tops can easily be identified on seismic sections. The checkshot values are used to identify well tops on seismic sections and they are available for 3 wells in the study area (see Figures A.6–A.8 in Appendix for more information). If the geometry of checkshots are entered properly, some programs or excel calculation sheets can be used to calculate the formation velocities in each well (see Tables A.4–A.7 in Appendix A for more information) by using a simple formula of $Velocity = \text{distance} / \text{time}$ (Tables 3.1 and 3.2). Since the well top values and velocity are known from well data and checkshot calculation, the seismic interpretation Petrel™ software can identify the well tops on seismic sections (Figures 3.2 and 3.3). The criteria for choosing a reflection or horizon to map are usually event strength and continuity. Karababa Formation is one of the strongest, continuous and recognizable reflections. Deposition of Sayındere Formation is affected by this fault. Thus,

Sayindere Formation and Karababa Formation are chosen for seismic interpretation (Figures 3.4–3.7). Well name, checkshot, Wavelet, closest seismic, Sonic, velocity and density logs are used to generate synthetic generation. This process is applied to both D.B-2 and BA-1 on seismic lines AD-03-229 and AV-00-113, because they are the closest seismic section to these wells, respectively.

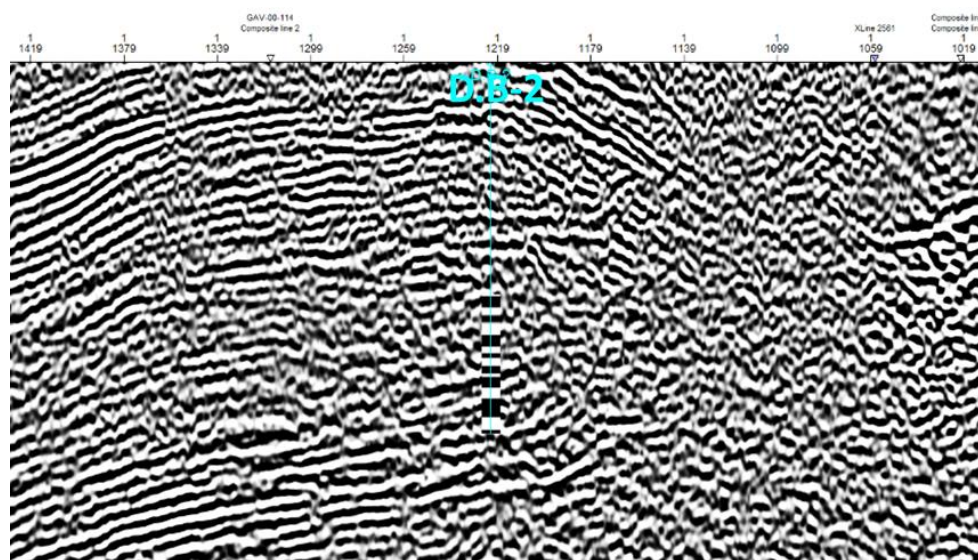


*Hi wt g'500*The synthetic seismogram calculated by using check shot data and sonic log for the well BA-1. TVD- True vertical depth; TWT- Two Way Time; RHOB- Sonic log; RC- Reflection coefficient. The formation contacts have been identified by using both cutting samples and well log information gathered from well.

3.2.1. Fault and Seismic Horizon Interpretation

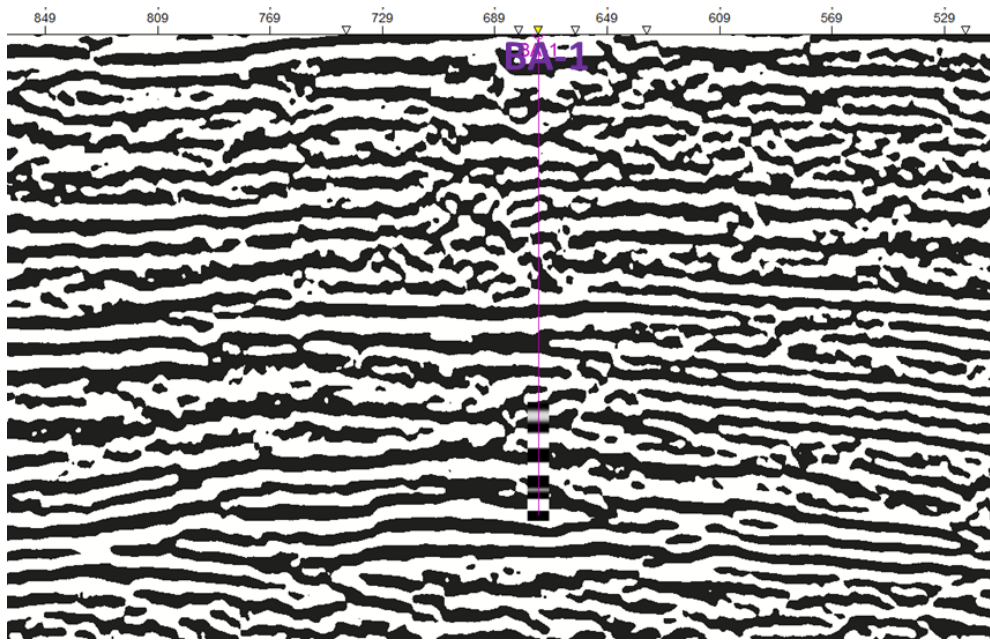
The actual interpretation of seismic sections is the most important stage of seismic methods. The validity of the remaining work rests on having an accurate and geologically correct interpretation of the available data. The seismic sections are examined with the structural elements on geological map and tectonic history of the area. The reflections at seismic sections represent a layer. The sharp broken reflections could refer to faults. The faults can easily be identified on seismic sections that are perpendicular to faults (Figure 3.10) and this is done manually. It is hard to distinguish faults in seismic sections running parallel to faults. When a fault is described in a

seismic section, the continuity of this fault should be searched in adjacent seismic sections. Corresponding faults in different seismic sections should be named the same.

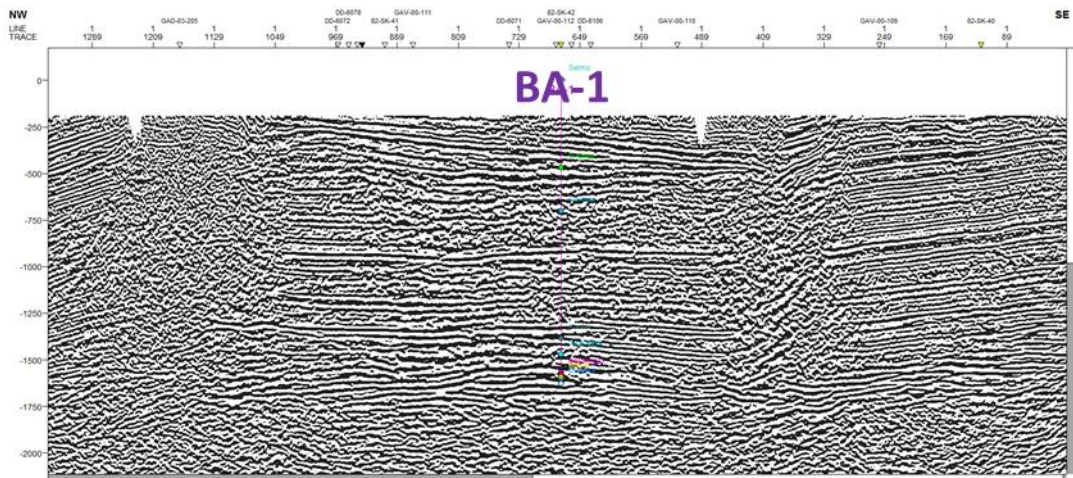


*Hki wt g'560*Horizon picks based on synthetic seismogram calibrated by sonic log and check-shot data on well D.B-2 in seismic section line AD-03-229. Top of the Karababa Formation (third black stripe from the top) is calibrated with well-log information to interpret the key horizon level.

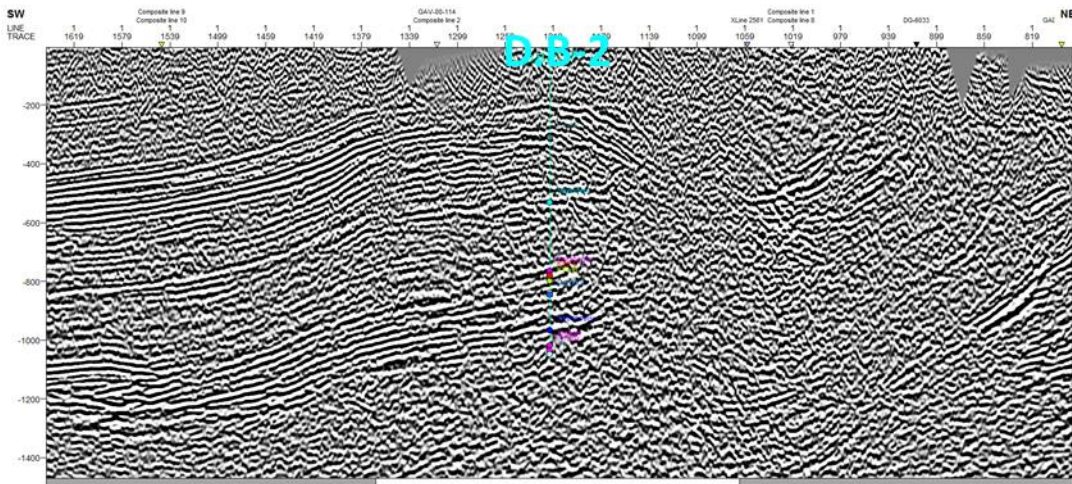
The horizons should be picked on seismic sections. The depth of formation is gathered from well data (Figure 3.11). Also, time value can be gathered from checkshot values and/or sonic logs of the wells. The well logs are loaded into seismic interpretation Petrel™ software with their coordinates, Kelly bushing and total depth. Seismic sections contain numerous reflections, and it is obvious that it would not be possible or practical to map every one of reflections.



Hki wt g'5070 Horizon picks based on synthetic seismogram calibrated by sonic log and check-shot data on well BA-1 in seismic section line AV-00-113. Top of the Karababa Formation (third black stripe from the top) is calibrated with well-log information to interpret the key horizon level.



Hki wt g'5080 Horizon picks based on synthetic seismogram calibrated by sonic log and check-shot data on well BA-1 on seismic section line AV-00-113. Formation tops are calibrated with well-log information to interpret key horizon levels of top of the Gaziantep, Germav, Kastel, Sayındere, Karaboğaz, Karababa, Derdere and other older formations (see Table 3.1 for more information).



Horizontal picks based on synthetic seismogram calibrated by sonic log and check-shot data on well D.B-2 on seismic section line AD-03-229. Formation tops are calibrated with well-log information to interpret key horizon levels of top of the Gaziantep, Germav, Kastel, Sayindere, Karaboğaz, Karababa, Derdere and other older formations (see Table 3.1 for more information).

The seismic horizons to map should be decided carefully. The criteria for choosing a reflection or horizon to map are usually based on event strength and continuity of reflection. The reflections across fault and fracture surfaces commonly indicate sharp contrasts. The most recognizable and continuous reflections will be the effortless to trace through a grid of data. Strongest and most continuous events should be selected to map whenever/wherever possible.

The actual interpretation of seismic sections is the most important part of seismic methods. The validity of the work rests on having accurate and geologically correct interpretation of the seismic data. A basic understanding of the reflection seismic method is needed before seismic data can be interpreted correctly. The main objective is to extract the information from the interpreted data and transfer it onto the map, because maps are commonly used more effectively. Transferring the interpreted data to a map is called as '*raqıpi*'.

Table 3.10 Hqt o cvkqp'vqr 'xcwgu'qhl'y gmu'D/3.'D/4.'DC/3.'F(D/3.'c'pf 'F(D/4'wugf 'ecrewr:vg'ij g'xgnqekf'xcwgu'qhl'
 hqt o cvkpu'vukpi "c'uko rrg'urt gcf uj ggv'o gpw0"

Well top spreadsheet for 'Well Tops-eski'

Edit point: None Filtering: [ON]

	Well identifier	Surface	X	Y	Z	MD	TWT picked	TWT auto
635	B-1	Kastel	403066.35	4175418.86	709	0.00		-323.97
636	B-1	Sayindere	403066.35	4175418.86	341	368.00		218.02
637	B-1	Karaboqaz	403066.35	4175418.86	94	615.00		329.39
638	B-1	Kbb-C	403066.35	4175418.86	85	624.00		332.46
639	B-1	Kbb-B	403066.35	4175418.86	64	645.00		339.37
644	B-1	Kbb-B	403066.35	4175418.86	-147	856.00		431.11
640	B-1	Kbb-A	403066.35	4175418.86	18	691.00		354.21
641	B-1	Derdere	403066.35	4175418.86	10	699.00		357.47
642	B-1	Sabunsuyu	403066.35	4175418.86	-87	796.00		402.34
643	B-1	Areban	403066.35	4175418.86	-137	846.00		426.32
647	B-1	SD	403066.35	4175418.86	-541	1250.00		620.01
645	B-1	Bakük	403066.35	4175418.86	-360	1069.00		533.23
646	B-1	Uludere	403066.35	4175418.86	-490	1199.00		595.55
693	B-2	Kastel	402752.42	4175041.82	695	50.00		52.00
648	B-2	Sayindere	402752.42	4175041.82	412	333.00		121.00
649	B-2	Karaboqaz	402752.42	4175041.82	127	618.00		181.25
650	B-2	Kbb-C	402752.42	4175041.82	119	626.00		183.26
651	B-2	Kbb-B	402752.42	4175041.82	96	649.00		189.17
652	B-2	Kbb-A	402752.42	4175041.82	38	707.00		199.00
653	B-2	Derdere	402752.42	4175041.82	31	714.00		201.17
654	B-2	SD	402752.42	4175041.82	-26	771.00		210.83
692	B-2	Kocali	402752.42	4175041.82	745	0.00		38.81
242	BA-1	Selmo	425867.60	4164721.43	603	0.00		-4.74
243	BA-1	Germav	425867.60	4164721.43	-109	712.00		702.06
233	BA-1	G.Antep	425867.60	4164721.43	164	439.00		468.98
234	BA-1	Kastel	425867.60	4164721.43	-1320	1923.00		1384.97
235	BA-1	Sayindere	425867.60	4164721.43	-1546	2149.00		1470.75
236	BA-1	Karaboqaz	425867.60	4164721.43	-1837	2440.00		1569.25
237	BA-1	Kbb-C	425867.60	4164721.43	-1871	2474.00		1579.59
238	BA-1	Kbb-B	425867.60	4164721.43	-1920	2523.00		1594.51
239	BA-1	Kbb-A	425867.60	4164721.43	-1973	2576.00		1610.64
240	BA-1	Derdere	425867.60	4164721.43	-2000	2603.00		1618.85
241	BA-1	SD	425867.60	4164721.43	-2027	2630.00		1627.07
624	D.B-1	Kastel	406843.36	4174475.87	598	24.00		4.35
625	D.B-1	Sayindere	406843.36	4174475.87	422	200.00		202.42
626	D.B-1	Karaboqaz	406843.36	4174475.87	189	433.00		363.41
627	D.B-1	Kbb-C	406843.36	4174475.87	183	439.00		367.99
628	D.B-1	Kbb-B	406843.36	4174475.87	175	447.00		374.10
629	D.B-1	Kbb-A	406843.36	4174475.87	155	467.00		388.65
630	D.B-1	Derdere	406843.36	4174475.87	147	475.00		394.37
631	D.B-1	Sabunsuyu	406843.36	4174475.87	39	583.00		467.11
632	D.B-1	Areban	406843.36	4174475.87	-66	688.00		523.88
633	D.B-1	Sosink	406843.36	4174475.87	-86	708.00		534.37
634	D.B-1	SD	406843.36	4174475.87	-157	779.00		570.16
777	D.B-2	Kastel	411091.28	4172012.90	172	459.00		376.62
778	D.B-2	Sayindere	411091.28	4172012.90	-141	772.00		562.75
779	D.B-2	Karaboqaz	411091.28	4172012.90	-468	1099.00		699.88
780	D.B-2	Kbb-C	411091.28	4172012.90	-489	1120.00		706.93
781	D.B-2	Kbb-B	411091.28	4172012.90	-516	1147.00		717.92
782	D.B-2	Kbb-A	411091.28	4172012.90	-576	1207.00		739.93

Use in geo.mod: All None Use in depth conv: All None Sync. well symbol Apply OK

There are two important purposes at tying seismic data. First, it creates a relationship between the traces of surfaces seen on seismic lines. In other words, tied data provides that a given trace of a geologic surface interpreted on one line is indeed the same surface as interpreted on an intersecting line. The ability to project the horizon being mapped into areas where well control may not exist is the second benefit of tying seismic data. Many wildcat prospects are created by this basis and have wells drilled through them. Seismic data could be used to extend a mapped horizon into areas with little subsurface control. The extracting faults and fractures is done manually.

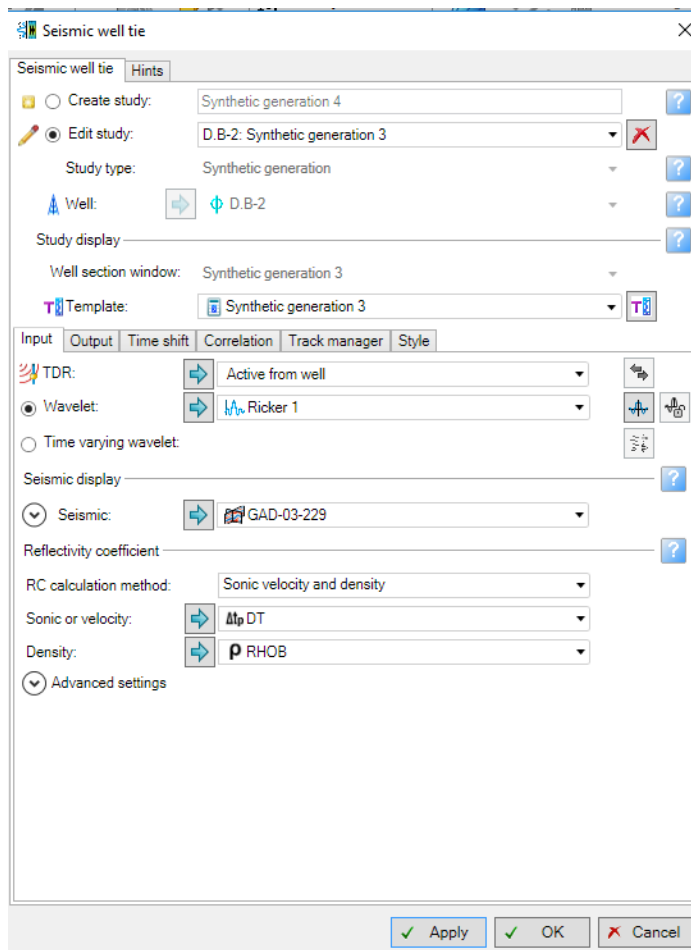


Figure 50 Seismic synthetic menu that is used in well-tying, that is conversion of the well-log measurements from depth to the time domain.

Table 3.20Ej gemij qv'xgrqekkgu'htq'f kktg pvv'htq o c'v'kpu'ecrewr'v'f 'ht qo 'ej gemij qv'xcwgu'0'

	D.P-1	KB-622.33	GL-517.33	AIRGUN616	SRD-600	X:	Y:						
FORMASYONLAR	KP'DEN DERİNLİK (m)	AIRGUNDAN ALICIYA KADAR GEÇEN ZAMAN (msn)	AIRGUN SEVİYESİNE GÖRE DÜŞEY DERİNLİK	AIRGUN İLE ALICIYASINDAKİ UZAKLIK	SRD'YE GÖRE DÜŞEY DERİNLİK	SRD'YE GÖRE ORTALAMA HIZ	SRD'YE GÖRE ARA HIZ	SRD'YE GÖRE TEK ZAMAN (msn)	SRD'YE GÖRE ÇİFT ZAMAN (msn)				
KASTEL	23	55	21.7	20.2	59.1	5.7	1075	1075	5.3	11			
	175	83	173.7	79.1	182.2	157.7	2195	2578	64.2	128			
SAYINDERE	200	99	198.7	95.4	206.1	182.7	2082	1535	80.5	161			
	223	107	221.7	103.9	228.4	205.7	2134	1453	96.4	193			
	259	113	257.7	110.5	263.5	241.7	2332	5406	103.0	206	KB'YI	SRDYI	AIRGUN
	348	133	346.7	131.4	351.0	330.7	2639	4269	123.9	248			AIRGUN
	384	142	382.7	140.6	386.6	366.7	2723	3914	133.1	266	617.33	600	616
	420	149	418.7	147.7	422.3	402.7	2834	5017	140.2	280			55
KARABOĞAZ	432	150	430.7	148.8	434.2	414.7	2894	5828	141.3	283			
KBB-C	439	152	437.7	150.8	441.1	421.7	2902	3461	143.3	287			
KBB-B	447	156	445.7	154.8	449.1	429.7	2879	1994	147.3	295			
KBB-A	467	158	465.7	156.9	468.9	449.7	2968	9597	149.4	289			
DERDERE	475	162	473.7	160.9	476.9	457.7	2944	4595	153.4	307			
	554	175	552.7	174.1	555.4	536.7	3174	5975	166.6	333			
SABUNSUYU	582	179	580.7	178.2	583.3	564.7	3258	6892	170.7	341			
	607	183	605.7	182.3	608.2	589.7	3323	6176	174.8	350			
AREBAN	687	200	685.7	199.4	687.9	669.7	3439	4963	191.9	384			
SOSİNK	707	206	705.7	205.4	707.8	689.7	3436	3324	197.9	396			
SD	780	223	778.7	222.4	780.6	762.7	3500	4277	214.9	430			

3.2.2. Structural Maps

Seismic sections are in time domain. To picture the subsurface independent of velocity, time domain should be altered to depth (Figure 3.9). If time is multiplied by velocity, depth information can be obtained. There are 4 wells around study area. Since there are sonic logs and checkshot values for wells are available, velocity maps can be prepared. In order to make a velocity map, the velocity and checkshot data need to be extrapolated. If two-way-time (TWT) map is multiplied by Velocity map, the result would be a 'structure contour map' by using a formula of $X=V*T/2$.

These processes will eventually lead to the preparation of 2D and 3D fault models, velocity, two-way-time (TWT), structural and 3D maps for the Karababa and Sayındere formations; the results will be presented and discussed in Chapter 4.

Depth conversion is an important step of the seismic reflection method, which converts the acoustic wave travel time to actual depth, based on the acoustic velocity of subsurface medium (sediments, rocks, water). A good seismic image is not enough for an exploration or field development interpretation. Good well ties and reliable depth conversion are also required.

3.3. Ground Truthing

Once the structural interpretation of the seismic sections is complete, there is a need for ground truthing of identified faults. The Adiyaman Fault displays in part typical strike-slip morphology (Figures 1.11–1.14). During field studies, the geological map of the study area is revised (Figure 1.10) and confirmation of structural elements are made. A special emphasis is given to the fault(s) that are observed to be cut and displaced by the Adiyaman Fault as it has significance on the offset of the AF. The results will be discussed in Chapter 4.

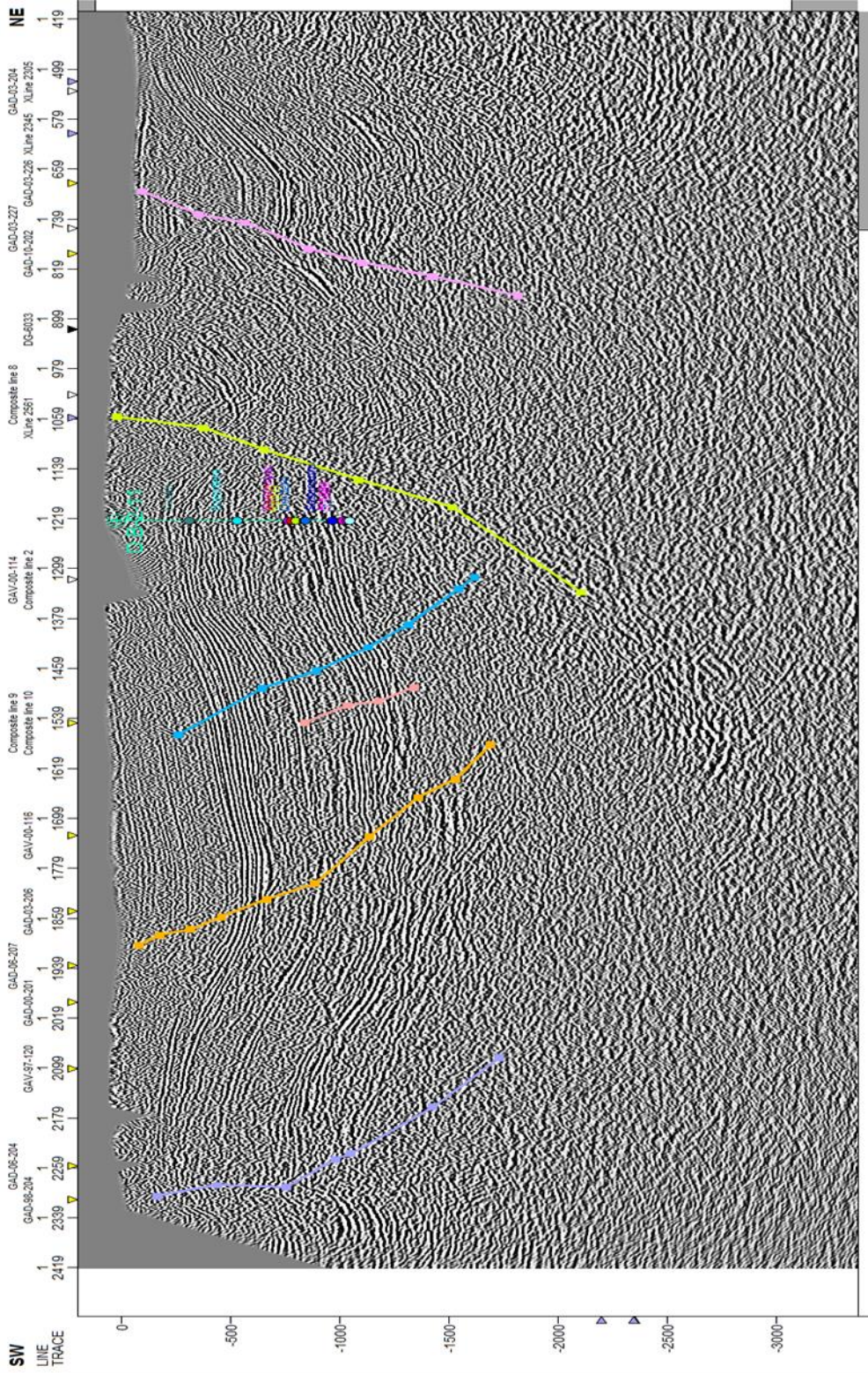


Figure 3.9. Fault interpretation on seismic line AD-03-229

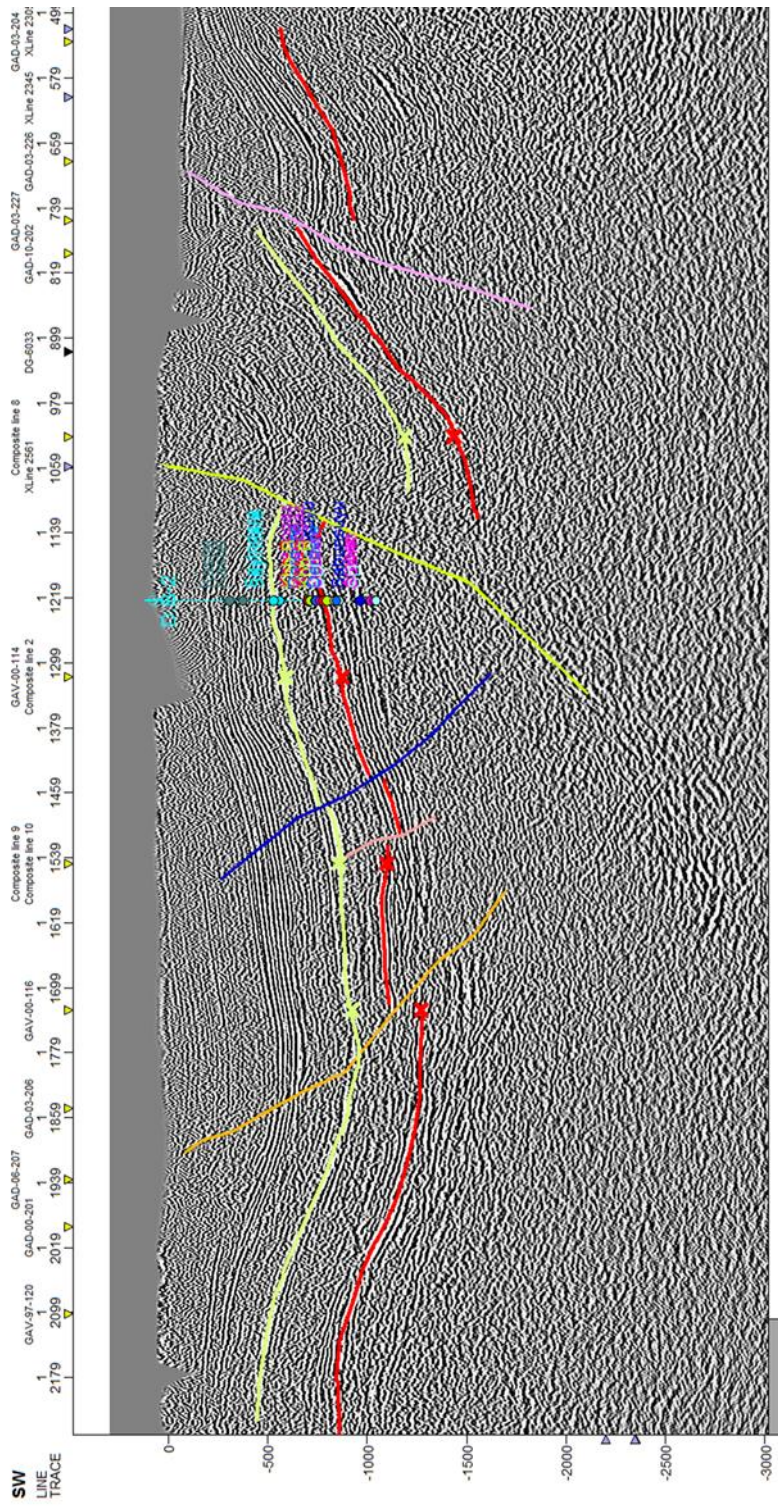


Figure 3.10. Top of the Karababa (red) and Sayindere (green) formations, and Fault interpretation on seismic line AD-03-229.

CHAPTER 4

INTERPRETATION OF THE SUBSURFACE DATA

4.1. Seismic Fault Interpretation Results

The 2D seismic sections are examined and then interpreted based on the structural elements on geological map and tectonic history of the study area. The reflections at seismic sections represent a layer. The broken reflections could refer faults. Two stratigraphic horizons, tops of the Karababa and Sayindere formations, are chosen to pick for seismic interpretation and geological calibration of the seismic sections. The Coniacian–Santonian Karababa Formation is picked because it is considered as one of the well-known target rocks for hydrocarbon exploration in the naturally fractured Şambayat field around Adıyaman and forms continuous reflections in the seismic sections. The Campanian Sayindere Formation also is considered as the cap rock of the Şambayat oil field. The oil field is interpreted as a positive flower structure formed in association with the sinistral Adıyaman Fault (Figure 1.15–1.17). This study has resulted in the identification of a new fault, herein named as Şambayat Fault.

Five seismic sections (Figure 3.1) are interpreted in order to define the fault and, to clarify and shed lights on the existing controversies over the presence of the Şambayat Fault (ŞF) and the offset of the Adıyaman Fault. The details of the seismic interpretation will be given in the following sections. Four of these seismic lines (AD-03-229, AD-00-202, AV-00-110 and D-6071) trend in NE–SW direction, almost parallel to the general orientation of the Adıyaman Fault, and perpendicular to the orientation of the inferred Şambayat Fault. The other seismic line trends in NW–SE direction and is almost orthogonal to the Adıyaman Fault (Figure 3.1).

4.2. Seismic Line AD-03-229

The NE–SW-trending seismic line is oriented almost parallel to the general orientation of the Adıyaman Fault, and almost perpendicular to the orientation of the inferred Şambayat Fault; it passes through the well D.B-2 (Figures 3.1, 4.1 and 4.2). The seismic line is therefore forms an ideal section to examine the existence and other possible characteristics of the Şambayat Fault. Horizons are picked based on synthetic seismogram calibrated by sonic log and check-shot data on well D.B-2.

The seismic section is therefore geologically calibrated with well-log information and tops of the Gaziantep, Germav, Kastel, Sayındere, Karaboğaz, Karababa, Derdere and other older formations are interpreted (Figure 4.2). Similarly, sharp broken reflections are interpreted as subsurface discontinuities/faults (Figures 4.3). Six steeply-dipping fault segments (F1 to F6 from southwest to northeast) are defined; four appears to dip to northeast, the two towards southwest. By means of velocity values gathered from checkshot values, key horizons –tops of the Sayındere and Karababa formations– are interpreted, drawn on the seismic section and integrated with the interpreted fault segments (Figure 4.4). The relative positions of the tops to the two formations on either block of these faults suggest that the faults appear to have reverse component. The displacement along Fault F5 is pronounced with a considerable amount of dip-slip component. The trace of tops to the Sayındere and Karababa formations appear to form a drag fold confirming the reverse component (Figure 4.4). Similarly, displacement along Fault F6 is also pronounced. The displacement along F4 is relatively small. The faults F3 and F2 appear to displace the top of the Karababa Formation but there is no observable displacement of the top of the Sayındere Formation. The F4 (blue) and F5 (green) faults are interpreted to represent the inferred Şambayat Fault; it appears that the area in-between oppositely dipping faults is uplifted, like a pressure ridge. If this interpretation is correct, then the Şambayat Fault is composed of fault segments that have reverse components and thrust towards northeast and southwest (Figure 4.4).

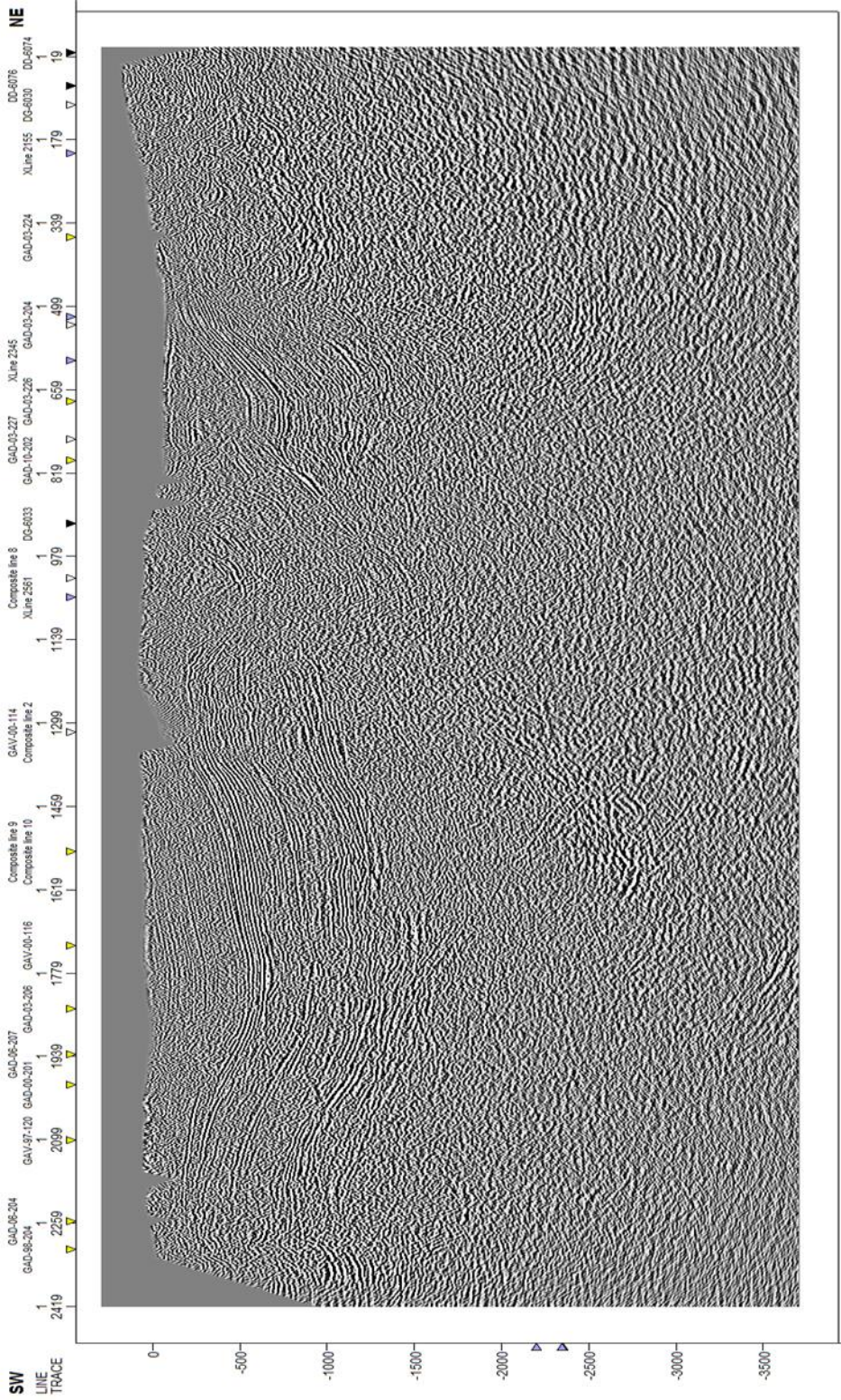


Figure 4.1. Un-interpreted seismic section AD-03-229 (migration). See Figure 3.1 for location.

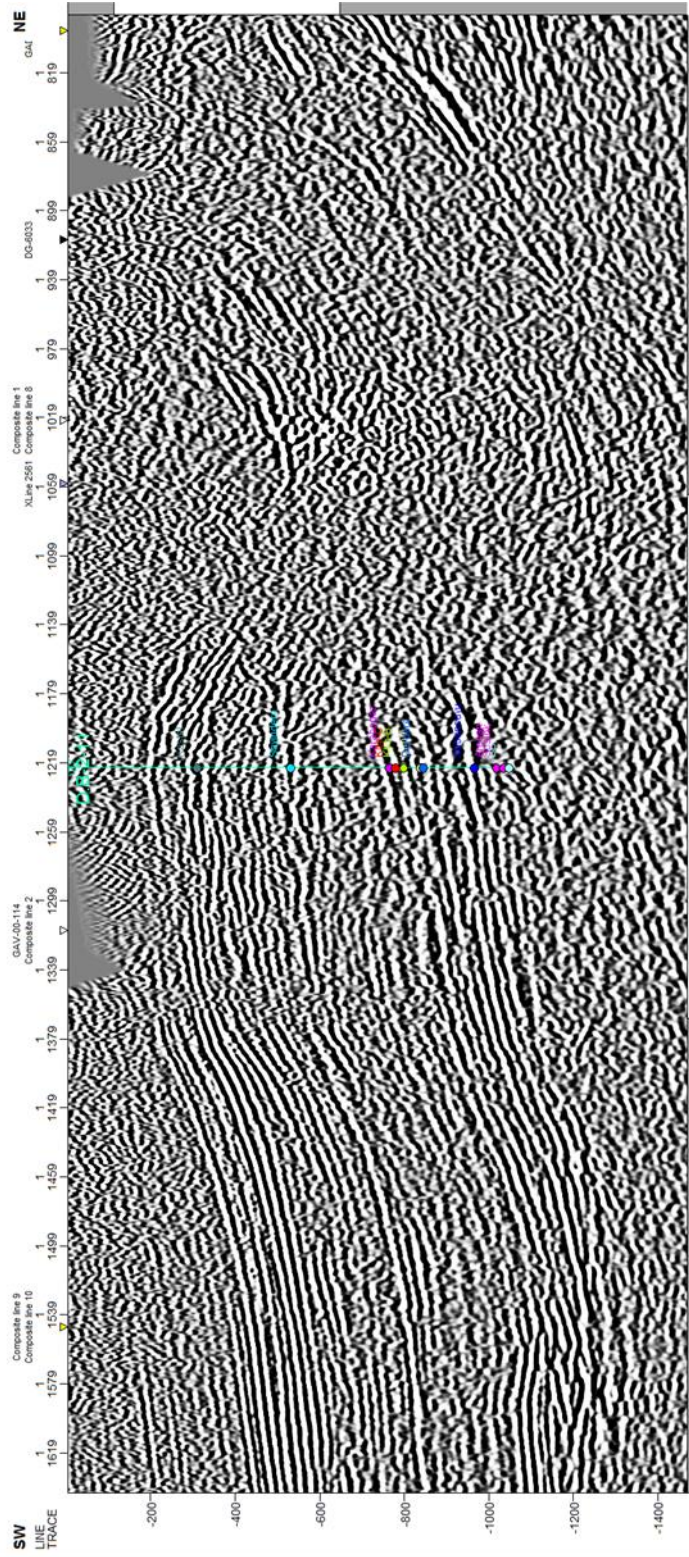


Figure 4.2. Horizon picks based on synthetic seismogram calibrated by sonic log and check-shot data on well D.B-2 on seismic section line AD-03-229. Formation tops are calibrated with well-log information to interpret key horizon levels of top of Gaziantep, Germay, Kastel, Sayindere, Karaboğaz, Karababa, Derdere and other older formations (see Table 3.1 for more information).

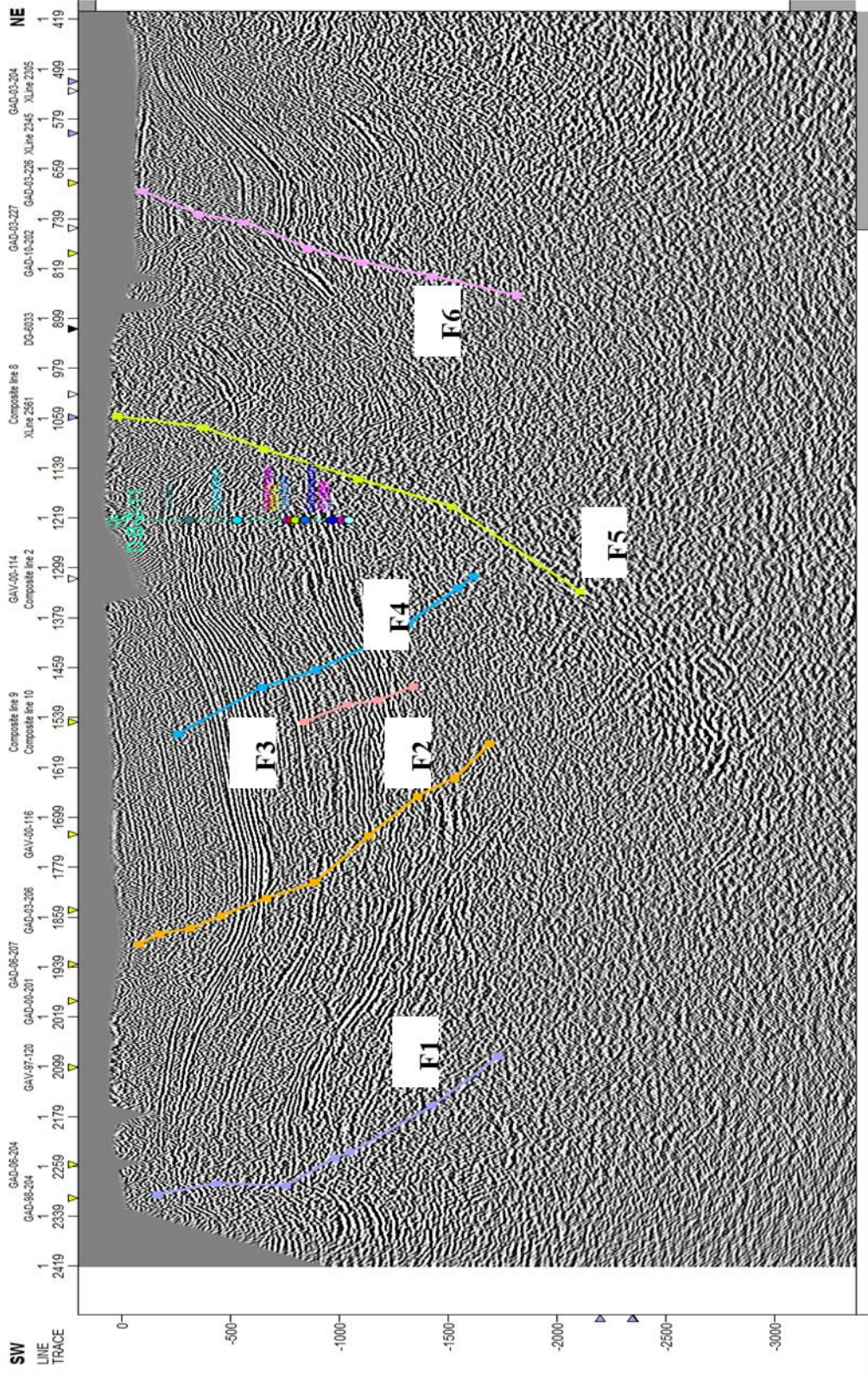


Figure 4.3. Fault interpretation on seismic line AD-03-229.

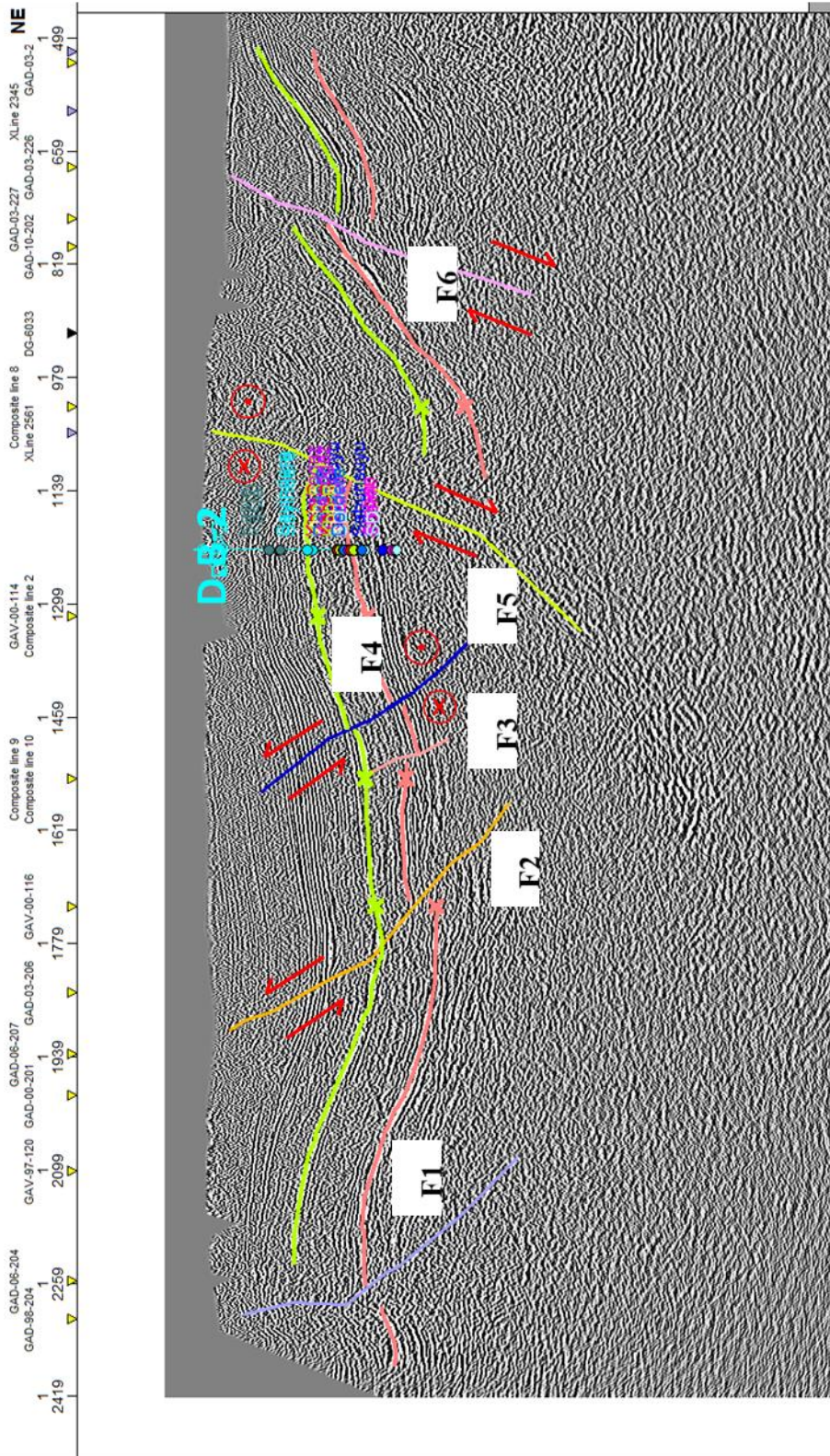


Figure 4.4. Top of the Karababa (red) and Sayndere (green) Formations, and Fault interpretation on seismic line AD-03-229

4.3. Seismic Line AV-00-113

The NW–SE-trending seismic line is oriented almost perpendicular to the general orientation of the Adıyaman Fault, and almost parallel to that of the inferred Şambayat Fault; it passes through the well BA-1 (Figures 3.1, 4.5 and 4.6). The seismic line is therefore forms an ideal section to examine the Adıyaman Fault.

Horizons are picked based on synthetic seismogram calibrated by sonic log and check-shot data on well BA-1. The seismic section is therefore geologically calibrated with well-log information and tops of the Gaziantep, Germav, Kastel, Sayındere, Karaboğaz, Karababa, Derdere and other older formations are interpreted (Figure 4.6). Similarly, a sharp broken reflection is interpreted as a subsurface discontinuity/fault (Figures 4.6).

By means of velocity values gathered from checkshot values, key horizons –tops of the Sayındere and Karababa formations– are interpreted, drawn on the seismic section and integrated with the interpreted fault segment (Figure 4.7). The relative positions of the tops to the two formations on either block of the fault suggest that the Adıyaman Fault has a pronounced displacement with a considerable amount of dip-slip reverse component. The Adıyaman Fault appears as steeply NW-dipping structure whereas dip direction changes with depth where it starts to deep steeply towards SE (Figure 4.7); a characteristic typical for strike-slip faults.

4.4. Seismic Line AD-00-202

The NE–SW-trending seismic line is oriented almost parallel to the general orientation of the Adıyaman Fault, and almost perpendicular to the orientation of the inferred Şambayat Fault (Figures 3.1 and 4.8). The seismic line is therefore forms an ideal section to examine the existence of the Şambayat Fault.

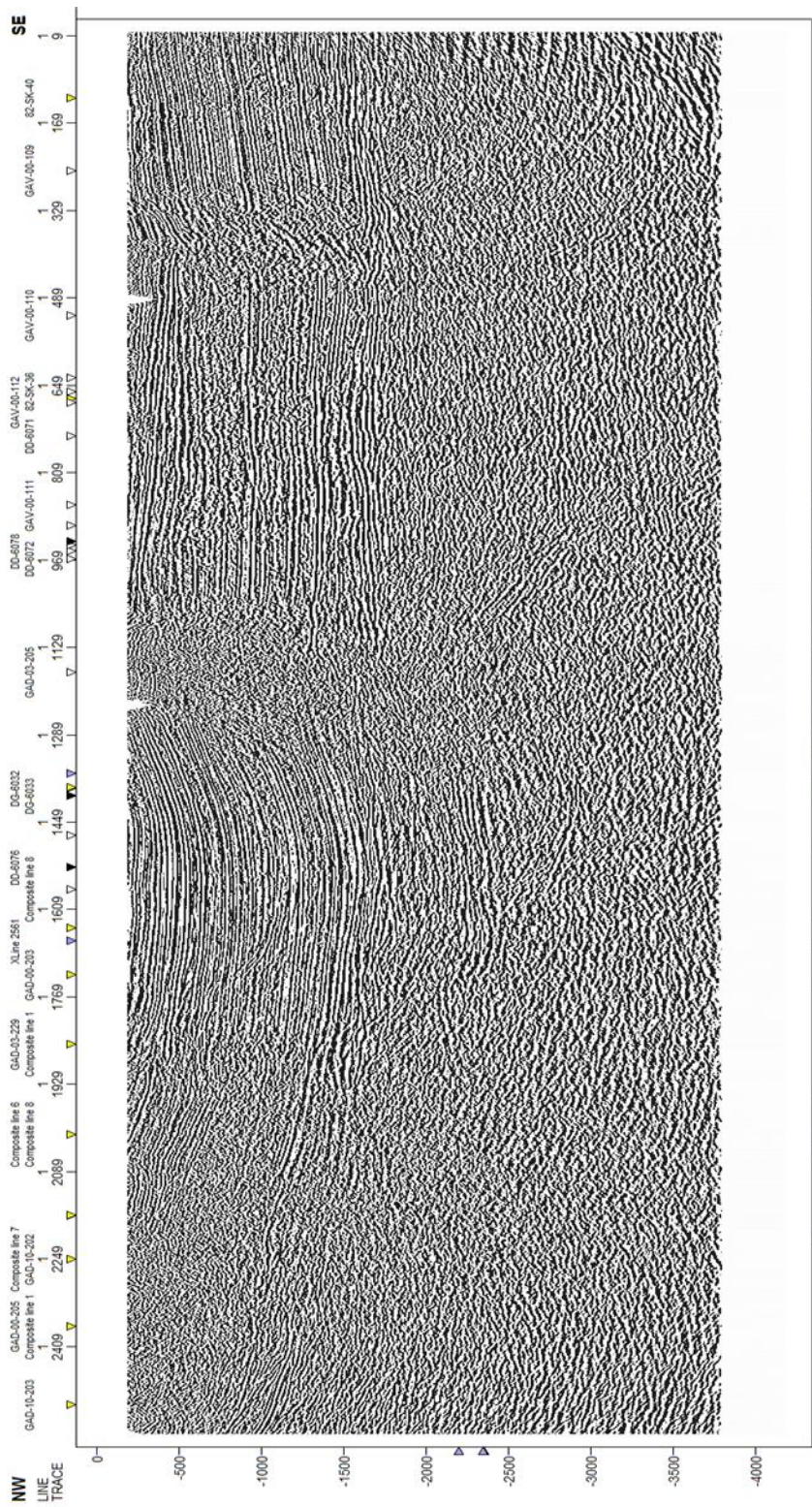


Figure 4.5. Uninterpreted seismic section AV-00-113 (migration). See Figure 3.1 for location.

Sharp broken reflections on the seismic section are interpreted as subsurface discontinuities/faults (Figures 4.9). Five steeply-dipping fault segments (F1 to F5 from southwest to northeast) are defined; they appear to dip both towards northeast southwest. The fault F5 appears to display a pronounced bend along dip: the fault dip steeply northeast at its uppermost section whereas a southwest steep dip at its lower section; differently dipping two parts of the fault is connected by a relatively gently northeast dipping section (Figure 4.9).

By means of velocity values gathered from checkshot values, key horizons –tops of the Sayındere and Karababa formations– are also interpreted, drawn on the seismic section and integrated with the interpreted fault segments (Figure 4.10). The relative positions of the tops to the two formations on either block of the faults suggest reverse component. The trace of tops to the Sayındere and Karababa formations appear to form a drag folds confirming the reverse components of faults F2 and F4 (Figure 4.10). Similarly, dip-slip reverse displacements along these faults are pronounced.

4.5. Seismic Line DD-6071

The NE–SW-trending seismic line is oriented almost parallel to the general orientation of the Şambayat Fault, and almost perpendicular to the orientation of the inferred Adıyaman Fault; it passes through the well BA-1 (Figures 3.1, 4.11 and 4.12). The seismic line is therefore forms an ideal section to examine the existence of the Şambayat Fault. Horizons are picked based on synthetic seismogram calibrated by sonic log and check-shot data on well BA-1.

The seismic section is therefore geologically calibrated with well-log information and tops of the Gaziantep, Germav, Kastel, Sayındere, Karaboğaz, Karababa, Derdere and other older formations are interpreted (Figure 4.12).

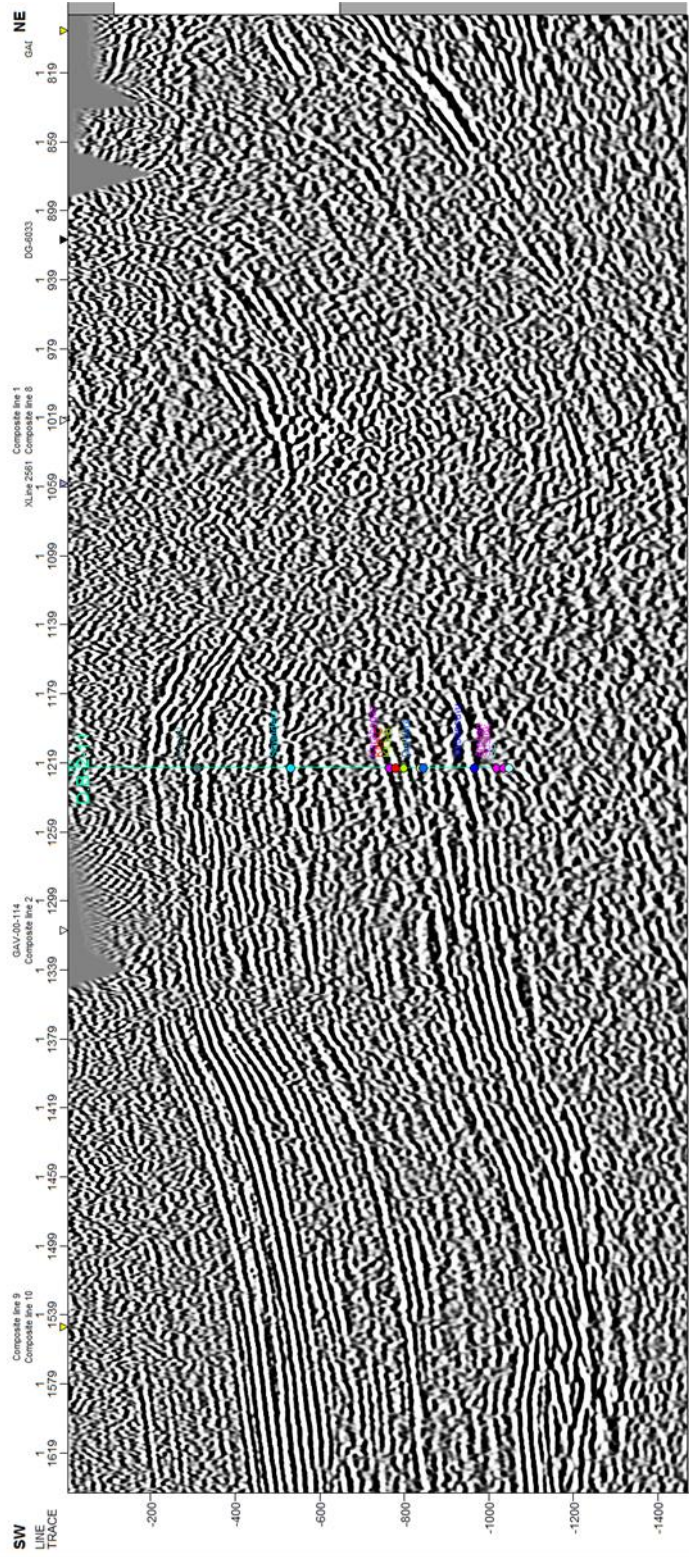


Figure 4.2. Horizon picks based on synthetic seismogram calibrated by sonic log and check-shot data on well D.B-2 on seismic section line AD-03-229. Formation tops are calibrated with well-log information to interpret key horizon levels of top of Gaziantep, Germay, Kastel, Sayindere, Karaboğaz, Karababa, Derdere and other older formations (see Table 3.1 for more information).

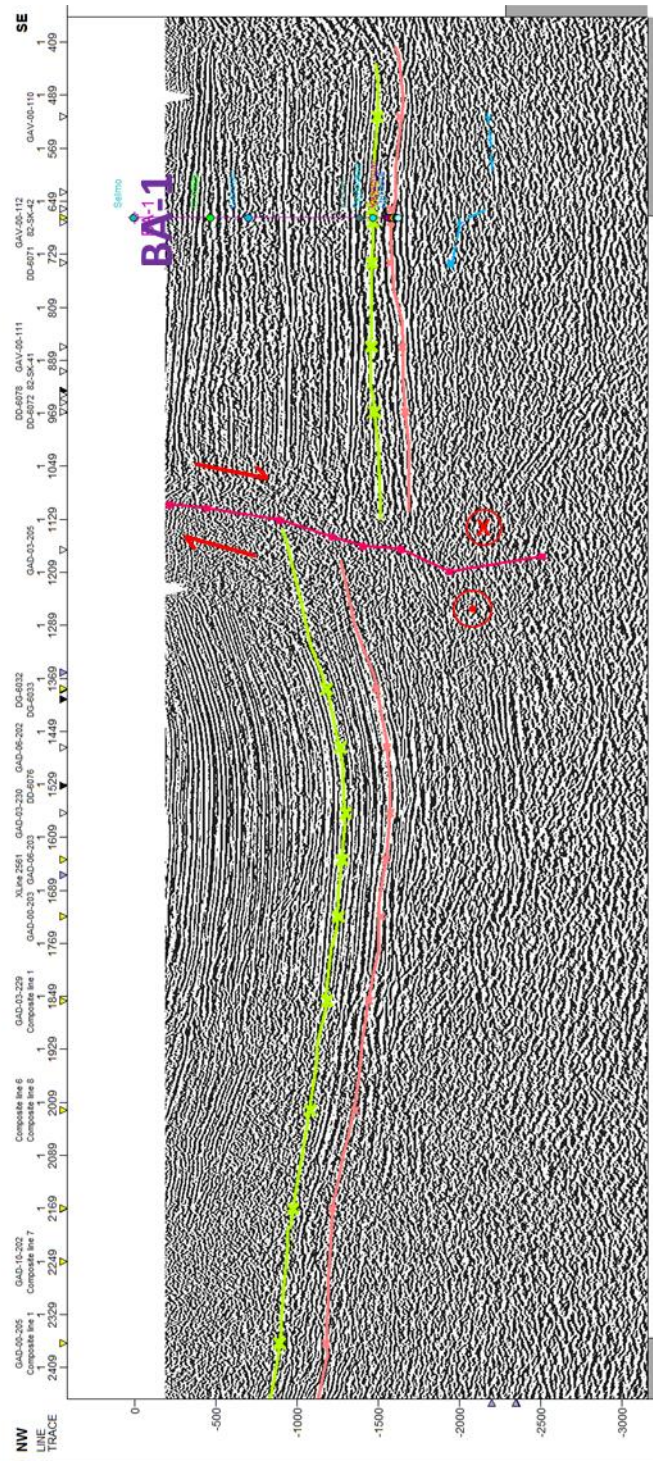


Figure 4.7. Top of the Karababa (red) and Sayindere (green) Formations, and fault interpretation on seismic line AV-00-113.

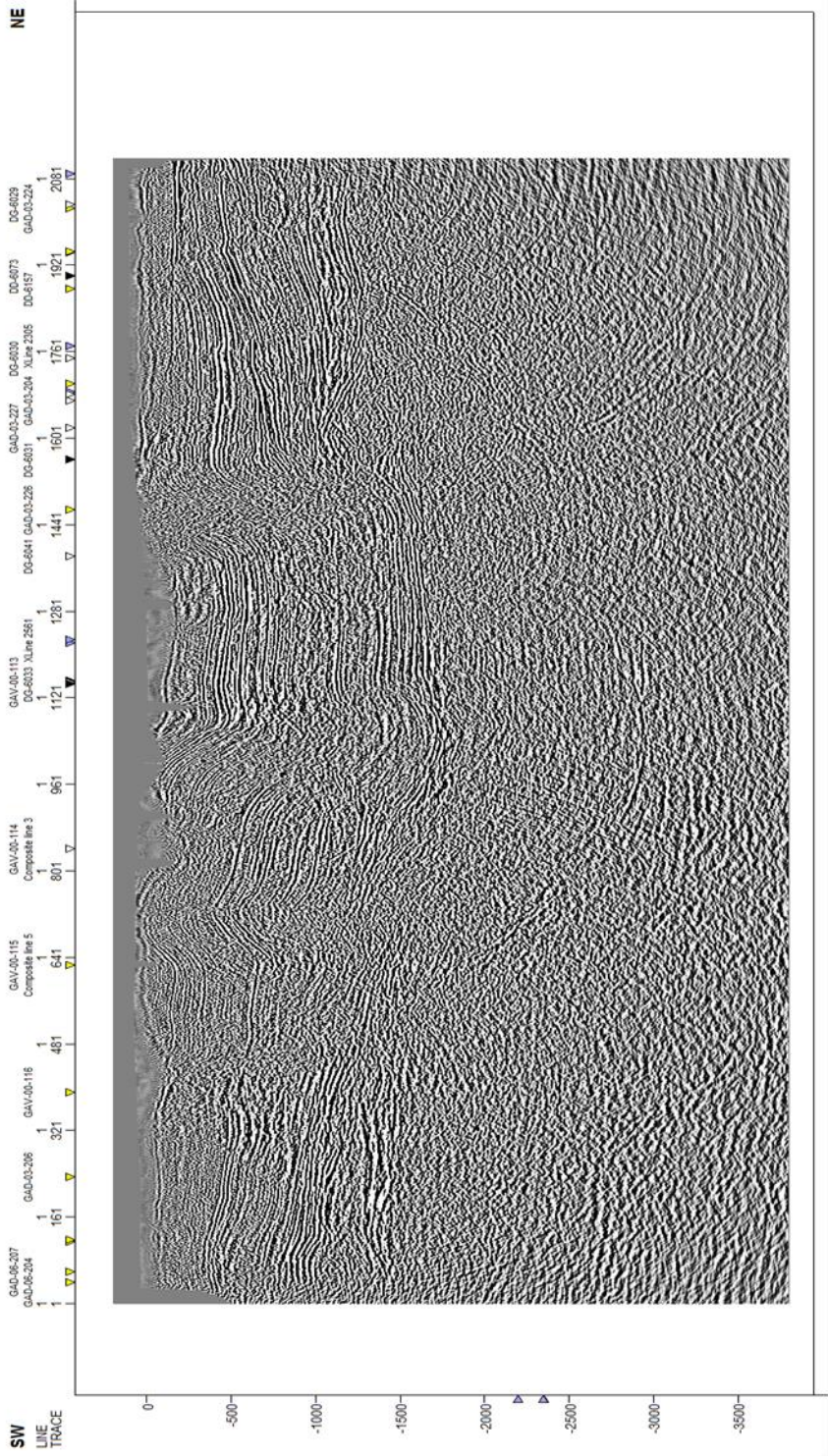


Figure 4.8. Uninterpreted seismic section AD-00-202 (migration). See Figure 3.1 for location.

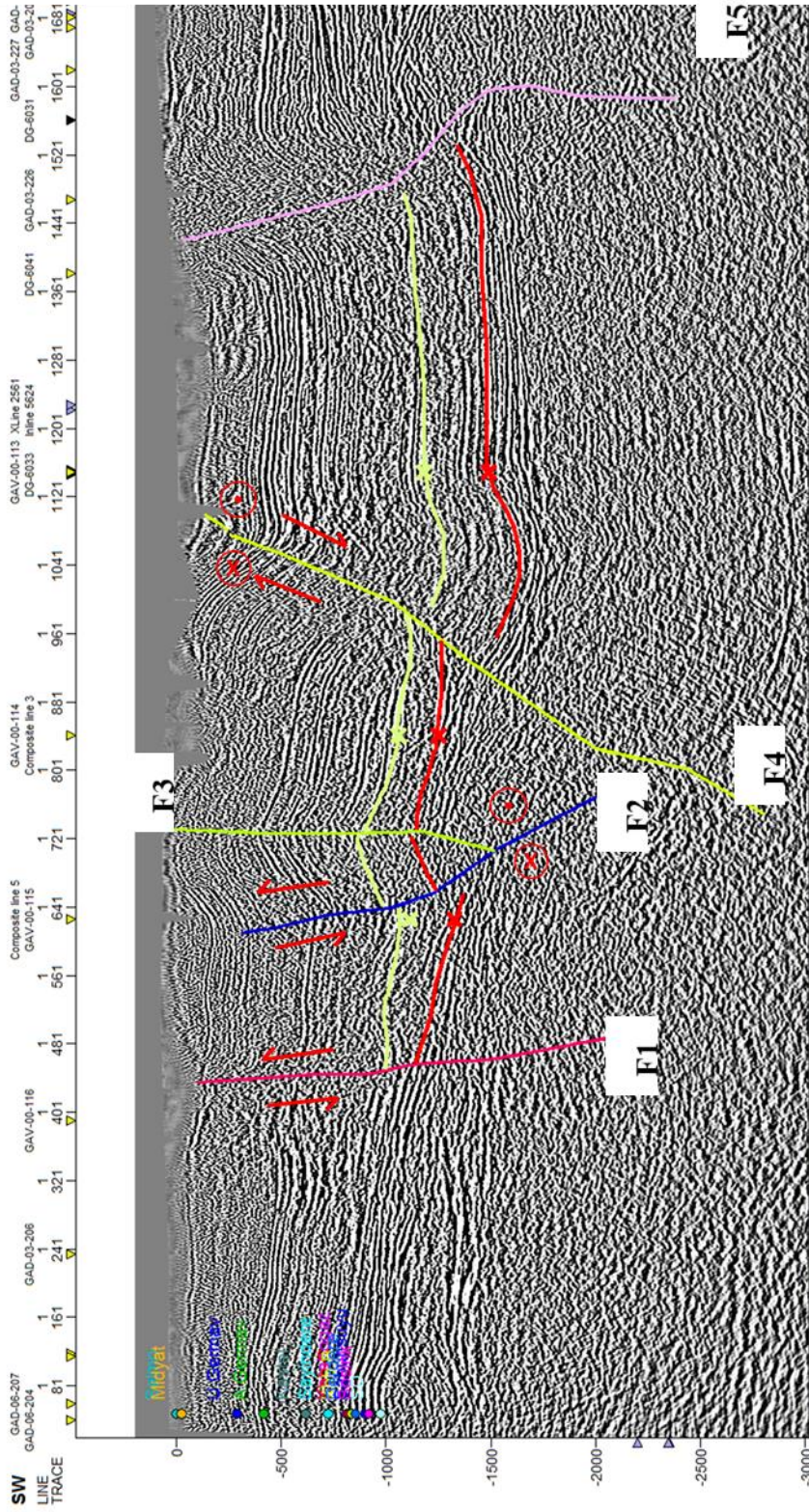


Figure 4.10. Top of the Karababa (red) and Sayundere (green) Formations, and fault interpretation on seismic line AD-00-202.

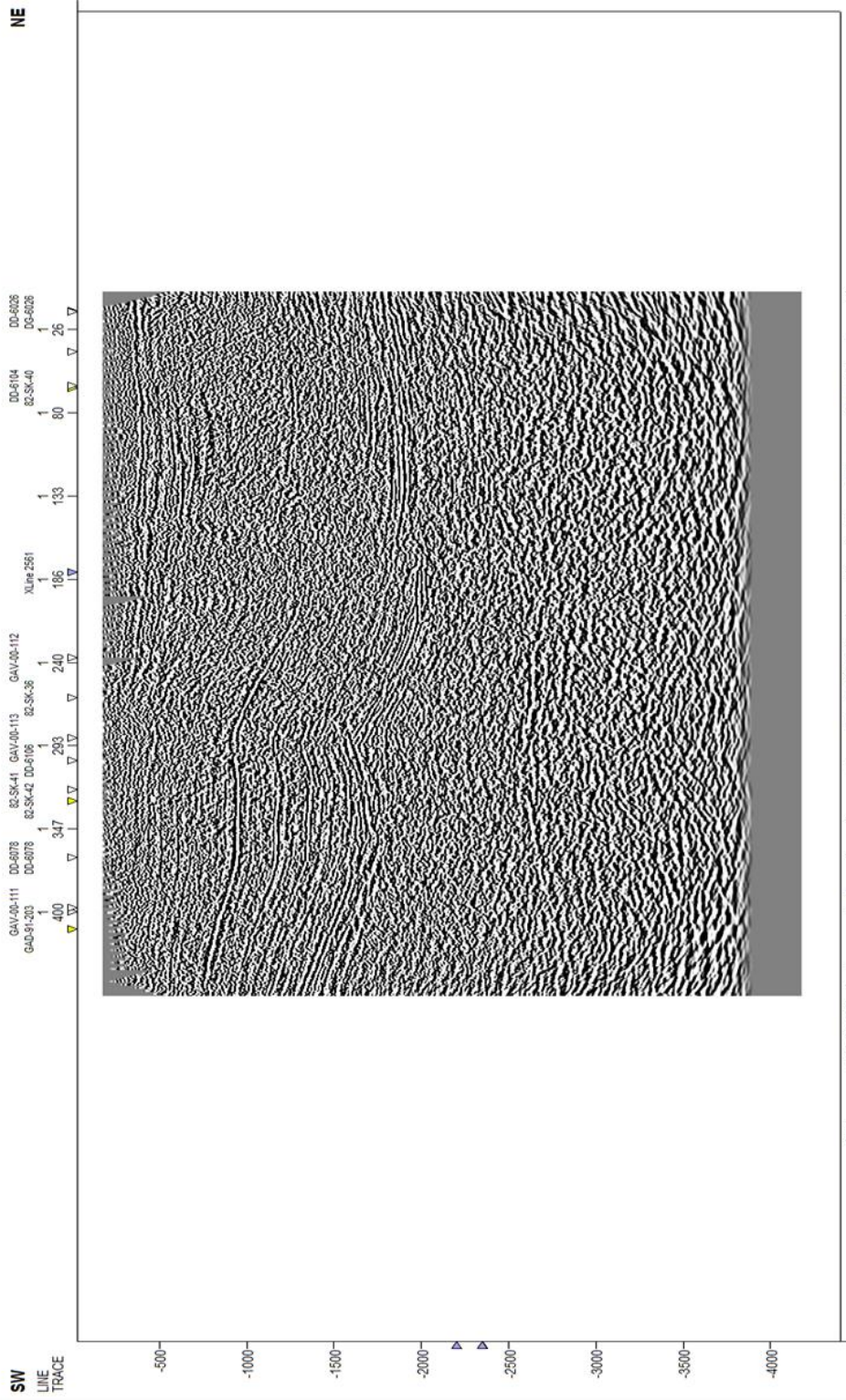


Figure 4.11. Uninterpreted seismic section D-6071 (migration). See Figure 3.1 for location.

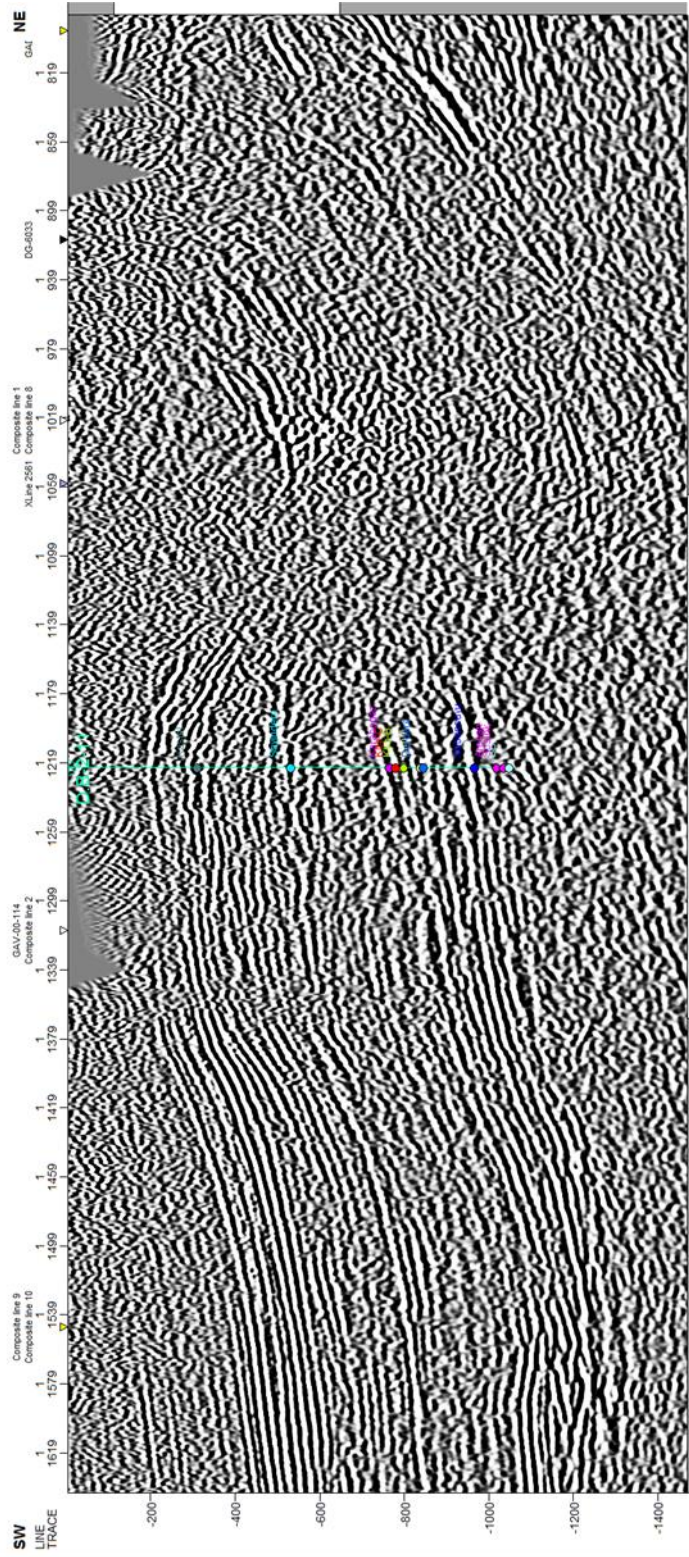


Figure 4.2. Horizon picks based on synthetic seismogram calibrated by sonic log and check-shot data on well D.B-2 on seismic section line AD-03-229. Formation tops are calibrated with well-log information to interpret key horizon levels of top of Gaziantep, Germay, Kastel, Sayindere, Karaboğaz, Karababa, Derdere and other older formations (see Table 3.1 for more information).

Similarly, sharp broken reflections are interpreted as subsurface discontinuities/faults (Figure 4.12). Two steeply-dipping fault segments (F1 and F2 from southwest to northeast) are defined; they dip in opposite directions to northeast and southwest. By means of velocity values gathered from checkshot values, key horizons –tops of the Sayındere and Karababa formations– are interpreted, drawn on the seismic section and integrated with the interpreted fault segments (Figure 4.13). The relative positions of the tops to the two formations on either block of these faults are consistent with minor reverse component. The area between the two faults appears as an antiformal structure; it seems the well BA-1 penetrated the core of this structure. Seismic Line AV-00-110

4.6. Seismic Line AV-00-110

The NE–SW-trending seismic line is oriented almost parallel to the general orientation of the Şambayat Fault, and almost perpendicular to the orientation of the inferred Adıyaman Fault; it passes through the well BA-1 (Figures 3.1, 4.14 and 4.15). The seismic line is therefore forms an ideal section to examine the existence of the Şambayat Fault. Horizons are picked based on synthetic seismogram calibrated by sonic log and check-shot data on well BA-1.

The seismic section is geologically calibrated with well-log information and tops of the Gaziantep, Germav, Kastel, Sayındere, Karaboğaz, Karababa, Derdere and other older formations are interpreted (Figure 4.15). Similarly, sharp broken reflections are interpreted as subsurface discontinuities/faults (Figures 4.15). Two steeply-dipping fault segments (F1 and F2 from southwest to northeast) are defined; they dip in opposite directions to northeast and southwest. The structural pattern of this section is very similar to seismic section DD-6071.

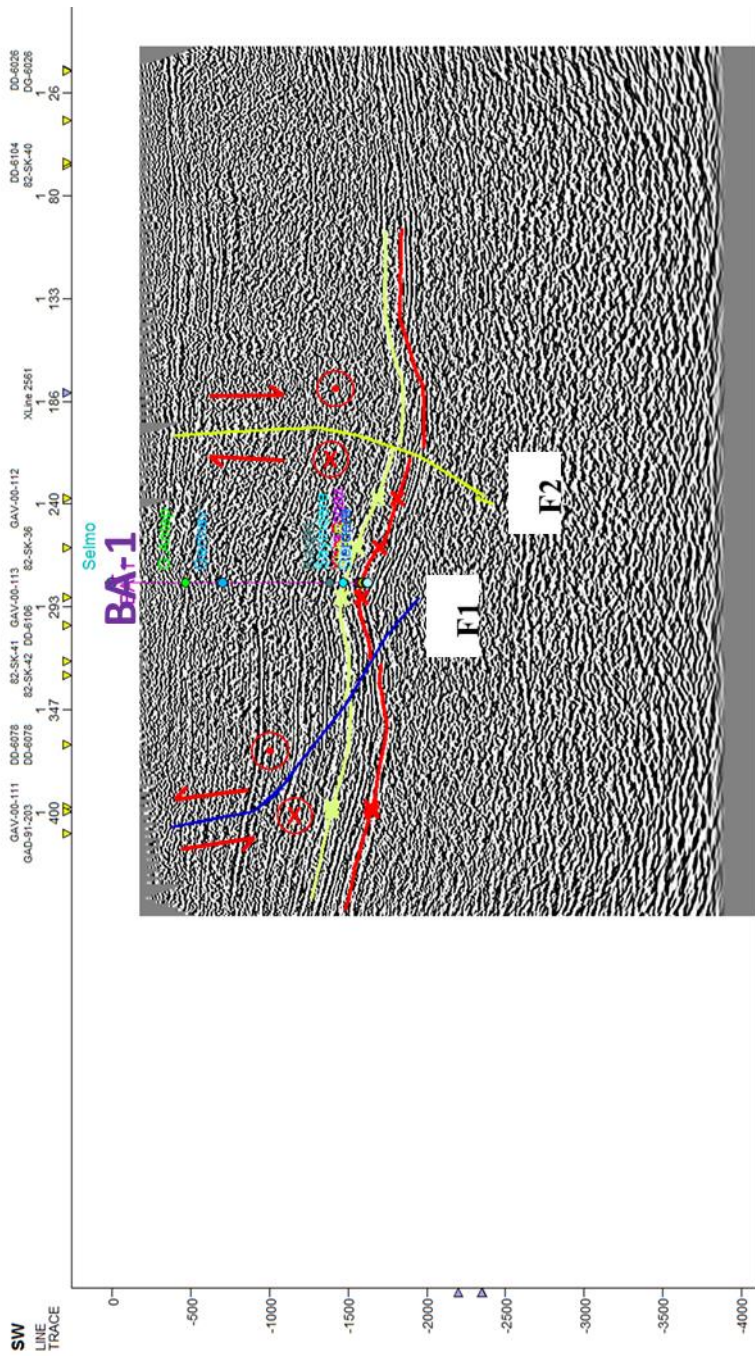


Figure 4.13. Top of the Karababa (red) and Sayndere (green) Formations, and fault interpretation on seismic line D-6071

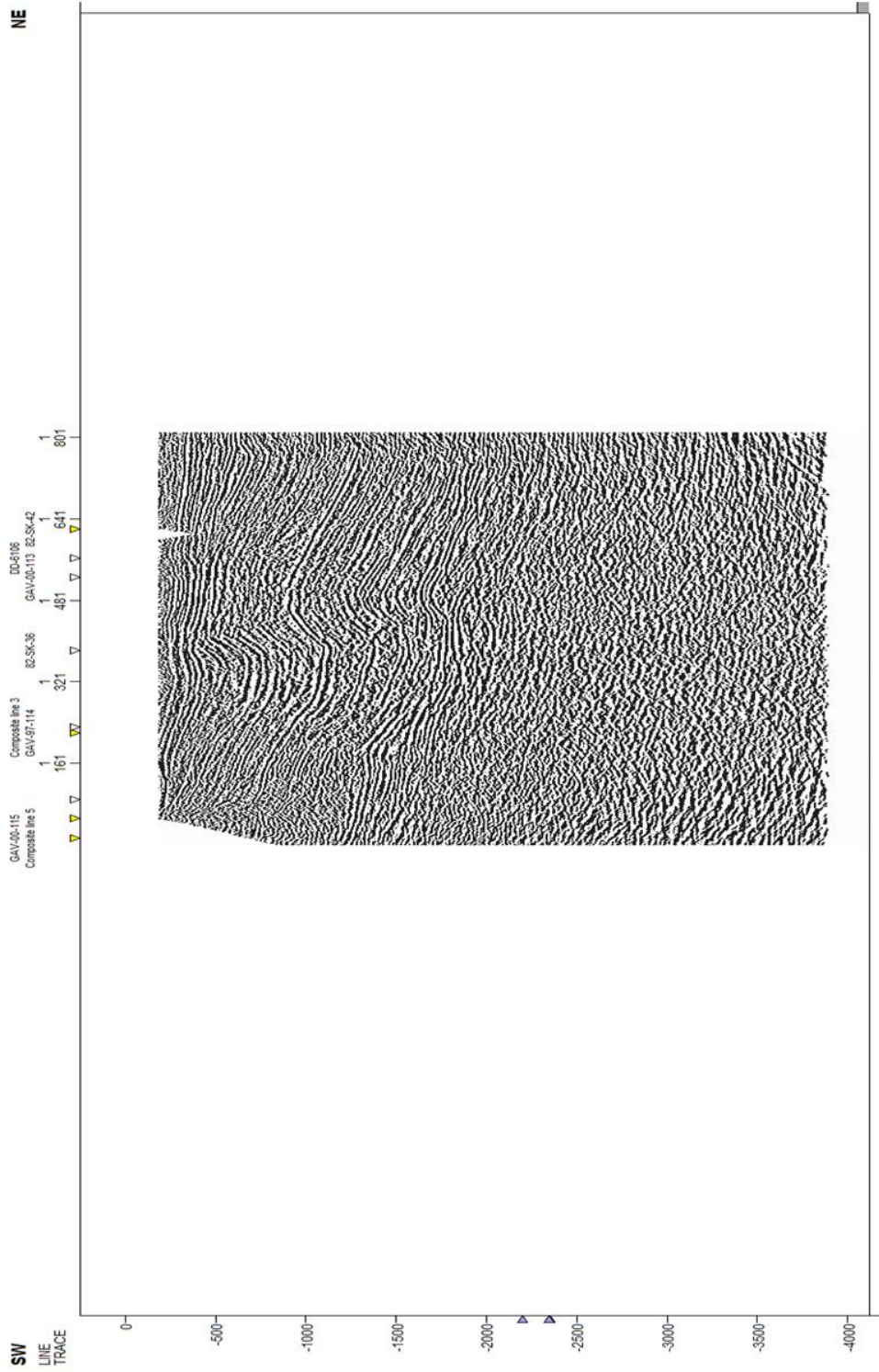


Figure 4.14. Uninterpreted seismic section AV-00-110 (migration). See Figure 3.1 for location.

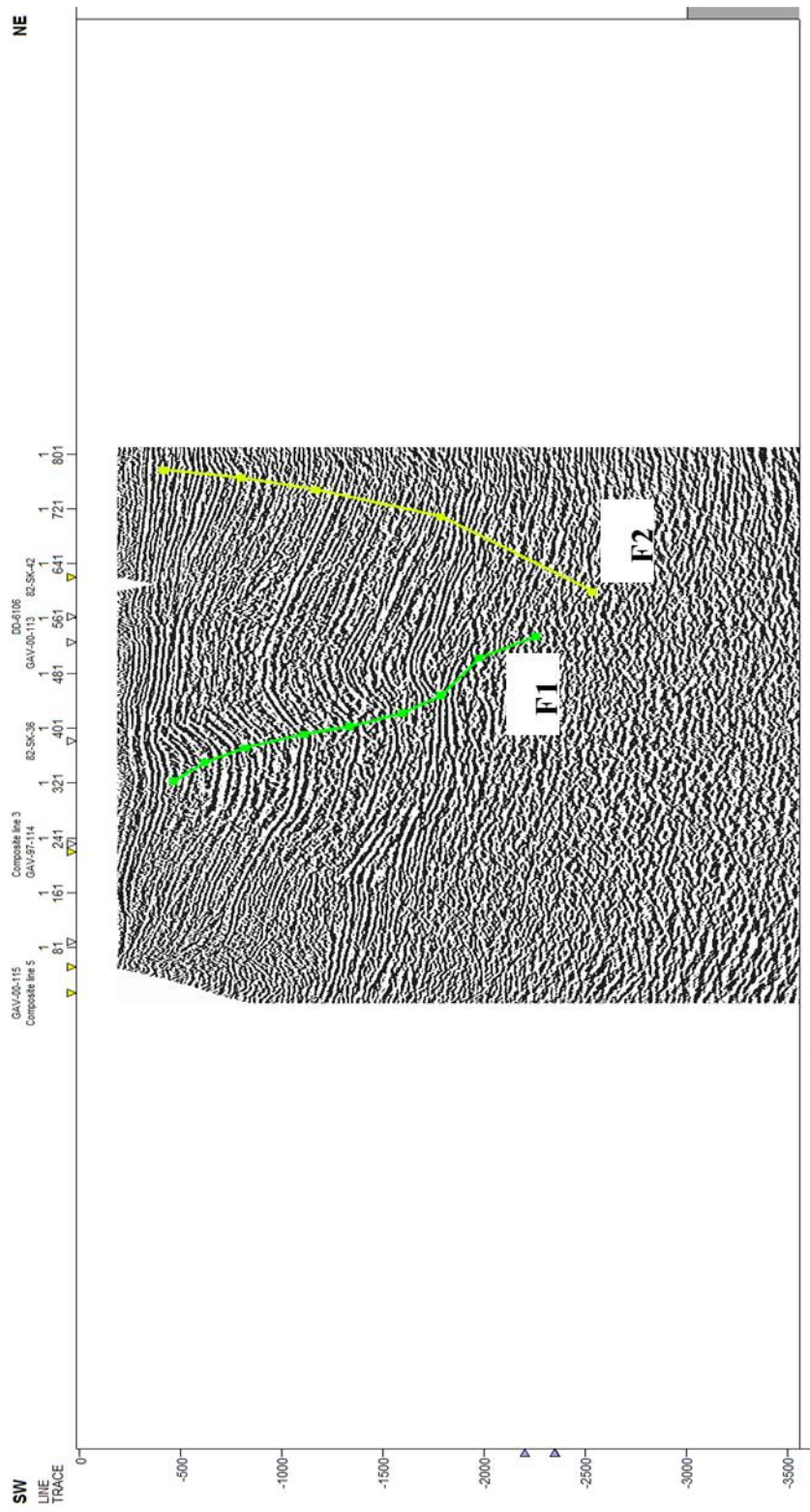


Figure 4.15. Fault interpretation on seismic line AV-00-110.

By means of velocity values gathered from checkshot values, key horizons –tops of the Sayındere and Karababa formations– are interpreted, drawn on the seismic section and integrated with the interpreted fault segments (Figure 4.16). The relative positions of the tops to the two formations on either block of these faults are consistent with minor reverse components. A drag fold in the footwall of the fault F1 is consistent with reverse dip-slip motion.

Geological map (2D image) of different structures interpreted in five seismic sections is prepared. The maps clearly show that segments of the Şambayat Fault are present on either blocks of the Adıyaman Fault. The correlation of these structures displays a fault pattern where the segments of the Şambayat Fault are cut and displaced sinistrally by the Adıyaman Fault (Figures 4.17 and 4.18).

4.7. Seismic Horizon Interpretation

The interpretation of the five seismic sections indicates the fact that sharp broken reflections (that are interpreted as faults) appear to continue from one section to another and they can be correlated (Figures 4.17–4.19). It is therefore possible to transfer these recognizable and continuous reflections on to map(s) through a grid of data. The maps can therefore be effectively used to address the main objectives of the present research.

Picked horizons, tops of the Karababa and Sayındere formations, are also interpolated and converted to surface models. Two-way-time (TWT) maps of these formations, accordingly 3D view maps are prepared by interpretation and interpolation of the available data. TWT maps are also integrated with faults to see vertical displacements.

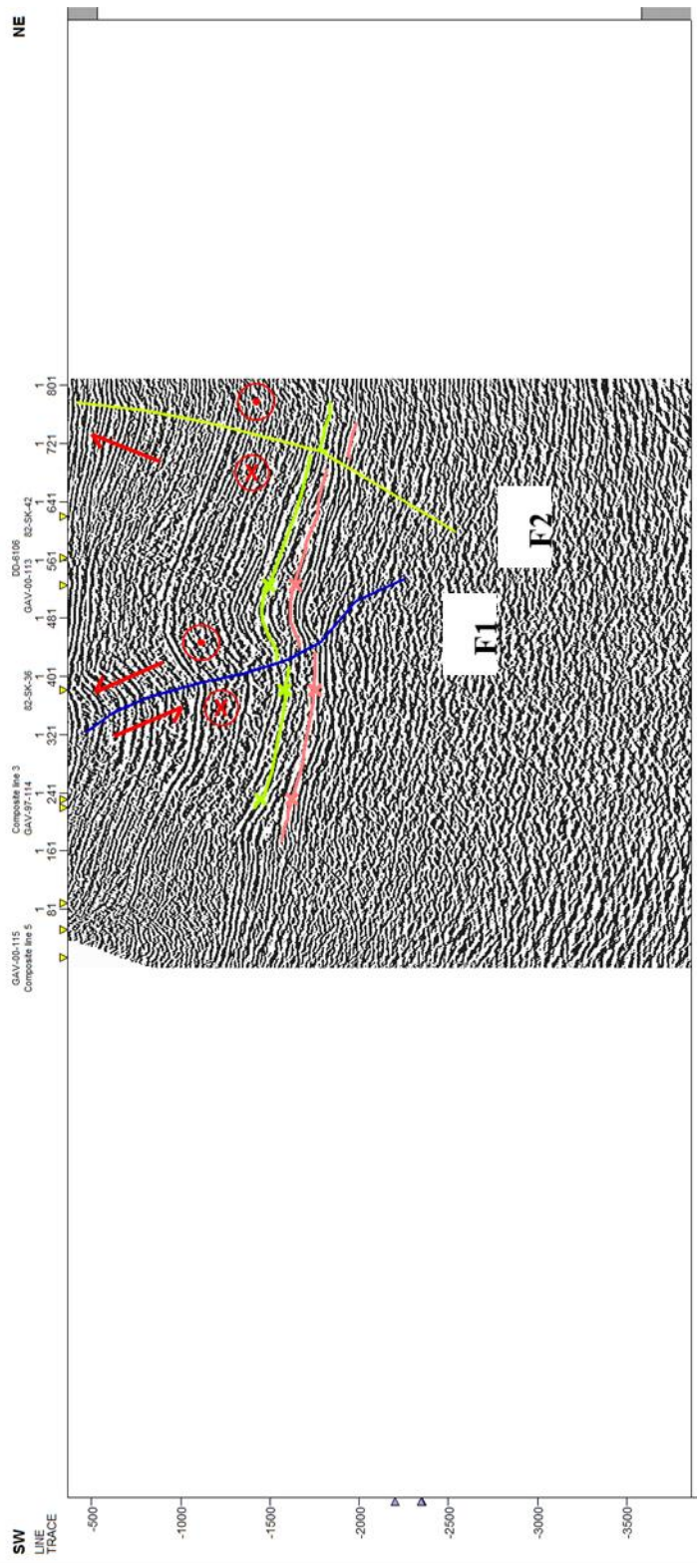
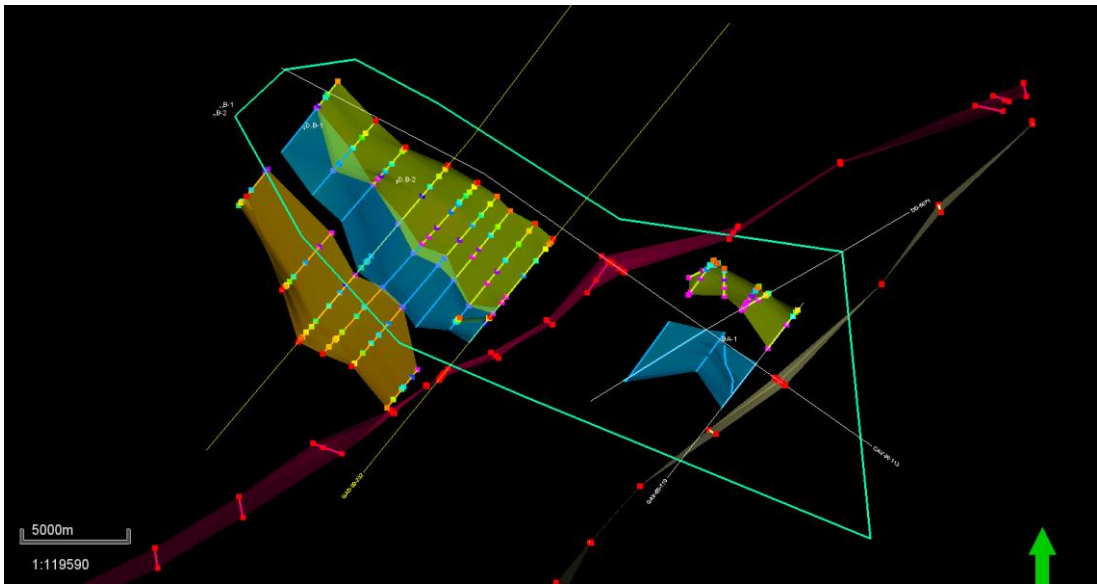


Figure 4.16. Top of the Karababa (red) and Sayndere (green) Formations, and Fault interpretation on seismic line AV-00-110.



Hki wt g'6Ø902D image of the fault planes interpreted in five seismic sections. The correlation of the fault segments (blue and green planes) indicates that the Adiyaman Fault (red) forms a domain boundary between the fault segments. The relative position of the segments is consistent with a sinistral displacement along the Adiyaman Fault.



Hki wt g'6Ø: 02D image of the fault planes on Google Earth™ image. See Figure 4.20 for explanation.

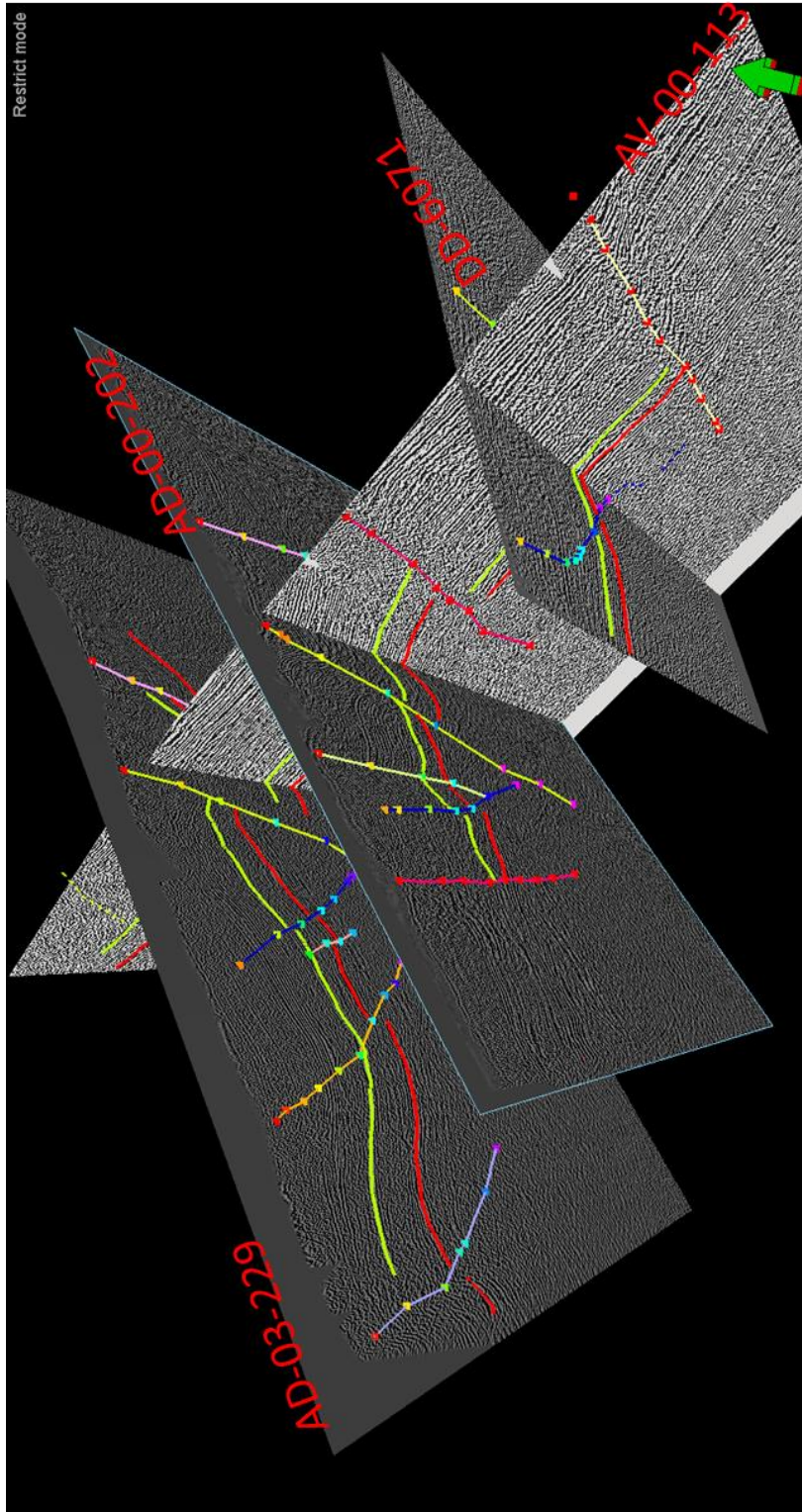


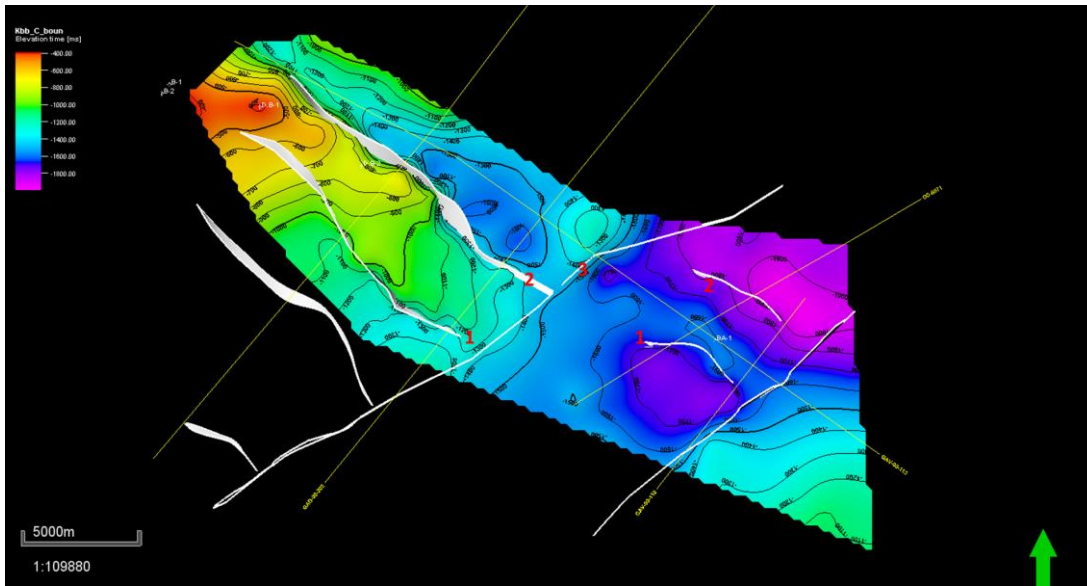
Figure 4.19. The interpretation and correlation of seismic sections analyzed during this research.

Two-way-time (TWT) maps of the Karababa and Sayindere formations are prepared by using 250*250 grid and minimum curvature method. Fault polygons (white) are also created through intersection of the formation and interpreted fault planes in the seismic sections. Contour interval is 100 (Figures 4.20 and 4.21). There is a very good correlation between the TWT contours and the faults; the faults appear to occur where there is a sharp break in contours and/or where contour lines are closer with steeper slope (Figures 4.20 and 4.21).

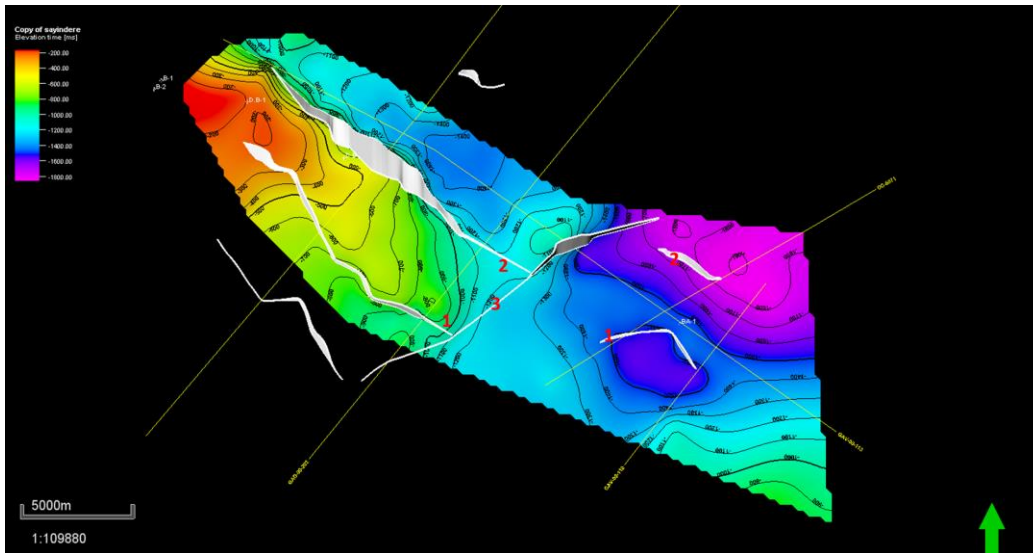
The Adıyaman Fault (AF) is marked by a sudden break in the contour lines and by the juxtaposition of relatively shallow and deep true vertical depths. Similarly, the segments of the Şambayat Fault are also evident in the TWT maps. The relative configuration of TWT contours in the northwestern block of the Adıyaman Fault is consistent with a well-developed pressure ridge between two segments (faults 1 and 2) of the Şambayat Fault (Figures 4.20 and 4.21). The pressure ridge is consistent with the dip-slip reverse component of the Şambayat Fault and confirms interpretation of this structure in seismic sections.

Although TWT contours maps support the existence of the Şambayat Fault in the northwestern block of the Adıyaman Fault, contour pattern in the southeastern block is not supportive (Figures 4.20 and 4.21) because of limited seismic resolution. The TWT maps are also helpful in correlation of the fault segments on either blocks of the Adıyaman Fault.

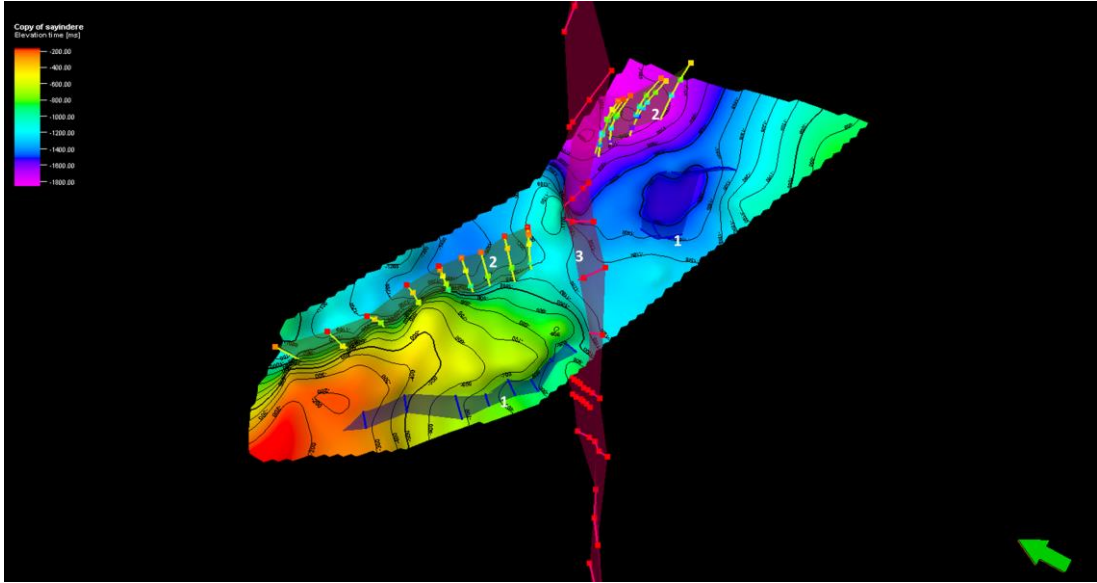
Similarly, the 3D views of the Sayindere and Karababa formations are also prepared (Figures 4.22 and 4.23). These maps confirm the structural pattern devised by TWT maps. The push-up structure is more pronounced; there is a gradual increase in the uplift amount from southeast to northwest. The bounding faults segments of the push-up structure are more pronounced and confirm the existence of the Şambayat Fault. These maps also indicate the fact the TWT values for both formations are much deeper in the southeastern block of the Adıyaman Fault; the fault is more pronounced and easy to trace.



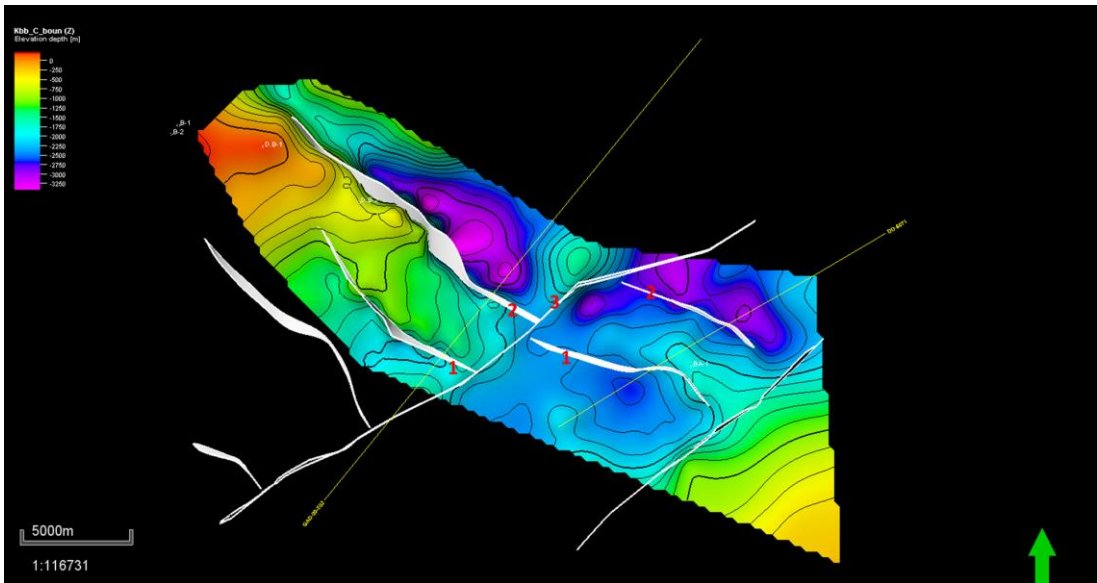
Hki wt g'60420 Two Way Time (TWT) map of the Karababa Formation. Contour interval is 100 m. The white lines show fault planes. Faults 1 and 2 represent the Şambayat Fault, 3 the Adıyaman Fault. Note that the Adıyaman Fault marks a sudden break in TWT contours. Note also that fault segments 1 and 2 in the northwestern block of the Adıyaman Fault bounds an area of low true vertical depths that is interpreted as a push-up structure. The sudden break in TWT contours across the fault segments 1 and 2 of the northwestern block of the Adıyaman Fault is more pronounced, whereas they are not evident in the southeastern block. The fault segment to the east of the Adıyaman Fault may be an artifact of poor seismic resolution."



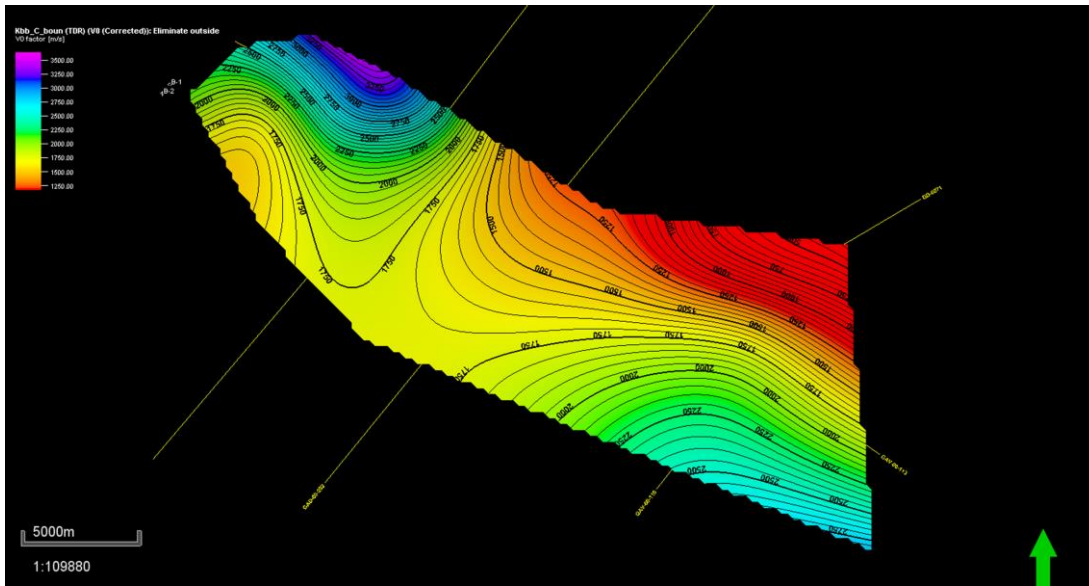
Hki wt g'60430 Two Way Time (TWT) map of the Sayındere Formation. See Figure 4.23 for more information.



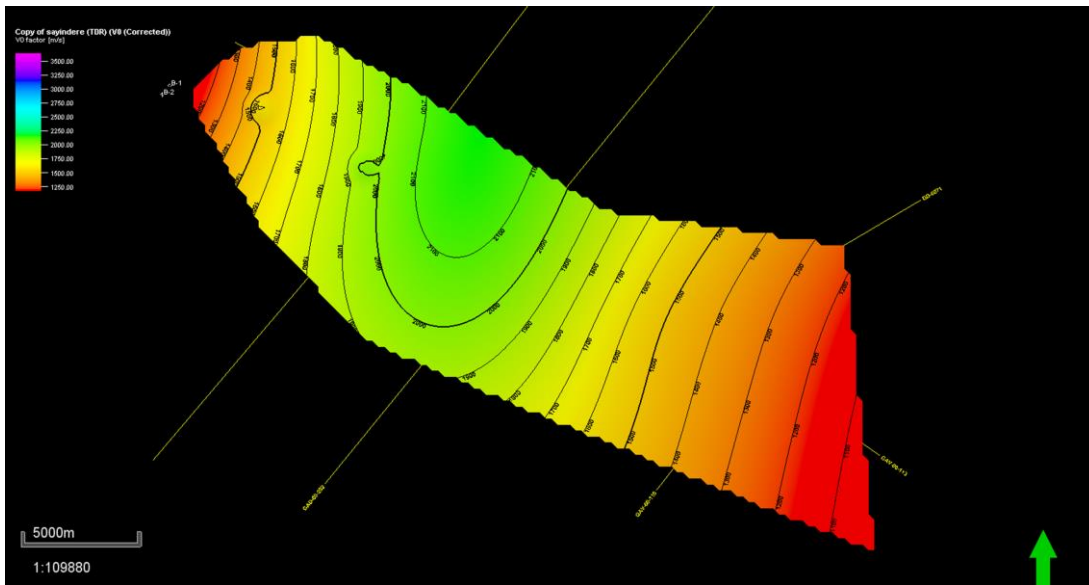
Hki wt g'604403D view of the Sayıdere Formation with seismic sections AV-00-202 and D-6071. See Figure 4.23 for labelling of faults.



Hki wt g'604503D view of the Karababa Formation with seismic sections AV-00-202 and D-6071. See Figure 4.23 for labelling of faults.



Velocity map of the Karababa Formation.



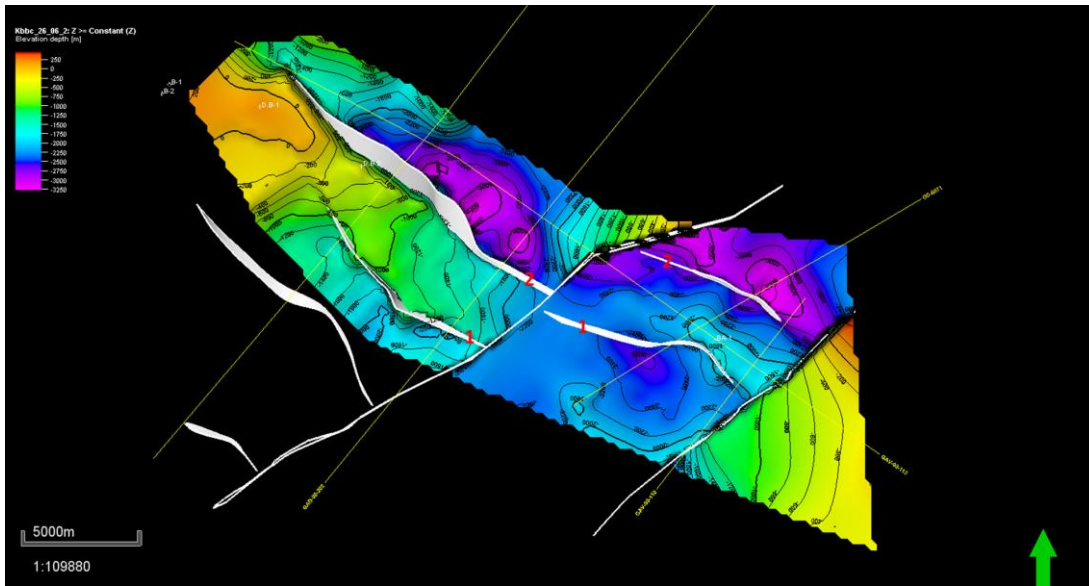
Velocity map of the Sayıdere Formation.

The velocity maps of the Karababa and Sayindere formations are also prepared by using sonic logs and checkshot values of five wells (D.B-1, D.B-2, BA-1, B-1, B-2) (Figures 4.24 and 4.25). These maps are in fact used in the preparation of the structural maps for both formations (Figures 4.26 and 4.27) (see section 3.1.3 for more information). The fault polygons (white) are created by the intersection of the formations and fault planes. 250*250 grid and minimum curvature method is used to prepare structural contour maps of the Karababa and Sayindere Formation. Contour interval is 100 m.

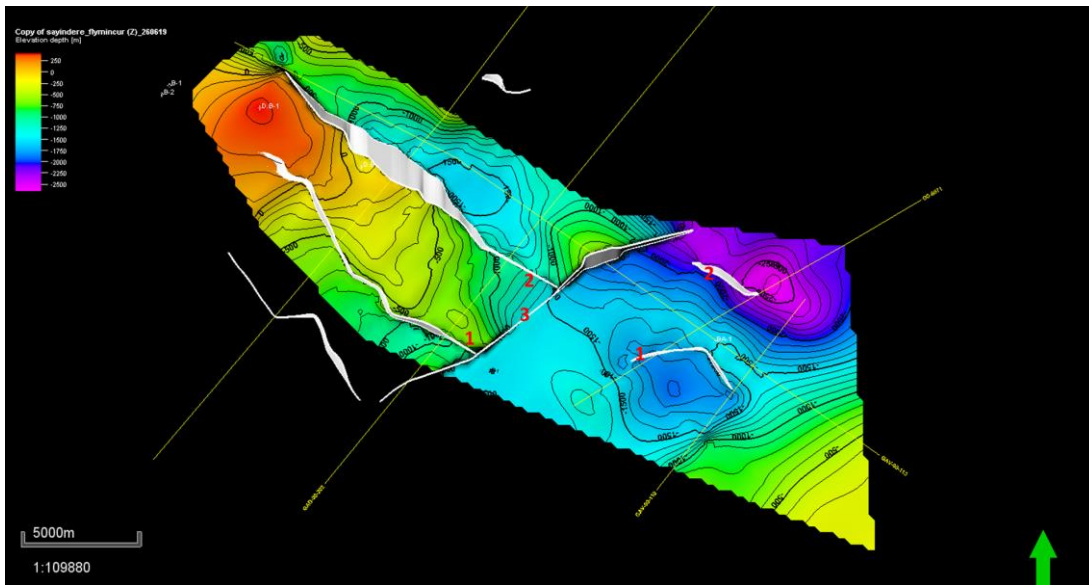
The structural map of the Karababa Formation (Figure 4.26) clearly shows that the fault segments 1 and 2 bounds an uplifted area (push-up structure) in either blocks of the Adıyaman Fault. The push-up is more pronounced in the northwestern block than the southeastern block. Similar observation can be communicated for the structure map of the Sayindere Formation but the push-up structure in the southeastern block of the Adıyaman Fault appears relatively weak (Figure 4.27). Nevertheless, these maps also indicate that correlation of these faults segments in either block of the Adıyaman Fault is sound. The sinistral displacement of the fault segments and push-up structure along the Adıyaman Fault is therefore evident.

It is attempted to calculate the vertical displacements of the fault segments 1 and 2 on either blocks of the Adıyaman Fault. To avoid effect of Şambayat Fault, the vertical displacement of the lower parts of fault segments are correlated. For Karababa Formation, on the northwestern block of the Adıyaman Fault, the vertical displacement of fault 1 is 320 m – 340 m, respectively. Similarly, the displacements of fault 2 in the southeastern block are 370 m – 380 m, respectively. For Sayindere Formation, on the northwestern block of the Adıyaman Fault, the vertical displacement of fault 1 is 430 m. Similarly, the displacements in the southeastern block are 450m (Figures 4.28 and 4.29).

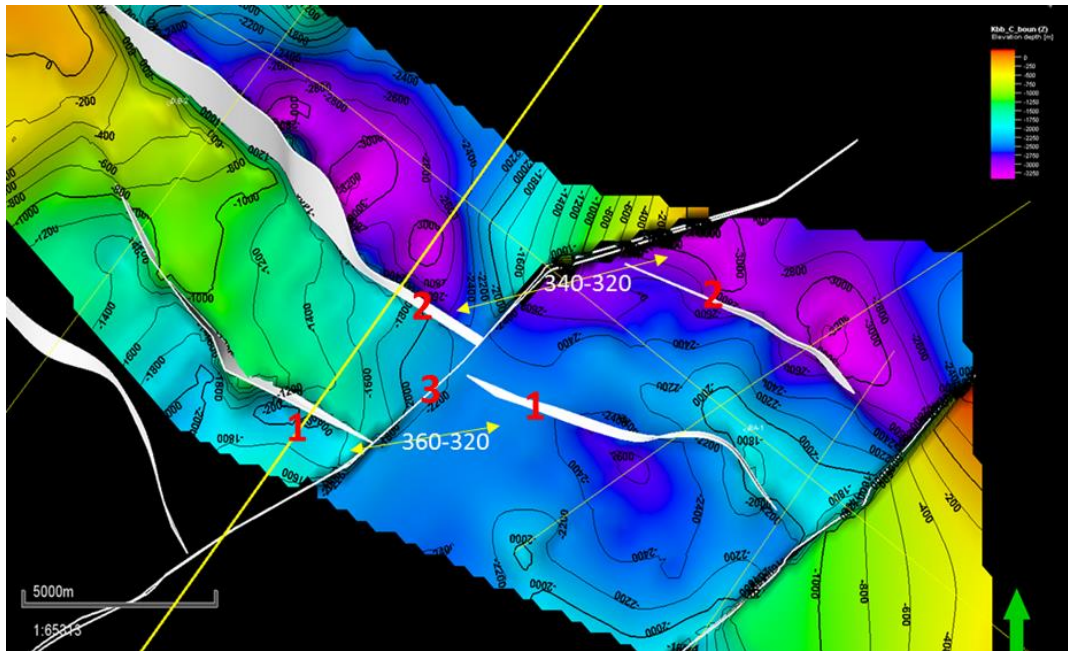
"



Hki wt g'60480 Structure map of the Karababa Formation. See Figure 4.23 for labelling of faults.



Hki wt g'60490 Structure map of the Sayindere Formation. See Figure 4.23 for labelling of faults



Hki wt g'60A:. Structure map of Karababa Formation, showing vertical displacements. See Figure 4.23 for labelling of faults. The vertical displacement amount is varying from 320–340 at northern part of Şambayat Fault and it is varying from 320–360 at Southern part of Şambayat Fault at the man of the top of Karababa Formation.

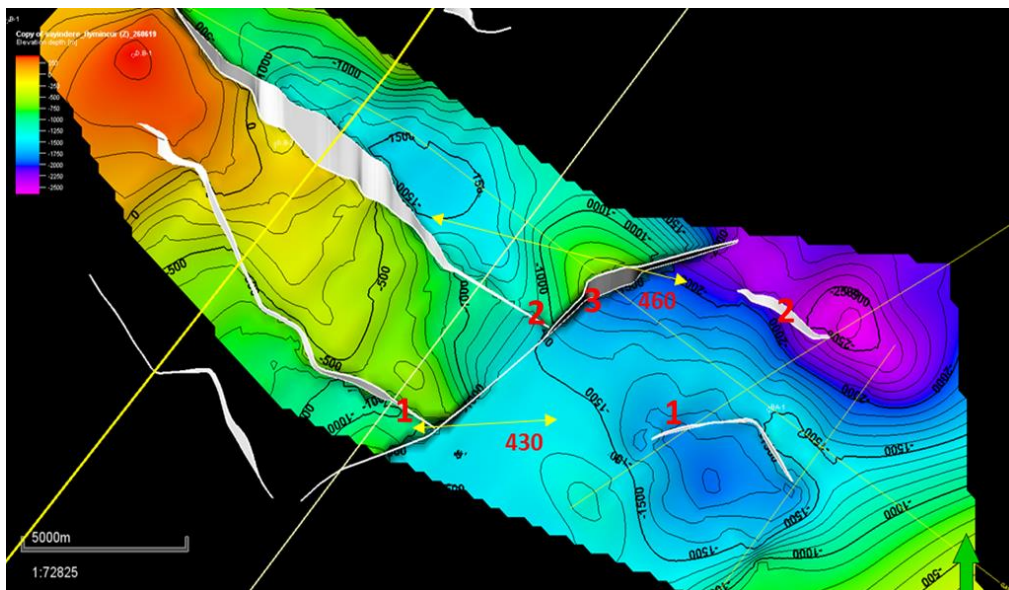


Figure 4.29. 'Structure contour map of top of Sayindere Formation. The vertical displacement amount at the northern part of Şambayat Fault is about 460m. The displacement amount at the Southern part of Şambayat Fault is 430 m. the difference between Karababa Formation and Sayindere Formation vertical amounts is caused by the distance between Seismic sections that is called seismic resolution. If Seismic is 3D the results could be more similar to each other.

The calculated vertical displacement values are not accurate because 2D seismic sections are employed as there is no 3D section. And there is no real measured data to test the calculated values. These values are therefore all extrapolated data and should be considered as approximate values. The most realistic value for the vertical displacement of the Adıyaman Fault is 320–360 m because these data are least affected by the Şambayat Fault. These observations confirm that there is considerable amount of reverse motion along the Adıyaman Fault.

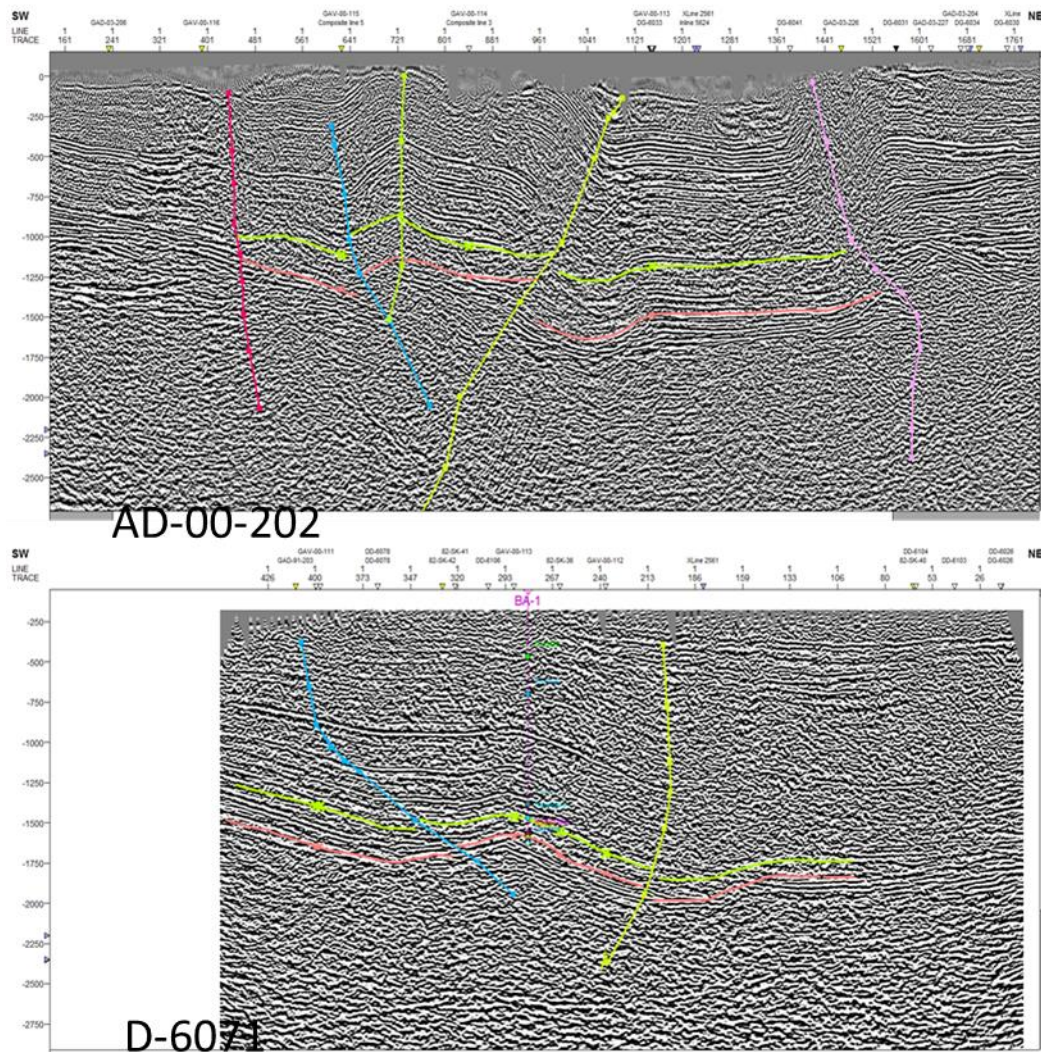
The results of the seismic interpretation also suggest that the depositions of the Coniacian–Santonian Karababa and the Campanian Sayındere Formation are controlled by Şambayat Fault and that the basin depth is not equal between the opposite sides of fault (Figure 4.30).

Similarly, the amount of sinistral displacement along the Adıyaman Fault is calculated, based on the relative configuration of fault segments 1 and 2 on either blocks of the fault, as about 4400 m. This approach is based on the interpretation that similarly trending faults in both blocks of the Adıyaman Fault are exactly the same structures.

4.7. Ground Truthing

Once the seismic sections are interpreted, the study area is visited to relate the described structures to real features on the ground. The lineament of the Adıyaman Fault can be visualized on a relief map (Figure 4.31). The fault has a linear trend in the area between Kutluca in the southwest and Çaltılı in the northeast. Alidağ pressure is regarded as an important structural element of the fault and can easily be distinguished on this relief map.

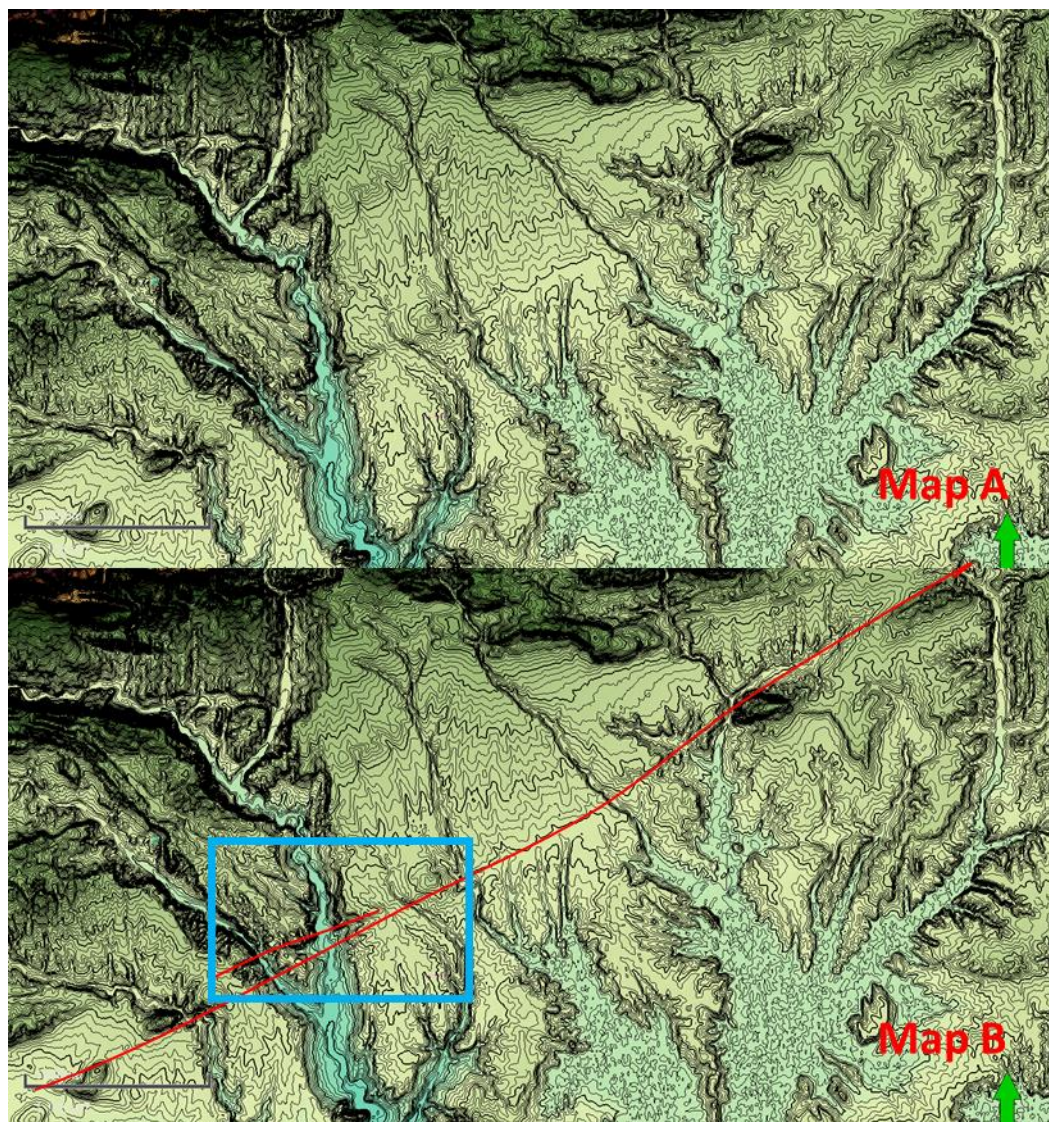
Despite of the Adıyaman Fault, the Şambayat Fault has no surface expression and it cannot be traced in the field.



Hki wt g'60520 These sections, which are at the opposite side of Adıyaman Fault, shows that the Sayındere Formation is syntectonic. The formation is thicker in the North and South of the Şambayat Fault. This proves that they are the same fault.

During field studies, a special emphasis is given to find/observe geological evidence of the Şambayat Fault; but this was almost not possible because the Adıyaman Fault area is mostly covered by upper Miocene–lower Pliocene Şelmo Formation and/or loose continental sediments of Plio–Quaternary age (Figure 4.32). The geological evidence is therefore none or scarce. Even if there is evidence, it must have been buried beneath younger sediments. The recognition of the Adıyaman fault and

calculation of its sinistral displacement are therefore solely based on seismic interpretation.



Hki wt g'6030(a) Relief map showing the surface expression of the Adiyaman Fault. Note the pronounced linear trace of the fault; (b) the interpretation of the DEM map; the red lines represent the Adiyaman Fault. Blue rectangle indicates location of the study area.”

The geological map of the Adiyaman area is therefore revised in-line with the information gathered from the interpretation of five seismic lines; two field studies

have been performed to investigate and map the faults in the region. First took four weeks and the second, a week. Field mapping was performed to verify the revised geological maps, lithostratigraphy of the region and to collect structural data (bedding and fault-slip data). During this study, contacts between several rock units are checked, the dip-strike of the exposed fault planes are measured, slip sense on slickenlines of fault planes (pitch/rake) are determined. The geological map of the study area is finally verified and revised (Figure 4.32). The results of this part of the research lie outside the scope of the present thesis and therefore they are not presented here.

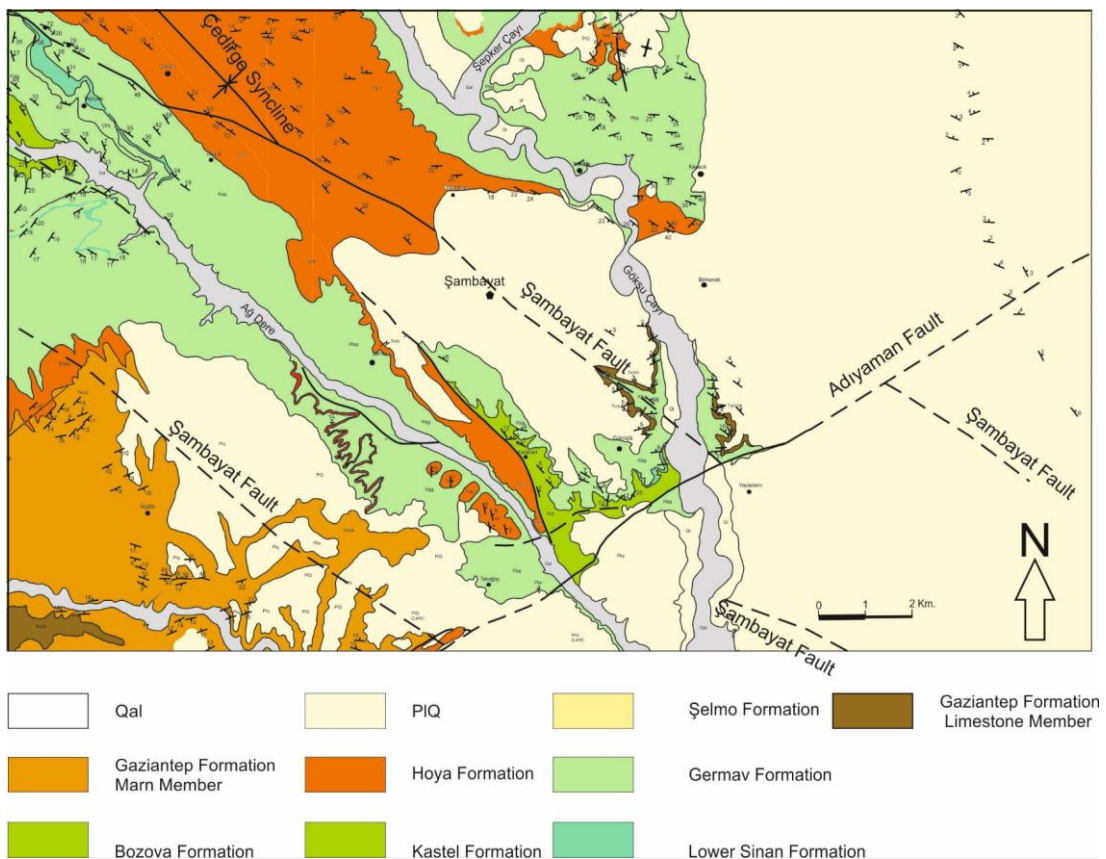


Fig. 4.32 Geological map of the study area (from Aksu et al., 2012). The faults are modified during this fieldwork. The trace of the Şambayat Fault is placed according to field observations and seismic interpretation. Qal– Quaternary alluvials, PIQ– Plio–Quaternary loose sediments.

The trace of the Şambayat fault is therefore mapped for the first time during this study (Figure 4.32). The fault trace runs through exposures of Sinan, Germav and Hoya formations. There appears the fault does not affect the upper Miocene–lower Pliocene Şelmo Formation and/or Plio–Quaternary loose sediments. In addition, Çedirge syncline terminates against Şambayat Fault (Figure 4.32). There is however no apparent offset of the formation boundaries. The Germav and Hoya formations are exposed within the valley but not offset is also observed. These observations confirm that the Şambayat Fault is an older structure; it was initially active during sedimentation of the Campanian Sayındere Formation. The fault was then reactivated during Early Miocene. Because upper Miocene–Early Pliocene Şelmo Formation and younger loose sediments display no evidence of deformation, it would not be possible to comment on the recent activity of the Şambayat Fault.



Figure 4.32 Google Earth™ image showing Şambayat Fault (green), Adıyaman Fault (red), Halfeti Fault (blue) and Bozova Fault (purple).

Şambayat Fault and Bozova Fault appear as parallel structures (Figure 4.33). In this case, the results of this thesis seem to be consistent with the hypothesis by Sungurlu (1972); he stated that the Bozova Fault has controlled deposition of the rock units during Coniacian–Santonian time interval and that it was reworked as a normal fault during the Miocene. Whereas Perinçek et al. (1987) reinterpreted the Bozova Fault as strike-slip fault with reverse component.

CHAPTER 5

DISCUSSION AND CONCLUSION

The primary objectives of the present research are: (i) to introduce and provide evidence for the existence and age of the inferred Şambayat Fault (ŞF); (ii) to map and define the previously unknown Şambayat Fault, (iii) to investigate the relationship between the Şambayat Fault and the Adıyaman Fault (AF) and (iv) to calculate the total amount of offset along the Adıyaman Fault.

The simplest and the cheapest way of addressing all of these questions may rely on field geology method to study the geological structures and their relationships with the lithological units. The area of the inferred Şambayat Fault and the Adıyaman Fault in this particular locality is largely covered by upper Miocene–lower Pliocene Şelmo Formation and/or Plio–Quaternary loose sediments and there is no such geological and pronounced morphological evidence that supports the existence of faults.

The existence of ~E–W-trending blind thrusts (e.g., Çakırhüyük blind thrust, Araban blind thrust, Yavuzeli blind thrust and Gemrik-Karababa blind thrust) is reported in the region to the south of the study area (Şahbaz and Seyitoğlu, 2018). The asymmetric anticlines (e.g., Faldağı anticline, Suvarlı anticline, Karadağ anticline; Figure 1.5) are interpreted as surface expression of the blind thrusts. As the Şambayat Fault is also a buried structure, its nature and geometry are further examined. Neither field observations nor geological maps (Figure 4.18 and 4.32) confirm the existence of anticline in the area.

TPAO has five 2D seismic sections in the area of interest. In order to address the main objectives of this research, structural interpretation of five 2D seismic sections are

carried out. The logs of five boreholes are carefully examined and evaluated; they are used in geological calibration of the 2D seismic sections. Coniacian–Santonian Karababa and Campanian Sayındere formations are considered as reservoir and cap rocks, respectively, of the naturally fractured Şambayat field. By the help of calculated check shot values, the formation well tops can be calculated and shown on seismic sections. The tops of these formations are picked as stratigraphic horizons and, are interpolated and converted to surface models. True vertical depths to the two formations are therefore calculated; this data is used to develop TWT maps, 3D views and structural maps of these formations.

Sharp broken reflections are interpreted as faults. The interpreted faults and various maps of the Karababa and Sayındere formations are integrated to develop structural models and to calculate vertical displacements along these fault segments.

The fault interpretation of the seismic sections indicates existence of an unknown fault(s) within the study area; this structure is herein named as Şambayat Fault (ŞF). It is interpreted as one of the major structural elements of the Adıyaman region. The fault is mapped and described for the first time in this study (Figure 4.32). The Şambayat Fault is a NW–SE-trending structure that parallels the Bozova Fault. It is made up of several parallel fault segments with differing dip-direction (Figures 4.4, 4.7, 4.10, 4.13, 4.16–4.19, 4.20–4.23, 4.26, 4.27 and 4.28). The different segments of the Şambayat Fault also controls a push-up structure in both blocks of the Adıyaman Fault and this is manifested by variation in true vertical depths to the tops of the two formations (Figures 4.20–4.23, 4.26, 4.27 and 4.28). The presence of similar push-up structures on both blocks of the Adıyaman Fault made it possible to correlate push-bounding fault segments, and in turn, to calculate the offset amount along the Adıyaman Fault. Şambayat Fault is therefore cut and displaced by the Adıyaman Fault; this is used as a firm evidence to comment on the offset amount along the Adıyaman Fault, which is calculated about 4.4 km (Figures 4.17–4.19).

The structural maps of the Sayındere and Karababa formations are also prepared as these maps are simple multiplication of velocity and TWT maps that are obtained by seismic interpretation method. The structural maps are used to calculate vertical displacement of the segments of the Şambayat Fault along the Adıyaman Fault. There appear differences in displacement amounts for different segments of the Şambayat Fault on either blocks of the Adıyaman Fault (Figure 4.28); this discrepancy is attributed to the 2D nature of the seismic data; if 3D sections are available, the results would have been closer. The TWT maps of the Karababa and Sayındere formations shows that vertical displacements of two formations along the Adıyaman Fault are about 320–360 m and 420–460 m, respectively and that the Adıyaman Fault has a considerable amount of reverse component.

The Şambayat fault and Bozova Fault are interpreted to control an uplifted area during Cretaceous, has then controlled the Coniacian–Campanian sedimentation of the Karababa and Sayındere formations. As a result, the thickness of the Sayındere appears different in either blocks of the Adıyaman Fault whereas thickness of the Karababa Formation seems to be the same. That is why, the displacement amount of the Karababa Formation (320–360 m) is interpreted as the vertical displacement of the Adıyaman Fault. The variation in thickness of the Sayındere Formation on either blocks of the Adıyaman Fault is interpreted to provide firm evidence about the geometry, age and evolution of the Şambaya fault. Thus, it is thought that if variation and change in thickness of the Sayındere Formation on opposite sides of the Adıyaman Fault is well documented, it may give clues to recognize and map the Şambayat Fault. The interpretation of the seismic sections has focused on this topic. The Sayındere Formation is therefore interpreted as syn-tectonic with respect to the activity of the Şambayat fault. In addition, Şambayat fault was reactivated during the Early Miocene, because Şambayat fault on map view (Figure 4.32) appears to cut and deform the Eocene Hoya Formation and Oligocene Gaziantep Formation but not the upper Miocene–lower Pliocene Şelmo Formation and/or Plio–Quaternary loose sediments.

At the end of the research, the study area was visited for ground thruthing. The geological map of the area is therefore revised and the traces of the Şambayat fault is mapped (Figure 4.32). The southern continuum of the Şambayat fault within the Plio–Quaternary loose sediments was not possible to trace on the ground. Similarly, the recognition of fault within the marl facies of the Gaziantep Formation was not possible as well.

The TWT maps, 3D views and structure maps of the Karababa and Sayindere formations therefore confirm that: (i) the Şambayat Fault is tectono-sedimentary fault for the Campanian Sayindere Formation, it appears thicker along the northern part of the fault on seismic sections AV-00-202 and D-6071; (ii) the fault must therefore was active during at least Campanian. In addition Germav, Hoya, Gaziantep formations are affected by the Şambayat fault but not the upper Miocene–lower Pliocene Şelmo Formation and the Plio–Quaternary terrestrial loose sediments. This relationship is interpreted to suggest that the Şambayat fault was reactivated possibly during at least Early Miocene but its recent activity is debated; (iii) the fault segments 1 and 2 on either blocks of the Adıyaman Fault represent the Şambayat Fault and they bound a pronounced push-up structure; (iv) these segments have a reverse component; (v) they are cut and displaced by the Adıyaman Fault where the amount of sinistral offset is about 4400 m; and (vi) the southeastern block of the northwesterly-dipping Adıyaman Fault appears as the downthrown block, thus confirming sinistral and reverse nature of the Adıyaman Fault.

The results of the present study need to be tested by new and possible 3D seismic sections and their structural interpretation

REFERENCES

- Açıkbaş, D. & Baştuğ, C. (1975). V. Bölge Cacas-Hani yöresi kuzey sahalarının jeoloji raporu ve petrol olanakları. *VRCQ'Tgrqtv'Pq<'39"*
- Açıkbaş, D., Sungurlu, O., Akgül, A., & Erdoğan, T. (1979). Geology and petroleum possibilities of Southeast Turkey. *VRCQ'tgrqtv'pq<'3632"*
- Açıkbaş, D., Akgül, A., & Erdoğan, L. T. (1981). Güneydoğu Anadolu'nun hidrokarbon olanakları ve Baykan-Şirvan-Pervari yöresinin jeolojisi. *VRCQ" tgrqtv'pq<'3765*
- Agard, P., Omrani, J., Jolivet, & L., Mouthereau, F.(2005). Convergence history across Zagros (Iran), Constraints from collisional and earlier deformation. *İpvtpcv'qpcn'Lqwtpcn'qhl'Gctvj "Uekpegu"; 6(3), 401-419*
- Ahmed, R. (1975). Geology of the area Southwest of Dicle (Diyarbakır-Turkey). *VRCQ" Gzr'qt cvkqp'I tqwr "Tgrqtv'Pq0'; ; 6, 48*
- Akarsu, İ. (1968). V. Bölge Cizre-Şırnak-İdil-Midyat ve Nusaybin çevresinin Petrol imkanları. *VRCQ"Gzr'qt cvkqp'Tgrqtv'Pq0648, 24*
- Aksoy, E., İnceöz, M. & Koçyiğit A. (2007). Lake Hazar Basin: A negative flower structure on the East Anatolian Fault System (EAFS), SE Turkey. *Vwtnkuj " Lqwtpcn'qhl'Gctvj "Uekpegu"38, 319–338.*
- Aksu, A. (1980). *Ncv" S wvgt'pct{" Ut cvki tcrj {" Rcrwgqgpxkt qpo gpvqrqi {" cpf " Ugf ko gpvc'kqp" J kvqt {" qh' Dc'hlk" Dc {" cpf " F cxku" Ut ck0 (Ph.D.), Dalhousie University, 771 pp.*
- Aksu, R. & Mülayim, O. (2015). Adıyaman ve Çevresinin Jeolojisi Teknik Gezi Kilavuzu, *VRCQ"Gzr'qt cvkqp'I tqwr "Tgrqtv'Pq<'7792. 22-23*
- Aksu, R.,& Durukan B.A. (2014). Adıyaman Bölgesi Geç Kretase İstifindeki Yeni Bulgular Ve Öneriler. *VRCQ'Ctco c'Fckg'Dc m'pn , "Ct k'k" Tcrqt'pq<'7724"*
- Aksu, R. (2016). *Vj g'İpvt c/Rj cvg'kp'vj g'Uqwj gcwgt'p'Cpcvqrk0* The Eocene Tectonics. Paper presented at 69th Geological Congress of Turkey, 548-549
- Aktuğ, B., Özener, H., Dogru, A., Sabuncu, A., Turgut, B., Halicioğlu, K., Yılmaz, O. & Havazlı, E. (2016). Slip rates and seismic potential on the East Anatolian Fault System using an improved GPS velocity field. *Lqwtpcn'qhl'I gqf {pco keu" ; 6/; 7,1-12*
- Ala, M.A. and Moss, B.J. (1979). Comparative petroleum geology of southeast Turkey and northeast Syria. *Lqwtpcn'qhl'Rgt qrgwo 'I gqrqi {" :3*6± 3–27.*

- Alavi, M. (1994). Tectonics of the Zagros orogenic belt of Iran: new data and interpretations. *Vgevpqrj {ukeu'44; (3-4), 211-238*
- Allen M. B. & Armstrong H. A. (2008). Arabia-Eurasia collision and the forcing of mid-Cenozoic global cooling. *Rcrwgqi gqi tcrj {." Rcrwgqerko cvqrji {." Rcrwgqgeqrji { '487, 52-8.*
- Altinli, İ. E. (1952). Siirt Güneydoğusunun Jeolojik İncelenmesi. *OVC"Trqt"Pq<" 3; 99"*
- Amaco, (1985) Turkey ESRI report no. ET 85/1 geological studies in SE TURKEY (Pervari- Beytüşşebap, Hazro, Mardin). *VRCQ"Gzrrqtcvkqp" I tqwr" Tgrqtv0437, 214*
- Araç, M. & Yilmaz, E. (1991). XI ve XII. Bölge Güneyindeki Kuyularda Kesilen Cudi ve Mardin Gruplarının Sedimantolojisi ile Fasiyes Diyajenez ve Rezarvar Özellikleri. *VRCQ"Ctckwko c'Trqtv0'Pq03937, 1-32*
- Arpat, E., & Şaroğlu, F. (1972). Doğu Anadolu Fayı ile ilgili bazı gözlemler ve düşünceler. *OVC'Fgti kuk9: .33-39*
- Arpat, E., & Şaroğlu, F. (1975). Türkiye'deki bazı önemli genç tektonik olaylar. *VĀnkġ g'Lgqrġlk'Mwt wo w'DĀngpk'3: , 91-101*
- Badgley, P. C. (1957). Tidewater Oil Company geological report on the Softekstructure Mardin and Siirt vilayets, Southeast Turkey (Licence no.154). *I gpgt cn'Fkt gevqt cvg"qhlRgt qrgwo "Chcktu."dqz 454. Tgrqtv'Pq4, 17*
- Bakkal, B., Çinku, M. C & Heller, F.(2019). Paleomagnetic results along the Bitlis-Zagros suture zone in SE Anatolia, Turkey: Implications for the activation of the Dead Sea Fault Zone. *Lqwt pcr'qhl'Gctvj 'Uekpegu'394. '14-29*
- Baraganzi M., Sandvol, E. & Seber, D. (2006). Structure and tectonic evolution of the Anatolian plateau in eastern Turkey. *I gqrqi kecn'Uqekvġ "qhl'Co gt kec "Urgeken' Rcr gt. '62; , 463-473*
- Barka, A. A. & Kadinsky-Cade, K.(1988). Strike-slip fault geometry in Turkey and its influence on earthquake activity. *Vgevpkeu.'9. '663-684*
- Baştuğ, M.C., (1980). *Ugf ko gpwvkqp. "F gġqt o cvkqp."cpf "O grvpi g"Go rrv ego gpv'kp" Nkeg" Dcukp. "F kerg/nctcdgi cp" Ctgc. "Uqwj gcw" Vwtngf. (Ph.D), Middle East Technical University, 282*
- Berberian M. King G.C.P. (1981). Towards a paleogeography and tectonic evolution of Iran. *Ecpcf kcp' Lqwt pcr'qhl'Gctvj 'Uekpeg. '3: (2), 210-285.*
- Best, J.A., Barazangi, M., Al-Saad, D., Sawaf T. & Gebran A. (1993). Continental margin evolution of the northern Arabian platform in Syria. *Co gt kecp" Cwqekcvkqp"qhlRgt qrgwo 'I gqrqi kmu'Dwngvkp. '99(2), 173-193.*

- Cater, J.M. & Tunbridge, I.P. (1992). Paleozoic tectonic history of the SE Turkey. *Lqwt pcr'qlh'Rgt qrgwo 'I gqrqi {.*'37, 35-50
- Cavazza, W. I., Cattò, S., Zattin, M., Okay, A. I. & Reiners, P., (2018). Thermochemistry of the Miocene Arabia-Eurasia collision zone of southeastern Turkey. *I gqrj gt g.'*36 (5), 2277-2293
- Coşkun, B. (2004). Arabian-Anatolian plate movements and related trends in southeast turkey's Oilfields. *Gpgti {'Uqwt egu.'*48, 978-1003.
- Çelikdemir, E., Görür, N & Dülger, S., (1987). GDA X., XI ve XII. Petrol Bölgelerinde Mardin Grubu Karbonatlarının Sedimantolojisi, Yayılımı, Fasiyes, Çökelme Ortamı ve Paleocografyası. *VRCQ'Gzrrqt cvkqp'I tqwr 'Pq<'* 4543
- Çelikdemir, E. & Dülger, S., 1990, Güneydoğu Anadolu'da Mardin Grubukarbonatlarının stratigrafisi, sedimantolojisi ve rezervuar özellikleri. *VRCQ'Gzrrqt cvkqp'I tqwr 'Tgrqt v'Pq04887,* 93
- Çelikdemir, E., Dülger, S., Görür, N., Wagner, C. & Uygur. K. (1991). Stratigraphy, sedimentology and hydrocarbon potential of the Mardin Group, SE Turkey. *Ur gekn'r wdrke cvkqp'qlh'GCRI .*'3, 439-454
- Çemen, İ. (1990). Araban tektonik bloğu doğu kısmının yapısal jeolojisi ve petrol potansiyeli. *VRCQ'gzrrqt cvkqp'i tqwr.'*4949, 37
- Çemen, İ., Perinçek, D., Ediger, V.Ş. & Akça, L. (1990). *I Āpglf q w'Cpcf qmwf cnk' Dq/qec'f q twmw'cv,o n'lc{,'Ā/ gt kpf gnk'knj ct gngv'vgt u'lc{rcpo c'qr cp'lc{rc t c' dk ''3/4pgn0* Paper presented in 8th Petroleum Congress of Turkey, Ankara, Turkey
- Çemen, İ., Bolgi, T., Peksu, M., & Akça, L (1991) Geology Map of XI District. *VRCQ'Gzrrqt cvkqp'I tqwr'0062/f'I gqrqi {'O cr0*
- Çetin, H., Guneyli, H. & MAYER, L. (2003). Paleoseismology of the Palu-Lake Hazar segment of the east Anatolian fault zone, Turkey. *Vgevppqrj {ukeu.'*596, 163-197.
- Çoruh, T., (1983). XII. Bolge Cemberlitas-4, 5, Adiyaman-1 ve Durukaynak-1 kuyularıyla, Karababa ve Inisdere OSK'larındaki Derdere ve Karababa formasyonlari hakkında yeni mikropaleontolojik bulgular. *VRCQ'Tgrqt v'76;* , 14.
- Çoruh, T. (1991). Adiyaman civarında (XI. Bölge kuzeybatısı ve XII. Bölge) yüzeyleyen Kampaniyen-Tanesiyen istifinin biyostratigrafisi ve paleocoğrafik evrimi. *VRCQ'Tgugctej 'Egpvgt.'Tgrqt v'pq<'3878,* 101
- Dağdelen, Y., (1970). AR/TPO/908 hak sıra nolu sahanın terk raporu," *VRCQ'Gzrrqt cvkqp'Tgrqt v'Pq0862,* 4

- Dean W.T. (1972). The trilobite genus *Holaspus* Matthew, 1985 in the Middle Cambrian rocks of Nova Scotia and eastern Turkey. *Ecpefkep "Lqwtpcn'qhl' Gctvj "Uekpeg" Qwqy c-θ;* , 266-278
- Dean, W.T., Martin, F., Monod, O., Demir, O., Rickards, R.B., Bultynck, P., & Bozdoğan N. (1997). Lower Palaeozoic stratigraphy, Karadere–Zirze area, central Pontides, northern Turkey, M.C. Göncüoğlu, A.S. Derman (Eds.), Early Palaeozoic Evolution in NW Gondwana." *Vwt nkuj " Cuiqekc vkap" qhl' Rgt qrgwo "I gqrqi kmu. "Ur gekcn'Rwdrkec vkap. "5. 32-38*
- Dean, W.T. (1975). Cambrian and Ordovician correlation and trilobite distribution in Turkey, *Hquuku"cpf "Ut cvc "7, 353–373.*
- Dean, W.T. (1980). The Ordovician System in the Near and Middle East, *Kvgtpcvkapcn' Wpkap"qhl' gqrqi kecn'Uekpegu. "4, 22*
- Dellaloğlu, A. A. & Pasin, C., (1984). Yalankoz ve Keldağ (Hatay) yörelerinin jeolojisi ve petrol olanakları. *VRCQ"Gzrrqt cvkap "I tqwr "Pq04233, 27*
- Demirel I.H. & Guneri S. (2000). Cretaceous carbonates in the Adiyaman region, SE Turkey: an assessment of burial history and source-rock potential. *Lqwtpcn'qhl' Rgt qrgwo "I gqrqi f. "45. 91–106.*
- Demirkol, C., (1988). Türkoğlu (K.Maraş) batısında yer alan Amanos dağlarının stratigrafisi, yapısal özellikleri ve tektonik evrimi. *"Dwngvtp"qhl'VC. "32: , 18-37*
- Dewey, J.F., Hemptom, M.R., Kidd, W.S.F., Saroglu, F. & Şengör, A.M.C. (1986). Shortening of continent young collision zone, in: Coward, M.P., Ries, A.C., eds, Collision tectonics. *"Drcemy grn'Uekgpvkte "Rwdrkec vkapu. "3/6, 3-36.*
- Duman, A. & Bozcu A. (2019). Source rock potential of the Sayındere Formation in the Şambayat oil field, SE Turkey. *Rgt qrgwo "Uekpeg"cpf "Vgej pqrqi f. "59(2), 171-180*
- Duman, T. Y. & Emre, O. (2013). The East Anatolian fault: geometry, segmentation and jog characteristics. *I gqrqi kecn'Uqekgvf. "594:495–529*
- Duran, O., Şemşir, D., Sezgin, İ., & Perinçek, D. (1988). Güneydoğu Anadolu'da Midyat ve Silvan Gruplarının stratigrafisi, sedimentolojisi ve petrol potansiyeli. *Lqwtpcn'qhl'Vwt nkuj "Cuiqekc vkap"qhl'Rgt qrgwo "I gqrqi kmu. "3*2), 99-126*
- Duran, O., (1991). Beşikli, Tokaris ve Bakacak sahalarının stratigrafisi, sedimentolojisi ve rezervuar özellikleri, *VRCQ" Tgugctej " Egpvgt " Tgrqt v" Pq07: 8, 43*
- Duran, O., Şemşir, D., Sezgin, İ., & Perinçek, D.(1989). Güneydoğu Anadolu'da Midyat ve Silvan Gruplarının stratigrafisi, sedimentolojisi ve petrol potansiyeli. *VRCQ"Gzrrqt cvkap "I tqwr. "4785, 78*

- Duran, O. & Aras M. (1990). [*gpkni4 "r gt qn'ucj cuk" *1 F "Cpcf qnw+O ctf kp" I twdw' nct d qpcwct k' eqngn' l vukf gu' xg" t g/ gt xwct " 3/4 gnknmt k0* Turkey 8. Petroleum Congress Geology Bulletin, 272-281
- Erdoğan, T. (1975). Gölbaşı civarının jeolojisi. *VRCQ "Gzrrnqt c v k q p" I t q w r " T g r q t v" P q Q 4; , 17*
- Erdoğan, B. & Yavuz, A.B. (2002). Relations between Miocene Paleogeography and marble deposits of southeast Anatolia, *L q w t p c n' q h G p i k p g g t k p i ' Ü e k p e g u ' F q m w' " G f n w i W p k x g t u k v f . 6 (2) , 5 3 - 6 4*
- Erkmen, U. & Bozdoğan, N. (1981) Cambrian acritarchs from the Sosink Formation in Southeast Turkey. *T g x k n e ' G u r c p q r e ' f g ' O k e t q r c r g q p t q r q i k e . ' 3 5 (1) , 4 7 - 6 0*
- Erenler, M. (1989). XI-XII. Bölge güney alanlarındaki kuyularda Mesozoyik çökel istifinin mikropaleontolojik incelenmesi. *VRCQ "g z r r n q t c v k q p" i t q w r . ' 3 5 8 6 , 4 4*
- Ertuğ, K. (1991). Güneydoğu Anadolu Kretase yaşlı Mardin Grubu ve Karaboğaz Formasyonu'nun palinostratigrafisi. *VRCQ "T g u g c t e j ' E g p v g t . ' 3 7 4 7 , 4 9*
- Girdler, R. W. & Styles. P. (1974). Two Stage Red Sea Floor Spreading, *P c w t g . ' 4 6 9 , 7 - 1 1*
- Gossage, D. W. (1956). Compiled progress report on the geology part of Petroleum District VI, Southeast Turkey. *' P O X O V w t m u g ' U j g m ' T g r q t v ' P q < 4 , 2 2*
- Gossage, D. W., (1959). Stratigraphic observations in the Tut area of District VI, Southeast Turkey: N. V. *V w t m u g ' U j g m ' T g r q t v ' p q 0 3 : , 4 8*
- Göncüoğlu M.C. & Turhan N. (1984). *I g q n q i { " q h ' v j g " D k r k u " o g w o q t r j k e " d g n ,* in Tekeli O. Göncüoğlu M.C., eds., Proceedings of the International Symposium on the Geology of the Taurus Belt: Ankara, Turkey, Mineral Research and Exploration Institute, 237–244.
- Görür, N., & Akkök, R., (1982). Adıyaman bölgesinde Mardin formasyonunun fasiyes analizi, diyajenezi ve hazne kaya niteliği. *VRCQ "G z r r n q t c v k q p" I t q w r " T g r q t v ' p q 0 ' 3 8 5 5 , 8 3*
- Görür, N., & Akkök, R., (1984). Facies analysis of the Midyat group (Lower Eocene to Lower Miocene) of the southeast Turkey. *' VRCQ ' G z r r n q t c v k q p" I t q w r " T g r q t v" p q . 2 1 8 7 , 5 7*
- Görür, N., Çelikdemir, E., & Dülger, S. (1987). Güneydoğu Anadolu X, XI. ve XII. Petrol Bölgelerinde Mardin Grubu Karbonatlarının Sedimantolojisi: Yayılım, fasiyes, çökelme ortamı ve paleocoğrafya. *VRCQ "G z r r n q t c v k q p" I t q w r " T g r q t v" p q . < 4 5 4 3*
- Günay, Y., & Sarıdaş, B., (1984). Amanos dağlarında Cudi-Mardin Grubu karbonatları ve Üst Kretase-Eosen yaşlı istifin konumu. *VRCQ "G z r r n q t c v k q p" I t q w r " T g r q t v ' p q . 2 0 2 1 , 2 2*

- Günay, Y., (1984). Amanos Dağları'nın jeolojisi ve Karasu-Hatay grabeninin petrol olanakları. *VRCQ'Gzrrıqt cvkqp'I tqwr'Tgrqt v'pq*. 1954, 98
- Günay, Y., (1986). Ergani-Dicle arasındaki Abdülaziz dağının jeolojisi ve yapısı. *VRCQ'Gzrrıqt cvkqp'I tqwr'Tgrqt v'pq04354*, 10
- Günay, Y., (1990). Güneydoğu Anadolu'nun jeolojisi (Yayınlanmamış). *VRCQ'Gzrrıqt cvkqp'I tqwr.'Cpnetc"*
- Güven, A., Dinçer, A., Tuna, M. E., Tezcan, Ü. Ş. & Çoruh, T. (1988). Güneydoğu Anadolu'da Mardin ve Midyat Grupları arasında yer alan birimlerin stratigrafisi (ön rapor). *VRCQ'Gzrrıqt cvkqp'I tqwr.'4636.'154*
- Güven, A., Dinçer, A., Tuna, E. M. & Çoruh, T. (1991). Stratigraphic evolution of the Campanian-Paleocene autochthonous succession of the South Anatolia. *Q/cp"Uıpi wtıw'Uıo rqukw 'Rt qeggf kpi u.'238-261*
- Hall, R. (1976). Ophiolite emplacement and the evolution of the Taurus suture zone, South-east Turkey, *I gqrıi kecn'Uqekıv' "ql'Co gt kec'Dwıngvıp."*: 9, 1078-1088.
- Handfield, R. W., Bryant, G. F. & Keskin, C. (1959). Measured section, Korudağ (American Overseas Petroleum). *VRCQ'Gzrrıqt cvkqp'i tqwr.745"*
- Hempton, M. R., Dewey, J.F., Şaroğlu, F. (1981). The East Anatolian transform fault: along strike variations in geometry and behavior. *Vtcpu'Co 'I gqrj {u'Wpkqp" GQU84,393*
- Hempton, M. R. (1985) Structure and deformation history of the Bitlis suture near Lake Hazar, southeastern Turkey. *I gqrıi kecn'Uqekıv' "ql'Co gt kec'Dwıngvıp."* ; 8(2), 233-243.
- Hempton M.R., (1987). Constraints on Arabia Plate motion and extensional history of the Red Sea. *Vgevıpkıeu.'8. 687-705.*
- Herece, E. (2008). Doğu Anadolu Fayı (DAF) Atlası. *OVC" | grıı c {,p'Ugt kık 'Pq<35, 359*
- Herece, E. & Akay, E. (1992). "Vj g"Gcıw'Cpcvırkcp"ıxıw"dgvy ggp"Mcıtrkqxc"cpf" Egrkıj cpö0In Ninth Petrol. Congr, 361-372. Turkish Association of Petroleum Geologist. Ankara, Turkey.
- Hill, R. (1959). Some basic principles in the mechanics of solids without a natural time. *Lqwtpcrı'qlııj g'O geı cpkeu'cıpf 'Rj {ıkeu'ql'Uırkıf u.'9(3), 209-225*
- Horstink, J. (1971). The Late Cretaceous and Tertiary geological evolution of eastern Turkey, *30Rgt qıgıw 'Mıpi t gık'*
- Husseini, M. I. (1989). Tectonic and Deposition Model of Late Precambrian-Cambrian Arabian and Adjoining Plates, *CCRI 'Dwıngvıp.'95(9), 1117-1131*
- Ilker, S., (1972). VI. Bölge Adıyaman kuzey ve kuzeydoğusundaki sahalar hakkında jeolojik rapor. *VRCQ'Gzrrıqt cvkqp'I tqwr'Tgrqt v'pq0; : 3, 27 s., Ankara.*

- İmamoğlu, M. Ş. (1993). *İncelenen Çöllerin, Çöllerin ve Çöllerin Marmara Bölgesi Üzerindeki Etkileri* (PhD). Unpublished, Ankara Üniversitesi Fen Bilimleri Enstitüsü, Ankara
- İmamoğlu, M. Ş. & Çetin, E. (2007). The Seismicity of Southeast Anatolian and Vicinity. *Journal of Ziya Gökalp Faculty of Education*, 9, 93-103.
- İnceöz, M. & Zengin, E. (2014). Morphotectonic and Structural Features of the Adıyaman Fault Zone. *Harita ve Jeoğrafya Dergisi*, 46 (2), 131-148.
- Jolivet, L. & Faccena, C. (2000). Mediterranean extension and the Africa-Eurasia collision. *Tectonics*, 19(6) 1095-1106
- Karabacak V. Altunel E. Cakir Z., (2011). Monitoring aseismic surface creep along the North Anatolian fault (Turkey) using ground-based LIDAR. *Earth and Planetary Science Letters*, 304, p. 64–70
- Karaoğlu F., Parlak O., Klötzli U., Köller F. & Rızaoğlu T.(2013). Age and duration of intra-oceanic arc volcanism built on a suprasubduction zone type oceanic crust in Southern Neotethys, SE Anatolia. *Geosci. Frontiers*, 4, 399-408.
- Kellogg, H.E. (1960) Stratigraphic report, Derik-Mardin area, Petroleum District V, Southeast Turkey (American Overseas Petroleum (AMOSEAS) Report). *General Directorate of Petroleum Affairs, box: 126, 3, 34.*
- Ketin, İ. (1964) Güneydoğu Anadolu Paleozoyik teşekküllerinin jeolojik etüdü hakkında rapor. *Turkish Petroleum Corporation Search Group Report*, 287, 36
- Ketin, İ. (1966) Tectonic units of Anatolia (Asia Minor). *Miner Resources Exploration Institute Bulletin*, 66, 23–34
- Khalifa, A., Çakir, Z., Owen, L.A., & Kaya, Ş., (2019). Evaluation of the Relative Tectonic Activity of the Adıyaman fault within the Arabian-Anatolian plate boundary (eastern Turkey). *Geologica Acta*, 17(6), 1-17.
- Kıratlıoğlu, E., (1964). AR/TPO/674 nolu sahanın jeolojik raporu: *TPAO Exploration Group Report No: 324*, 13
- Kıratlıoğlu, E. & Bolgi, T. (1961). AR/TPO/609 nolu Kastel sahası ve civarının jeolojik etüdü. *TPAO Exploration Group no: 220*, 36
- Koaster, E. A. (1963). Petroleum geology of District V, Turkey with special reference to licence n. 649 of Aladdin Middle East Ltd. (AME Report). *General Directorate of Petroleum Affairs, box: 126, 3, 34.*
- Köylüoğlu, M., (1986). Chronostratigraphy, microfacies and microfossils of the autochthonous units of the SE Anatolia. *TPAO Exploration Group, Report No: 1986*

- Mahmoud, Y., Masson, F., Meghraoui, M., Cakir, Z., Alchalbi, A., Yavasoglu, H., Yönlü, O., Daoud, M., Ergintav, S. & Inan S. (2013). Kinematic study at the junction of the East Anatolian fault and the Dead Sea fault from GPS measurements. *Journal of Geodynamics*, 89. 30–39
- Maxson, J. H. (1936). Geology and petroleum possibilitied of the Hermis Dome. *OVC eqo rkrvkqp*. '477, 25
- McQuarrie, N., & D. J. J. van Hinsbergen(2013). Retro-deforming the Arabia-Eurasia collision zone: Age of collision versus magnitude of continental subduction. *I gqrqi {.*'63. 315–318
- Meriç, E. (1978). Güneydoğu Türkiye’de Sinan Formasyonu alt üyesi ve Besni Formasyonu’nun fauna özellikleri. *Dwngvkp'qhlI gqrqi kecnEqpi t guu'qhlVwt ngf.* " 43(2), 95-96
- Meriç, E., Oktay, F.Y. & Özer, S., (1985). New observations about the stratigraphic developpement of the Besni Formation in the northwest of Alıdamı (Kahta-Adıyaman), southeastern Anatolia. *Dwngvkp'qhlIj g'I gqrqi kecnGpi kpggt kpi .*'47, 51-54
- Meriç E, Oktay FY, Toker V, Tansel İ, Duru M (1987) Sedimentary geology and biostratigraphy (foraminifera, nannoplankton and ostracods) of the Upper Cretaceous–Eocene sequence in the Adıyaman area, southeast Turkey. *Vwt nkuj "* I gqrqi kecnUqekgvf "Dwngvkp"52, 19–32
- Monod, O. & Dean, W.T. (1980). TPAO 1980 field season report. *VRCQ"Gzrrqt cvkqp"* I tqwr.'3: 97, 29
- Muehlberger R.W., Gordon M.B., (1987). Observations on the complexity of the East Anatolian Fault, Turkey. *Lqwtpcn'qhlUt wewt cnI gqrqi {.* ; , 899–903
- Mülayim, O., Mancini, E., Çemen, İ., Yılmaz, İ.Ö. (2016). Upper Cenomanian-Lower Campanian Derdere and Karababa formations in the Çemberlitaş oil field, southeastern Turkey: their microfacies analyses, depositional environments, and sequence stratigraphy. *Vwt nkuj "Lqwtpcn'qhlGct vj "Uekgpegu."*47, 46–63.
- Oberhänsli, R., Candan, O., Bousquet, R., Rimmelé, G., Okay A. & Goff J. (2010). Alpine high pressure evolution of the eastern Bitlis complex, SE Turkey. *I gqrqi kecnUqekgvf. "Nqpf qp. "Ur gekcnRwdrkecvkqpu."*562. 461-483,
- Oberhänsli, R., Bousquet, R., & Okay, O. (2012). Dating Subduction Events in East Anatolia, Turkey. *Vwt nkuj "Lqwtpcn'qhlGct vj "Uekgpegu."*43 (1), 1-17
- Oberhänsli, R., Koralay E., Candan, O., Pourceau A. & Bousquet, R.(2013). Late Cretaceous eclogitic high-pressure relics in the Bitlis Massif. *Lqwtpcn'qhl" I gqf kpcoc kecnCew.* "48(3-4)
- Okay, A. I., Armam, M. B., & Göncüoğlu, M. C. (1985) Petrology and phase relations of the kyanite-clogites from eastern Turkey. *Eqpvt kdwkqpu'vq'O kpgt crqi { 'çpf "* Rgvt qqrqi {.'; 3, 196–204

- Perinçek, D., (1981). Güneydoğu Anadolu'da jeokimya çalışması yapılacak Mesozoyik ve Tersiyer yaşlı anakaya olası birimlerin stratigrafisi. *VRCQ" Gzrñtçvkqp" I tqwr "Tgrqt v'Pq037; 3. "18*
- Perinçek, D. & Özkaya, İ. (1981). Arabistan levhası kuzey kenarı tektonik evrimi. *KwcpdwñLqwt pçñ'qñ'Gct vj "Uekpegu. "9 (8), 91-102.*
- Perinçek, D., (1989). Hakkari ili ve dolayının stratigrafisi, yapısal özellikleri, petrol imkanları. *VRCQ"gzrñtçvkqp" i tqwr. "4767, 127.*
- Perinçek, D., Günay, Y. & Kozlu, H. (1987). *Pgy "qdugtxcvkqp"qp"ñt kñg/urkr "lcwñu"kp" gcw" cpf "uqwj gcw" Cpcvñk0 Paper presented in 7th Biannual Petroleum Congress of Turkey, Ankara, Turkey*
- Perinçek, D., (1990). Hakkari ili ve dolayının stratigrafisi, GDA Türkiye. *"Dwñgvp"qñ' Vwtñkj "Cuuqekçvkqp"qñ'Rgt qñgwo "I gqrñi kñu. "4(1), 21-68*
- Perinçek, D., Duran, O., Bozdoğan, N. & Çoruh, T. (1991). *Utcvñi tcrj {" cpf" rcrñqi gqi tcrj kecn'gxqñwvkqp"qñ'ñj g"cwñqej vj qpqwu'ñgf ko gpwt {" t qem'kp"vj g"UG" Vwtñg/0Ozan Sungurlu Symposium proceedings, 274-304*
- Perinçek D. & Çemen İ., (1990). The structural relationship between the East Anatolian and Dead Sea fault zones in Southeastern Turkey, *Vgevppqrj {ukeu" 394, 331–340*
- Perinçek, D. & Çemen, İ. (1991). *Ncvg"Et gw egqw/Rcrñqi gpg"ñt wewt cñ'gxcñwçvkqp"qñ' vj g" ñt wewt cñ' j ki j u" qñ' Uqwj gtp" Cpcvñk. Ozan Sungurlu Symposium Notifications. 386-403*
- Perry, L. & Yalçın, K. (1957). Tavan Structure(south) section (Esso Standard (Turkey) Inc.) *Vrcq"Gzrñtçvkqp" I tqwr. 925*
- Poblet, J., & Lisle, R.J., (2011) Kinematic evolution and structural styles of fold-and-thrust belts. *I gqrñi kecn'Uqekvñ. "Nqpf qp. "Ur gekcñ'Rwdñkçvkpu. "56; , 1-24*
- Proctor, P. D. & Özkaya, İ., (1975). V. ve VI. Bölge şaryaj zonu, Maden, Ergani, Guleman, Dicle yöresi jeolojisi. *VRCQ"Gzrñtçvkqp" I tqwr "Tgrqt v'Pq0; 9: . 83*
- Reilinger R., McClusky S., Vernant P., & Lawrence S. (2006). GPS constraints on continental deformation in the Africa-Arabia-Eurasia continental collision zone and implications for the dynamics of plate interactions. *Lqwt pçñ'qñ' I gqrj {ukecñ'Tgugctej. "333"*
- Rigo de Righi, M., & Cortesini, A. (1964). Gravity tectonics in Foothills Structure Belt of southeast Turkey. *CCRI "Dwñgvp"6: , 1911–1937*
- Robertson A.H.F. (1998). *O guq/qkeóVgt vkt {"vgevppke"gxqñwvkqp"qñ'vj g"Gcñgt po quw" O gf kgttçpgcp" ctgc <"kpñgi tçvkqp" qñ' o ct kpg" cpf "rcpf dcugf " gñlf gpeg0 In Proceedings of the Ocean Drilling Program, Scientific Results, Robertson AHF, Emeis K-C, Richter C, Camerlenghi A (eds). 160: 723–782*

- Robertson, A.H.F. (2000). Mesozoic-Tertiary Tectonic-Sedimentary Evolution of a South Tethyan Oceanic Basin and its Margins in Southern Turkey, *I gqrqi kecn' Uqekv'.*395, 97-138,
- Robertson, A.H.F., Parlak, O., Rızaoğlu, T., Unlügenç, U., İnan, N., Taşlı, K. & Ustaömer, T. (2007). Tectonic evolution of the South-Tethyan Ocean: evidence from the Eastern Taurus Mountains (Elazığ region, SE Turkey). *CÖÖ Tkgu."TÖÖ Ö'Dwrgt."TÖÖ Ö'I tç co "Gf'üÖ" F glqt o c'kqp"ql'h'vj g"Eqp'kpgp'cn' Et wü<'Vj g'Ngi ceç"ql'Ö kng"Egy çtf."I gqrqi kecn'Uqekv' "ql'Nqpf qp"Ür gekcn' Rwdrkcc'kqpu.*494, 231-270.
- Rolland, Y., Perinçek, D., Kaymakçı, N., Sosson, M., Barrier, E., & Avagyan, A. (2012). Evidence for ~80–75 Ma subduction jump during Anatolide–Tauride–Armenian block accretion and ~48 Ma Arabia–Eurasia collision in Lesser Caucasus–East Anatolia. *Lqwt pçri'qhl' gqf {pco keu.'78ö79.* 76–85.
- Saltik, O., (1970). Cizre-Silopi-Rubai sahasına ait rekonesans jeoloji raporu. *VRCQ"Gzrrqt c'kqp'I tqwr'Tgrqt v'Pq.* 488, 9
- Saltik, O. & Saka, K., (1971). İnışdere tip stratigrafi kesiti. *VRCQ"Gzrrqt c'kqp'I tqwr" Tgrqt v'Pq.* 4308., 75 s.,
- Sarıdaş, B., (1987). Hazro, Malahermo, Belaşa dolayının jeolojisi ve petrol olanakları. *VRCQ"Gzrrqt c'kqp'I tqwr'Tgrqt v'Pq.* 2326, 48
- Sarıdaş, B., (1991). Cendere sahası ve Nemrut dağı dolayının jeolojisi (rezarvar çalışması). *VRCQ"Gzrrqt c'kqp'I tqwr'Tgrqt v'Pq.* 2826, 20
- Savci, H., & Dülger, S., (1980). Cacas-Sason-Kozluk dolayının jeoloji incelemesi ve petrol olanaklarının araştırılması. *VRCQ"Gzrrqt c'kqp'I tqwr'Tgrqt v'Pq.* 1442, 41
- Sayili, A. & Duran, O., (1994). XI. Bölge batısı ve XII. Bölge doğu alanlarında (GDA) Sabunsuyu, Derdere, Karababa, Karaboğaz ve Sayındere formasyonlarının fasiyes dağılımları ve rezervuar özellikleri. *VRCQ'Tgugct ej'Egpvt'Tgrqt v'Pq.* 1985, 41 s
- Schmidt, G.C. (1961). Stratigraphic nomenclature for the Adana region petroleum district VII. *Rgt qrgwo 'Cf o kpknt c'kqp'Dwrgkçp.'8,* 47-63
- Schmidt, G.C. (1963). A review of Permian and Mesozoic formations exposed near the Turkey (Iraq border at Harbol). *Rgt qrgwo 'Cf o kpknt c'kqp'Rwdrkcc'kqpu.'.* 39-49
- Schmidt, G.C. (1964). Proposed rock unit nomenclature Petroleum District V, SE-Turkey (Mobil Exploration Mediteranean Inc.). *I gpgt cn' Fkt gevqt cvg" ql'h' Rgt qrgwo 'Chçkt u.'5; 77(1)"*
- Schmidt, G. C. (1965). Proposed Rock Unit Nomenclature, Petroleum District V S.E. Turkey (autochthonous terrain). Chart 1. Revised Edition. Stratigraphy Committee, *Vwt nkuj 'Cuuqekc'kqp'ql'Rgt qrgwo 'I gqrqi knu.'wpr wdrkuj gf -Ö'*

- Sefünç, A. & Efeoğlu, T. (2005). Recognition of Wrench Faults on Seismic Sections, *VCRI 'Dwngvlp.* '39(1), 19-39
- Seyitoğlu, G., Esat, K. & Kaypak, B. (2017). The neotectonics of southeast Turkey, northern Syria, and Iraq: the internal structure of the Southeast Anatolian Wedge and its relationship with recent earthquakes. *Vwt nkuj 'Lqwt pcr'qhl'Gct yj "* *Ukpgpegu.* '48. 105-126.
- Seyitoğlu, G., Esat, K., Kaypak, B., Toori, M., Aktuğ, B., (2018). Internal deformation of the Turkish-Iranian Plateau in the hinterland of Bitlis-Zagros Suture Zone. In: Tectonic and Structural Framework of the Zagros Fold-Thrust Belt (Ed. Farzipour Saein, A.) *Gnugxkgt*, 161-244.
- Sinanoğlu, E. & Erkmén, U. (1980). *I ãpg{f q w" Cpcf qmw" Crukl gp/Crdkl gp" rcrkpwqt cvki tclhuk"xg"d³/ni gplp"Cw"Mt gxcug"rcrkpqr t qxgpungt k'kãpf gnik" {gt k* Proceedings of Fifth petroleum congress of Turkey. 51-59
- Sonel, N., Eker, N., Sarı, A. & Bağcı, S., (2002). Interpretation of Tokaris Area Adıyaman-Mardin Group Members Adıyaman-Kahta Rezervuar Properties in Elan Plus Software, *I gqrqi kecn'Dwngvlp'qhl'Vwt ngf.* '67(1),
- Soytürk, N. & Erdoğan, T., (1974). Bakük –Ceylanpınar-Derik-Mazıdağı dolaylarının jeolojisi ve hidrokarbon olanakları. *VRCQ'Gzrrqt cvkqp'I tqwr 'Tgrqt v'Pq0':* 87, 14
- Stratum, (1963). General geological report on the Petroleum District V with reference to the areas AR/ A.M.E/648, AR/C.M.E/657, 660, AR/P.E.R/650, 659 (Aladin Middle East Ltd. Report). *I gpgt cn'F kt gevqt cvg'qhl'Rgt qrgwo 'Chk kt u'Vej pkecn' Ctej kxg.'Dqz'pq0347.'Tgrqt v'pq09,* 19
- Sungurlu, O. (1972). VI. Bölge Gölbaşı-Gerger arasındaki sahanın jeolojisi, *VRCQ" tgrqt v'pq<: 24"*
- Sungurlu, O. (1973). VI. Bölge Gölbaşı-Gerger arasındaki sahanın jeolojisi. *VRCQ" Gzrrqt cvkqp'I tqwr.":* 24, 30
- Sungurlu, O. (1974) *I gqrqi {"qhl'XKOP qt vj gtp"ctgc.* Second Petroleum Congress of Turkey, Ankara, 85–107
- Sunkar, M., & Karataş, Z., (2015). Kahta Çayı Aşağı Havzası'nın (Adıyaman) jeomorfolojik özellikleri, *Vwt nkuj 'I gqi tcrj kecn'Tgxky.* '85
- Şafak, Ü. & Meriç, E., (1996) Kahta Geç Miyosen ostrakod topluluğu hakkında yeni görüşler, *¥wmt qxc "Wpkxgt ukf "Lqwt pcr'qhl'Gpi kpggt kpi "cpf "Ctej kgewt g."4;* , 171-197.
- Şahbaz, N. & Seyitoğlu, G., (2018). The neotectonics of NE Gaziantep: The Bozova and Halfeti strike-slip faults and their relationships with blind thrusts, Turkey, *Dwngvlp'qhl'y g'O kpgt cn'Tgugct ej "cpf 'Gzrrqt cvkqp.* '378, 17-40

- Şaroğlu, F., Emre, Ö., & Boray, A. (1987). Türkiye'nin Diri Fayları ve Depremsellikleri. *I gpgt cn' F kt gevqt cvg " qh' O kpgt cn' Tgugctej " cpf " Gzr rqt cvkqp. " Tgr qt v' pq < 81(74), 394 s., Ankara*
- Şaroğlu F., Emre Ö., & Kuşçu İ., (1992a). Active Fault Map of Turkey. *I gpgt cn' F kt gevqt cvg " qh' O kpgt cn' cpf " Tgugctej " Gzr rqt cvkqp " qh' Vwt ngf " Rwdrkecvkqp "*
- Şaroğlu, F., Emre, Ö., Kuşçu, İ. (1992b). The East Anatolian Fault zone of Turkey. *Annal. Tecton. 6:99–125*
- Şenel, M. & Ercan, T. (2002). 1:500000 Ölçekli Türkiye Jeoloji Haritası, Van Paftası. *I gpgt cn' F kt gevqt cvg " qh' O kpgt cn' cpf " Tgugctej " Gzr rqt cvkqp " qh' Vwt ngf " Rwdrkecvkqp*
- Şengör, A.M.C. & Kidd, W.S.F (1979). Post-collisional tectonics of the Turkish-Iranian plateau and a comparison with Tibet. *Vgevppqrj { ukeu. '77(3–4), 10 June 1979, Pages 361-376*
- Şengör, A.M.C & Yılmaz, Y. (1981). Tethyan evolution of Turkey: A plate tectonic approach. *Vgevppqrj { ukeu'97(3–4), 181-190, 193-199, 203-241*
- Şengör, A.M.C., Görür, N., & Şaroğlu, F., (1985). Strike-slip faulting and related basin formation in zones of tectonic escape: Turkey as a case study: in Biddle, K.T. and Christie-Blick, N., eds, Strike-slip Deformation, Basin Formation, and Sedimentation, *Uqe0Geqp0Rcrqgpı00 kp0Ur ge0Rwd0*59+ 227-264.*
- Şengündüz, N. & Aras, M., (1986). XI ve XII. Bölgelerde Mardin Grubu karbonatlarının ve Karaboğaz Formasyonu'nun fasiyes dağılımı, diyajenetik özellikleri ve çökme modeli, *VRCQ' Tgugctej 'Egpvgt 'Tgr qt v' P q03227, 75*
- Tardu, T., (1991). *C' ugs wpeg' iat cvki t crj ke' crrt qcej " vj' g' O ct f kp' I t qwr 0Vgevppkeu' cpf " j { f t qe c t d q p " r qv g p v k c n' qh' C p c v r k c " c p f " i m t q w p f k p i " t g i k p u.* In: Ozan Sungurlu Symposium Proceedings, Ankara, Turkey.
- Tarhan, N., (2002). Geological map of Turkey. 1:500.000 scale Erzurum sheet, No 11. *I gpgt cn' F kt gevqt cvg " qh' O kpgt cn' Tgugctej " cpf " Gzr rqt cvkqp " Rwdrkecvkqpı0*
- Tatar, O., Koçbulut, F., Polat, A., & Demirel, M. (2019). 02.03.2017 ve 24.04.2018 Samsat (Adıyaman) Depremleri ve Bölgesel Sismotektonik İçindeki Önemi, *I gqrqi kecn' D w r g v k p " qh' V w t n g f. '84. 167-180*
- Taylor, P. B. (1955). Stratigraphic studies Bozova (Urfa) area (Mobil Exploration Mediterranean Inc. Report). *I gpgt cn' F kt gevqt cvg " qh' R g t q r g w o " C h c k t u. " d q z < 554. '3, 14*
- Taymaz, T., H. Eyidogan, & Jackson, J. (1991). Source parameters of large earthquakes in the East Anatolian fault zone (Turkey). *I gqrj { ukecn' L q w t p c n' k p v g t p c v k p c n' 328, 537–550,*
- Tearpock, D. J & Bischke, R. E. (1990). Mapping throw in place of vertical separation - A costly subsurface mapping misconception. *Qkt' cpf " I cu' L q w t p c n' " : (29), 74-78*

- Thomas, E., Aytuna, S. & Özcan, O., (1986). Geological field report, Southeast Turkey, Akpınar license: ARCO International Oil and Gas Company Report. *VRCQ'Gzrrqt cvkqp'I tqwr'Tgrqt v'4469*. 62
- Tolun, N. (1948). Silvan ve Hazru mintıkası hakkında jeolojik notlar. *I gqrqi kecn'Dwngvkp'ql'Vwtngf*. '4. '1.
- Tolun, N. & Ternek, Z. (1952). Mardin bölgesinin jeolojisi. *I gqrqi kecn'Dwngvkp'ql'Vwtngf*. '5(2), 1-20
- Tolun, N. (1954). Güney - Doğu Anadolu'nun stratigrafisi ve tektoniği. *I gpgtcn'Fkt gevqt cvg'ql'O kpgtcn'Tgugctej 'cpf 'Gzrrqt cvkqp'Tgrqt v'Pq03469*, 39-41.
- Tolun, N., Erentöz, C. & Ketin, İ., (1962). 1/500.000 ölçekli Türkiye Jeoloji Haritası (Diyarbakır paftası). *I gpgtcn'Fkt gevqt cvg' ql' O kpgtcn' Tgugctej " cpf " Gzrrqt cvkqp'Rwdrkcvkqpu*, 69
- Tromp, S. W. (1940). Preliminary report on the oil possibilities of S.E. Turkey, based on a re-interpretation of microfaunal and sub-surface data (Cenubu Şarki Türkiye'nin stratigrafisi, strüktür veçleri ve petrol imkanları ile bunların mücavir mintikalarla mukayesesi). *Fkt gevqt cvg' ql' O kpgtcn' Tgugctej " cpf " Gzrrqt cvkqp'Ego rkrv'kp'pq03438*. 74
- Tuna, D. (1973). VI. Bölge litostratigrafi birimleri adlamasının açıklayıcı raporu. *VRCQ'Gzrrqt cvkqp'I tqwr*. ': 35. '131
- Tuna, D. (1974). *Nkj qwt cvki tcrj ke'pqo o gperxwt g'ql'wpku'ql'Fkmt kev'XK'UG'Vwtngf0* Proceedings of 2nd Turkish Petroleum Congress, Ankara, Turkey, 183–187.
- Turner, F., (1958). Kayık section (Esso Standart (Turkey) Inc.). *VRCQ'Gzrrqt cvkqp' I tqwr'Tgrqt v'Pq0983*
- Türkünal, S., (1955). Çukurca, Beytüşşebap ve Şırnak arasında kalan bölgelerin jeolojik etüdü: *I gqrqi kecn'Dwngvkp'ql'Vwtngf*. '8 (1), 41-49
- Ulu, Ü., Genç Ş., Giray S., Metin Y., Çörekçioğlu E., Örcen S., Ercan T., Yaşar T. & Karabıykoğlu M., (1991). Belveren-Araban-Yavuzeli-Nizip-Birecik Alanının Jeolojisi Senozoyik Yaşlı Volkanik Kayaçların Petrolojisi ve Bölgesel Yayılımı, *Fkt gevqt cvg'ql'O kpgtcn'Tgugctej 'cpf 'Gzrrqt cvkqp'Ego rkrv'kp'pq0 ; 448*
- Uygur, K. & Aydemir, V., (1988). Bolukyayla-Cukurtas sahalarında (XII. Bolge) Derdere, Karababa, Karabogaz ve Sayindere formasyonlarının yeraltı jeolojisi; petrografi sedimantoloji, ortam analizi, petrofizik ve goreceli olay kronolojisi. *VRCQ'Gzrrqt cvkqp'I tqwr'Tgrqt v'4776*. '259.
- Uzunçimen, S., Tekin, U.K., Bedi, Y., Perinçek, D., Varol, E. & Soycan, H. (2011). Discovery of the Late Triassic (Middle Carnian–Rhaetian) radiolarians in the volcano-sedimentary sequences of the Koçali Complex, SE Turkey: correlation with the other Tauride units. *"Lqwt pcn'ql'Cukcp"Gctvj "Uekgpegu"* 62,180–200

- Wagner, C. & Pehlivanli, M., (1985). Karst geological interpretation of Mardin carbonates in Cemberlitas oil field, a pilot study, *VRCQ"Gzrrnqt cvkqp" I tqwr" Tgrqt vPq<4273*, 19.
- Wagner, C., & Tuna, E., (1988). Campanian cycle IV carbonates in Southeast Turkey- depositional environments and paleogeography. *VRCQ"Gzrrnqt cvkqp" I tqwr" Tgrqt vPq<474: . '11*
- Westaway, R. (1998). Dependence of active normal fault dips on lower-crustal flow regimes. *Lqwt pcrn'qhl'ij g'I gqrqi kecn'Uqekgyl.377*, 233–253
- Westaway, R. (2004). Kinematic consistency between the Dead Sea Fault Zone and the Neogene and Quaternary left-lateral faulting in SE Turkey. *Vgevppqrj {ukeu" 5; 3*, 203–237
- Westaway, R., & Arger, J. (2001). Kinematics of the Malatya–Ovacık Fault Zone, *I ggf kpc o kec 'Cew'36*.103–131
- Wilson, H. H., & Krummenacher, R., (1957). Geology and Oil Prospects of the Gaziantep Region; Available Information in Technical Fields of NV Turkse Shell, Petroleum Activites In Turkey. *I gpgt cn' Fk gevqt cvg" qh' Rgt qrgwo " Chck u'Rwdrkecvkqp'Dwngvkp.":*
- Wilson, H. H. & Krummenacher, R. (1959). Geology and oil prospects of the Gaziantep Region, Southeast Turkey(N. V. Turkse Shell Report). *I gpgt cn' Fk gevqt cvg"qh'Rgt qrgwo 'Chck u."dqz-573. '4*, 53
- Workman, L. E. (1962). Subsurface geology of the Batman region, *VRCQ"Gzrrnqt cvkqp" I tqwr. '483(1)*, 29
- Yalçın, N. (1976). Geology of the Narince-Gerger area (Adıyaman province) and its petroleum possibilities. *Tgxwg"fg"rc "Hcewn² "fgu"Uekgpegu"fg"nWpkxgt uk² " f ø ucpdwiD63*, 57–82.
- Yalçın, N. (1977). Geology of the Narince-Gerger area (Adıyaman province) and its petroleum possibilities. *Dwngvkp"qh' ucpdwiWpkxgt uk² "Uekgpeg'Hcewnl. 'D/63*, 57-82
- Yalçın, N.,(1978). Kahramanmaraş-Gaziantep arasındaki allohton birimlerin ayırtlanması ve ilişkileri, *VRCQ"Gzrrnqt cvkqp" I tqwr "Tgrqt vPq0346; . 68*
- Yazar, B.B., (2009). *Kpxgwnki cvkqp"qh'Uwdumthceg'I gqrqi {'cpf 'Rgt qrgwo 'Rqukdkrkkgu" qh'Octf kp" I tqwr "Ectdqpcvgu"lp"Uqwj gtp"Cf k'co cp/"Mcj v "Ctgc "¶ cri cp/ Mctcm/rtÃ/Crkf c "Tgi ,qp-θ(M.S)*, Ankara University.
- Yazgan E (1983) *C" I gqt cxgtug"dgvy ggp"yj g"Ctdkcp"rrvqt o "cpf"yj g"Owp/wt" pcrngu*. In: Guide book for excursion V. Int Symp on Geology of the Taurus belt, Directorate of Mineral Research and Exploration, Ankara, Turkey, 17.
- Yazgan E, Michard A, Whitechurch H, Montigny R (1983) Le Taurus de Malatya (Turquie orientale), élément de la suture sudtéthysienne. *Dwngvkp'fg'rc"Uqek² v" I ² qnqi kswg'fg'Ht cpeg. '47*, 59–69

- Yıldırım, M. & Yılmaz, Y. (1991). Güneydoğu Anadolu Orojenik Kuşağının Ekayılı Zonu, *Dwngvlp'qlVwt nkuj 'Cuuqekv kqp'qlRgt qrgwo 'I gqrqi kmu.* 5(1), 57-73
- Yılmaz, Y., (1982). Amanos dağlarının tektoniği. *VRCQ'Gzrrqt cvkqp'I tqwr'Tgrqt v'Pq<3875.* 91
- Yılmaz, Y. (1984). Amanos dağlarının jeolojisi. *VRCQ'Gzrrqt cvkqp'I tqwr'Tgrqt v'Pq:* 1920.
- Yılmaz, Y., Demirkol, C., Gürpınar, O., Yalçın, N., Yetiş, C., Yiğitbaş, E., Günay, Y. & Sarıtaş, B. (1984). Amanos dağlarının jeolojisi. İstanbul Üniversitesi, Mühendislik Fakültesi, *VRCQ'Tgugctej 'I tqwr'Tgrqt v'Pq<3;* 42, 571.
- Yılmaz Y., Yiğitbaş E., & Yıldırım M. (1987). *I Āpgffq w'Cpcf qmf c "Vtkf cu"uqpw' vgmqpk' o cu,"xg"dwppw"lgqrqlkn'cprco ,07.* Petroleum Congress of Turkey, Ankara, Türkiye, 9-10
- Yılmaz, Y. (1990) Comparison of young volcanic associations of western and eastern Anatolia formed under a compressional regime: a review, *Lqwtpcn' qh' Xqrecpqrqi { 'cpf 'I gqvj gto cn'Tgugctej .* 66(1-2), 69-87
- Yılmaz, Y. (1991). Allocthonous Terranes in the Tethyan Middle East: Anatolia And The Surrounding Region. Allocthonous Terranes (Edited By Dewey, j.f., gass, i.g., curry, g.b. harris, n.b.w., and sengör, A.M.C.). *Eco dtkf i g"Wpkxgt ukv' Rt guu.* 155-168
- Yılmaz, Y. (1993). New evidence and model on the evolution of the southeast Anatolian orogen, *I gqrqi kecn'Uqekv' qh'Co gte c'Dwngvlp.* 327(2), 251-271.
- Yılmaz, Y., Yiğitbaş, E. & Genç, C.Ş. (1993) Ophiolitic and metamorphic assemblages of southeast Anatolia and their significance in the geological evolution of the orogenic belt. *Vgevxpkeu.* 34(5), 1280-1297.
- Yılmaz, E. & Duran, O. (1997). *I Āpgffq w'Cpcf qnw'D'4i guk'Qvqmqp"xg"Crqmqp" Dtko rgt " Ut cvki tclh' Cf rwo c" U'4rñ Ā" *Ngzkeqp+* Ankara: TPAO Eğitim Yayınları No.31
- Yılmaz, A., Yılmaz, H., Kaya, C. & Durmus, B. (2010). The nature of the crustal structure of the Eastern Anatolian Plateau, Turkey. *I gqf kpc o ke c' Cew.* 45(4), 167-183
- Yiğitbaş, E., Yılmaz, Y., & Genç, Ş. C. (1992). *I Āpgffq w'Cpcf qnw' qt qlgpkn' mw c ,pfc'Gqugp' pcr' { gtrg o guk' *Gqegpg' pcr r g' go r rwe go gpv'lp' vj g' uqwj gcw' Cpcvqrkcp' qt qi gpke" dgn+0* In Proceedings of the 9th Petroleum Congress and Exhibition of Turkey, 307–318.
- Yiğitbaş E. & Yılmaz Y., (1993). *Gqegpg' f glqto cvkpu" qp' vj g' pqt vj y guvgt p' Ctcdkcp' rrv'g" o cti kp." UG" Cpcvqrk.* European Union of Geosciences VII, STRASBOURG, FRANSA, 5(1), 273-273

- Yiğitbaş, E. & Yılmaz, Y. (1996). New evidence and solution to the Maden complex controversy of the Southeast Anatolian orogenic belt (Turkey), *İzmit Körfezi Jeolojisi*, 85(2), 250-263
- Yoldemir, O. (1985). Suvarlı (Adıyaman) yakın dolayının jeolojisi. *YERİNE KÖKÜ* 4335
- Yoldemir, O. (1987). Suvarlı-Haydarlı-Narlı Gaziantep arasında kalan alanın jeolojisi, yapısal durumu ve petrol olanakları. *YERİNE KÖKÜ* 4479
- Yürür M.T. & Chorowicz J., (1998). Recent volcanism, tectonics and plate kinematics near the junction of the African, Arabian, and Anatolian plates, *İzmit Körfezi Jeolojisi* 7, 1-15.

APPENDICES

A. Materials

Well Bore Litholog logs

ZR: 617.13 m.
KB: 622.33 m.

D.B-1 Exploration Well

Age	FORMATION	LITOLGY	DEPTH	EXPLANATION
QUATERNAR	QUATERNER		24 (+598)	Brownish beige, Brown, polygenic conglomerate
CRETACEOUS	KASTEL		176	Greenish grey, mediu-coarse graned, poorly sorted, angular, lithic arenit sandstone.
			200 (+422)	
	SAYINDERE		233	Light grey, cream, White, beige, wackestone-packstone clayey limestone.
			433 (+189)	Beige, wackestone-packstone Limestone with chert lamiae.
			439 (+183)	Beige, dolomitic limestone
	K.BOGAZ		475 (+147)	
	KARABABA		583(+39)	Fine-medium crystalline dolomite.
	DERDERE		688(-66)	Dolomite.
SABUNSUYU		708(-86)	Fine medium grained, poorly sorted, angular, quartz arenit Sandstone.	
AREBAN		708(-86)		
CAMBRIAN	SOSİNK			Fine – medium/ coarse grained, poorly sorted, angular, Sanstone with shale laminae.

Total Depth: 779(-157) m.

Hki wt g'CO Lithology log of well D.B-1

D.B-2 Exploration Well

ZR: 625.83 m

KB: 631.03 m

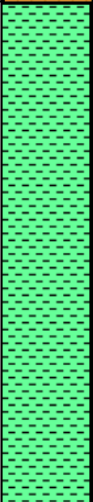
Age	FORMATION	LITOLOGY	DEPTH	EXPLANATION
QUATERNARY	QUATERNARY		16 (+615)	Various colored, polygenic, fine-medium, medium sorted, rounded conglomerate with fine claystone laminae
PALEOCENE	GERMAV		443	Light grey, grey, brittle, silty Marn with sandstone laminae.
			459 (+172)	
CRETACEOUS	KASTEL		313	Light brown, brown, brownish grey, brittle, silty shale
			772 (-141)	
	SAYINDERE		327	Beige, dark beige, hard, brittle, chalky, clayey limestone.
			1099 (-468)	
	K.BOGAZ		1120 (-489)	Brownish beige, brown, dark brown, blackish brown, hard, brittle limestone with chert sands. Dark brown, blackish brown very hard chert.
	KARABABA		1217 (-586)	Cream, white cream, beige, hard, brittle, chalky limestone.
	DERDERE		1412 (-784)	Beige, light beige, stiff, porous dolomitic limestone.
SABUNSUYU		1496 (-865)	Greyish white, brownish grey, stiff, sugar textured dolomitic limestone	
CAMBRIAN	AREBAN		1526 (-895)	Yellowish, fine-coarse grained, poorly sorted, semi rounded, Sandstone
	SOSINK			Translucent, semi translucent, pinkish, fine-medium grained, medium sorted, semi rounded, loose sandstone.

T.D. 1548 (-917) m

Lithology log of well D.B-2.

KB:603.26 m.
ZR:597.59 m.

BA-1 Exploration Well

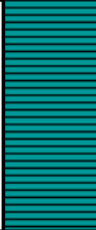
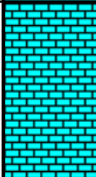
AGE	FORMATION	LITOLGY	DEPTH	EXPLANATION
UPPER MIOCENE	ŞELMO		439 (164)	Polygenic, various colored gravel, Light Brown, silty sandy marny claystone.
				Greenish grey, silty marn Light gray, brownish gray shale
OLIGOCENE	G.ANTEP		712 (-109)	White, cream colored, medium-hard, fossiliferous Limestone.
PALEOCENE	GERMAV FM.		1923 (-1320)	Greenish gray, calcareous Marn
UPPER CRETACEOUS				KASTEL
	S.DERE		2440 (-1837)	Beige, cream colored, medium-hard, clayey limestone
	K.BOGAZ		2474 (-1870)	Blackish Brown, Brown, microfractured, Limestone
	K.BABA		2523 (-1919) 2576 (-1973)	Beige, honey Brown, microfractured Limestone and cherty limestone.
	DERDERE		2603 (-2000)	Cream, beige dolomite with blackish Brown, dark Brown chert

Total Depth: 2630 (-2027) M.

Hikmet ÇOBOLithology log of well BA-1

B-1 EXPLORATION WELL

KB: 708.53 m.
ZR: 704.98 m.

AGE	FORMATION	LITOTOLOGY	DEPTH	EXPLANATION
UPPER CRETACEOUS	KASTEL		368 (341)	Green, grey hard, brittle shale, Sandstone and conglomerate alteration Purple shale with little calcereous shale.
	S.DERE			Marn, clayey Limestone
	K.BABA		615 (94)	Clayey, micritic, chert laminated dolomitic Limestone
	C		624 (85)	
	B		645 (64)	Beige, honey Brown, microfractured Limestone and cherty limestone.
	A		691 (18)	
DERDERE		699 (10)	Beige, cream dolomite	
LOWER CRETACEOUS	S.SUYU		796 (-87)	Cream,-White, hard, dense dolomite
	AREBAN		846 (-137)	
LOWER- MIDDLE TRIASIC	BAKÜK		856 (-147)	Dark grey, carstic hard dense dolomite
	ULUDERE		1069 (-360)	
CAMBRIAN	SOSİNK		1199 (-490)	Grey, green, poorly rounded sandstone with shale laminae.

TOTAL DEPTH: 1250 (-541)

Hikmet Çoçuk Lithology log of well B-1.

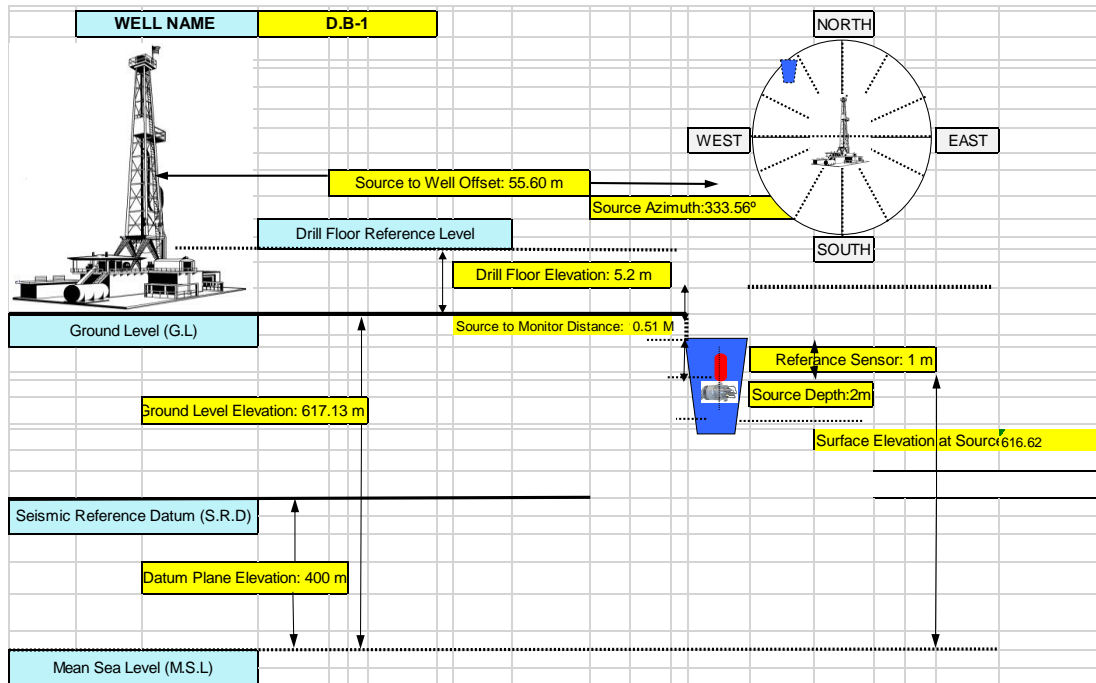
ZR: 739.38 m
KB: 744.58 m

B-2 EXPLORATION WELL

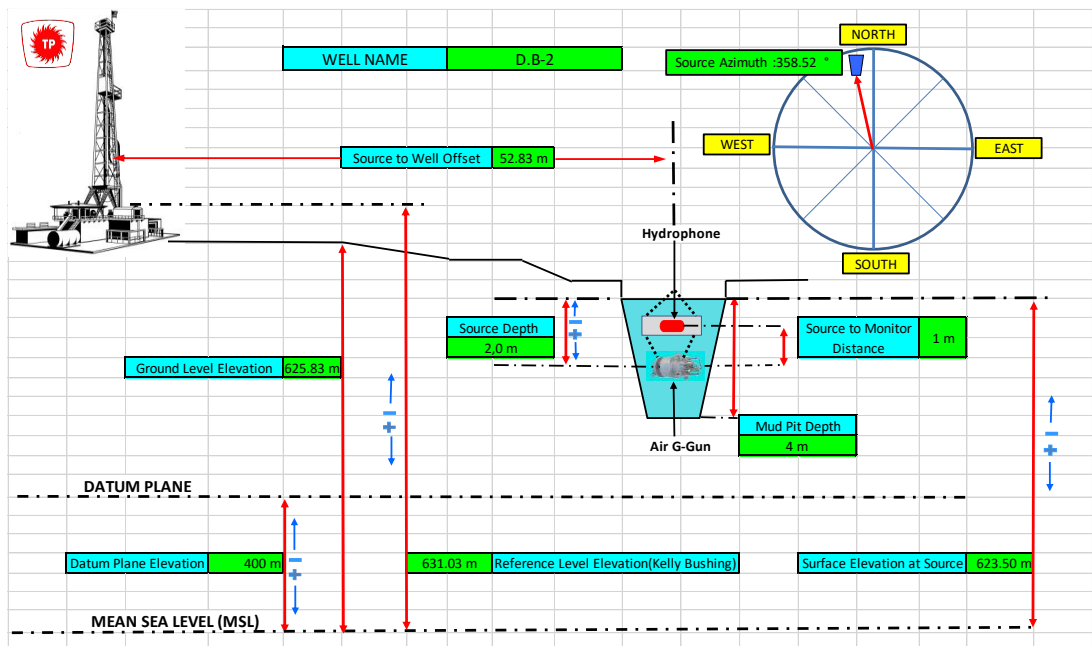
AGE	FORMATION	LITOLGY	DEPTH	EXPLANATION
UPPER CRETACEOUS	TJK	KOÇALI	50 (+695)	Beige, cream colored, stiff, silicified limestone, red, blueish grey, brittle silicified shale. <div style="text-align: right;">13 3/8" 78 m.</div>
		KASTEEL	283	Polygenic, various colored, fine-medium-coarse grained, poorly sorted, sandstone, dark grey, brittle, shale.
		SAYINDERE	333 (+412)	
			285	Cream, White, beige, stiff, clayey limestone. <div style="text-align: right;">9 5/8" 505 m.</div>
		K.BOGAZ	618 (+127) 626 (+119)	Beige, dark beige limestone with black, blackish Brown chert.
		KARABABA	714 (+31)	Cream, White cream stiff, brittle, limestone.
		DERDERE		Cream, beige, dolomitic limestone.

Hikmet Çiğdem Lithology log of well D.B-2.

B. Checkshot Geometries of Three Wellbores



Checkshot geometry of well DB-1.



Checkshot geometry of well DB-2

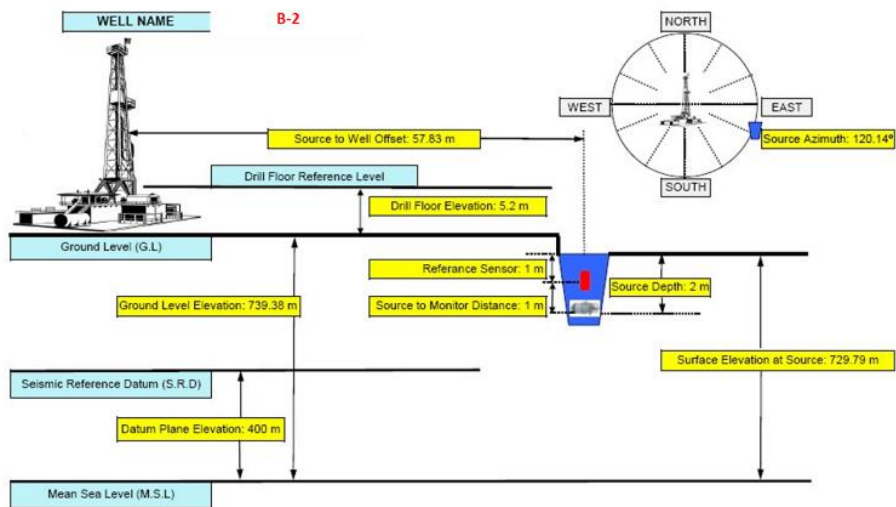


Figure B-2. Checkshot geometry of well B-2.

C. Checkshot Values for Wellbores

Table C.10Ej gemij qv'xcnwg'u'ql'ly gm'D/40'

B-2 Kuyusu check shot Degerlendirmesi

K.B.: 744.00m SRD: 400.00m AirGun: 727.00m AirGun Offset: 57.00m
 Saga(X) :4175223.00m Boylam: 0. 0. 0.0 G.L.: 739.00m
 Yukari(Y): 402767.00m Enlem: 0. 0. 0.0

KBGD = KELLY BUSHING E GORE KUYUDAKI ALICININ DERINLIGI
 AGKGZ = AIRGUN DAN ALICIYA KADAR GECEN ZAMAN (MS)
 AGKGDD = AIRGUN SEVIYESINE GORE DUSEY DERINLIK (M)
 AGKGDZ = AIRGUN SEVIYESINE GORE DUSEY ZAMAN (MS)
 AGKGED = AIRGUN ILE ALICI SEVIYESI ARASINDAKI UZAKLIK (M)
 RDGDD = REFERANS (SISMIK) DUZLEMINE GORE DUSEY DERINLIK (M)
 RDGOH = REFERANS (SISMIK) DUZLEMINE GORE ORTALAMA HIZ (M/S)
 RDGAH = REFERANS (SISMIK) DUZLEMINE GORE ARA HIZ (M/S)
 RDGTZ = REFERANS (SISMIK) DUZLEMINE GORE DUSEY TEK ZAMAN (MS)
 RDGCZ = REFERANS (SISMIK) DUZLEMINE GORE DUSEY CIFT ZAMAN (MS)

Atis No	KBGD (m)	AGKGZ (ms)	AGKGDD (m)	AGKGDZ (ms)	AGKGED (m)	RDGDD (m)	RDGOH (m/s)	RDGAH (m/s)	RDGTZ (ms)	RDGCZ (ms)	
								1267.			
1	50.00	52.00	33.00	26.05	65.86	-294.0	1267.	----	-232.1	-464.	KASTEL
								764.			
2	141.00	76.00	124.00	69.05	136.47	-203.0	1796.	----	-113.0	-226.	
								1763.			
3	333.00	121.00	316.00	119.08	321.10	-11.0	2654.	----	-4.1	-8.	SAYINDERE
								2744.			
4	369.00	128.00	352.00	126.35	356.59	25.0	2786.	----	9.0	18.	
								3055.			
5	469.00	152.00	452.00	150.81	455.58	125.0	2997.	----	41.7	83.	
								3332.			
6	504.00	160.00	487.00	158.92	490.32	160.0	3065.	----	52.2	104.	
								3784.			
7	558.00	169.00	541.00	168.07	543.99	214.0	3219.	----	66.5	133.	
								3806.			
8	617.00	181.00	600.00	180.19	602.70	273.0	3330.	----	82.0	164.	KARABOĞAZ
								3600.			
9	625.00	183.00	608.00	182.20	610.67	281.0	3337.	----	84.2	168.	KARBABA-C
								3550.			
10	648.00	189.00	631.00	188.23	633.57	304.0	3352.	----	90.7	181.	KARABABA-B
								4322.			
11	707.00	199.00	690.00	198.32	692.35	363.0	3479.	----	104.3	209.	KARABABA-A
								3203.			
12	713.00	201.00	696.00	200.33	698.33	369.0	3474.	----	106.2	212.	DERDERE
								4516.			
13	772.00	211.00	755.00	210.40	757.15	428.0	3588.	----	119.3	239.	

Table C.20Ej genij qv'xcwgu'qlly gniF D/30'

D.B-1

l kuyusu check shot Degerlendirmesi
 K.B.: 622.00m SRD: 400.00m AirGun: 616.00m AirGun Offset: 55.00m
 Saga(X) :4174657.00m Boylam: 0. 0. 0.0 G.L.: 617.00m
 Yukari(Y): 406858.00m Enlem: 0. 0. 0.0

KBGD = KELLY BUSHING E GORE KUYUDAKI ALICININ DERINLIGI
 AGKGZ = AIRGUN DAN ALICIYA KADAR GECEN ZAMAN (MS)
 AGKGDD = AIRGUN SEVIYESINE GORE DUSEY DERINLIK (M)
 AGKGDZ = AIRGUN SEVIYESINE GORE DUSEY ZAMAN (MS)
 AGKGED = AIRGUN ILE ALICI SEVIYESI ARASINDAKI UZAKLIK (M)
 RDGDD = REFERANS (SISMİK) DUZLEMINE GORE DUSEY DERINLIK (M)
 RDGOH = REFERANS (SISMİK) DUZLEMINE GORE ORTALAMA HIZ (M/S)
 RDGAH = REFERANS (SISMİK) DUZLEMINE GORE ARA HIZ (M/S)
 RDGTZ = REFERANS (SISMİK) DUZLEMINE GORE DUSEY TEK ZAMAN (MS)
 RDGCZ = REFERANS (SISMİK) DUZLEMINE GORE DUSEY CIFT ZAMAN (MS)

Atis No	KBGD (m)	AGKGZ (ms)	AGKGDD (m)	AGKGDZ (ms)	AGKGED (m)	RDGDD (m)	RDGOH (m/s)	RDGAH (m/s)	RDGTZ (ms)	RDGCZ (ms)
1	23.00	55.00	17.00	16.24	57.57	-199.0	1047.	1047.	-190.1	-380. KASTEL
2	175.00	83.00	169.00	78.93	177.72	-47.0	2141.	904.	-21.9	-44.
3	200.00	99.00	194.00	95.25	201.65	-22.0	2037.	2242.	-10.8	-22. SAYINDERE
4	223.00	107.00	217.00	103.72	223.86	1.0	2092.	2039.	0.5	1.
5	259.00	113.00	253.00	110.42	258.91	37.0	2291.	2297.	16.1	32.
6	348.00	133.00	342.00	131.31	346.39	126.0	2604.	2761.	48.4	97.
7	384.00	142.00	378.00	140.52	381.98	162.0	2690.	3039.	60.2	120.
8	420.00	149.00	414.00	147.70	417.64	198.0	2803.	3456.	70.6	141.
9	432.00	150.00	426.00	148.77	429.54	210.0	2864.	4453.	73.3	147. KARABOĞAZ
10	439.00	152.00	433.00	150.79	436.48	217.0	2872.	3134.	75.6	151. KBB-C
11	447.00	156.00	441.00	154.80	444.42	225.0	2849.	2345.	79.0	158. KBB-B
12	467.00	158.00	461.00	156.89	464.27	245.0	2938.	4547.	83.4	167. KBB-A
13	475.00	162.00	469.00	160.90	472.21	253.0	2915.	2341.	86.8	174. DERDERE
14	554.00	175.00	548.00	174.13	550.75	332.0	3147.	4225.	105.5	211.
15	582.00	179.00	576.00	178.19	578.62	360.0	3233.	4765.	111.4	223. SABUNSUYU
16	607.00	183.00	601.00	182.24	603.51	385.0	3298.	4653.	116.7	233.
17	687.00	200.00	681.00	199.35	683.22	465.0	3416.	4128.	136.1	272. AREBAN
18	707.00	206.00	701.00	205.37	703.15	485.0	3413.	3351.	142.1	284. SOSINK
19	780.00	223.00	774.00	222.44	775.95	558.0	3480.	3995.	160.4	321.

Table C.30Ej gemj qv'xcwgu'qhl'y gn'F D/40'

D.B-2

Kuyusu c'heck Shot Degerlendirmesi
 K.B.: 631.03m SRD: 400.00m AirGun: 623.83m AirGun Offset: 52.83m
 Saga(X) : 411106.50m Boylam: 0. 0. .0 G.L.: 625.83m
 Yukari(Y):4172194.00m Enlem: 0. 0. .0

KBGD = KELLY BUSHING E GORE KUYUDAKI ALICININ DERINLIGI
 AGKGZ = AIRGUN DAN ALICIYA KADAR GECEN ZAMAN (MS)
 AGKGDZ = AIRGUN SEVIYESINE GORE DUSEY DERINLIK (M)
 AGKGDZ = AIRGUN SEVIYESINE GORE DUSEY ZAMAN (MS)
 AGKGED = AIRGUN ILE ALICI SEVIYESI ARASINDAKI UZAKLIK (M)
 RDGDD = REFERANS (SISMIK) DUZLEMINE GORE DUSEY DERINLIK (M)
 RDGOH = REFERANS (SISMIK) DUZLEMINE GORE ORTALAMA HIZ (M/S)
 RDGAH = REFERANS (SISMIK) DUZLEMINE GORE ARA HIZ (M/S)
 RDGTZ = REFERANS (SISMIK) DUZLEMINE GORE DUSEY TEK ZAMAN (MS)
 RDGCZ = REFERANS (SISMIK) DUZLEMINE GORE DUSEY CIFT ZAMAN (MS)

Atis No	KBGD (m)	AGKGZ (ms)	AGKGDZ (m)	AGKGDZ (ms)	AGKGED (m)	RDGDD (m)	RDGOH (m/s)	RDGAH (m/s)	RDGTZ (ms)	RDGCZ (ms)
1	51.00	89.50	43.80	57.12	68.63	-180.0	767.	767.	-234.8	-470.
2	168.00	110.20	160.80	104.69	169.26	-63.0	1536.	1544.	-41.0	-82.
3	233.00	124.80	225.80	121.52	231.90	2.0	1858.	2090.	1.1	2.
4	341.00	162.10	333.80	160.11	337.95	110.0	2085.	2491.	52.7	105.
5	430.70	189.70	423.50	188.24	426.78	199.7	2250.	2451.	88.8	178.
6	460.80	200.80	453.60	199.45	456.67	229.8	2274.	2584.	101.0	202.
7	565.70	237.40	558.50	236.34	560.99	334.7	2363.	3147.	141.6	283.
8	685.50	269.00	678.30	268.19	680.35	454.5	2529.	3331.	179.7	359.
9	746.50	284.70	739.30	283.98	741.19	515.5	2603.	3513.	198.0	396.
10	772.50	291.00	765.30	290.31	767.12	541.5	2636.	3650.	205.4	411.
11	840.40	306.90	833.20	306.28	834.87	609.4	2720.	3905.	224.0	448.
12	888.30	317.30	881.10	316.73	882.68	657.3	2782.	4407.	236.3	473.
13	955.30	329.70	948.10	329.19	949.57	724.3	2880.	4392.	251.5	503.
14	1035.30	345.20	1028.10	344.75	1029.46	804.3	2982.	4335.	269.7	539.
15	1099.30	358.20	1092.10	357.78	1093.38	868.3	3052.	4997.	284.5	569.
16	1120.20	361.70	1113.00	361.29	1114.25	889.2	3081.	4447.	288.6	577.
17	1147.20	367.10	1140.00	366.71	1141.22	916.2	3109.	4804.	294.7	589.
18	1207.20	378.00	1200.00	377.63	1201.16	976.2	3178.	4354.	307.2	614.
19	1217.20	380.10	1210.00	379.74	1211.15	986.2	3186.	4826.	309.5	619.
20	1265.10	388.90	1257.90	388.56	1259.01	1034.1	3237.	5105.	319.4	639.
21	1346.10	402.90	1338.90	402.59	1339.94	1115.1	3326.	5006.	335.3	671.
22	1412.10	414.80	1404.90	414.51	1405.89	1181.1	3389.	5614.	348.5	697.
23	1496.10	428.00	1488.90	427.73	1489.84	1265.1	3481.	5088.	363.4	727.
24	1526.00	433.40	1518.80	433.14	1519.72	1295.0	3507.	4384.	369.3	739.
25	1548.00	438.20	1540.80	437.94	1541.71	1317.0	3518.	---	374.3	749.

D. Calculated Formation Velocities in Each Well

Table D.10 *Ec rēwcvgf 'ej genlij qv'xgrqekf 'xcwgu'qlhy gniF (D/30'*

Checkshot spreadsheet for 'Checkshots'

Well: Sonic log:

Depth in: Time in:

	MD	TWT	Average velocity	Interval velocity	Sonic time	Sonic Int. Vel
312	23.00	2.00	670.00	2156.03		
313	175.00	143.00	2135.24	1562.50		
314	200.00	175.00	2030.51	2705.88		
315	223.00	192.00	2090.31	4800.00		
316	259.00	207.00	2286.67	4139.53		
317	348.00	250.00	2605.36	3789.47		
318	384.00	269.00	2689.00	4800.00		
319	420.00	284.00	2800.49	12000.00		
320	432.00	286.00	2864.83	3500.00		
321	439.00	290.00	2873.59	2000.00		
322	447.00	298.00	2850.13	8000.00		
323	467.00	303.00	2935.12	2000.00		
324	475.00	311.00	2911.06	5851.85		
325	554.00	338.00	3145.98	7000.00		
326	582.00	346.00	3235.09	5555.56		
327	607.00	355.00	3293.92	4705.88		
328	687.00	389.00	3417.33	3333.33		
329	707.00	401.00	3414.81	4171.43		
330	780.00	436.00	3475.55			

< >

Table D.20 Ecrwrcvgf 'ej genlij qv'xgrqekf 'xcwgu'qhlj gmF (D/40'

Checkshot spreadsheet for 'Checkshots'

Well: Sonic log:

Depth in: Time in:

	MD	TWT	Average velocity	Interval velocity	Sonic time	Sonic Int. Vel
331	51.00	52.00	768.08	1857.14		
332	168.00	178.00	1538.99	3333.33		
333	233.00	217.00	1861.47	2700.00		
334	341.00	297.00	2087.34	3093.10		
335	430.70	355.00	2251.66	2617.39		
336	460.80	378.00	2273.92	2797.33		
337	565.70	453.00	2360.57	3686.15		
338	685.50	518.00	2526.91	3812.50		
339	746.50	550.00	2601.71	4000.00		
340	772.50	563.00	2634.00	4243.75		
341	840.40	595.00	2720.57	4561.90		
342	888.30	616.00	2783.34	5153.85		
343	955.30	642.00	2879.35	5000.00		
344	1035.30	674.00	2980.03	4923.08		
345	1099.30	700.00	3052.20	5971.43		
346	1120.20	707.00	3081.10	4909.09		
347	1147.20	718.00	3109.11	5454.55		
348	1207.20	740.00	3178.84	4000.00		
349	1217.20	745.00	3184.35	5635.29		
350	1265.10	762.00	3239.03	5586.21		
351	1346.10	791.00	3325.08	5500.00		
352	1412.10	815.00	3389.13	6214.81		
622	1496.00	842.00	3479.74	5454.55		
623	1526.00	853.00	3505.21	4888.89		
624	1548.00	862.00	3519.65			

Table D.30 Ecrewaxvgf 'ej gentij qv'xgrqeky 'xcmgu'qhty gniD/40'

Checkshot spreadsheet for 'Checkshots'

Well: Sonic log: Depth in: Time in:

	MD	TWT	Average velocity	Interval velocity	Sonic time	Sonic Int. Vel
766	50.00	52.00	-3637.69	7583.33	26.00	
767	141.00	76.00	-94.21	8533.33	48.20	4098.87
768	333.00	121.00	3114.38	10285.71	97.20	3918.24
769	369.00	128.00	3506.56	8333.33	104.96	4640.37
770	469.00	152.00	4268.68	8750.00	133.85	3462.06
771	504.00	160.00	4492.75	12000.00	141.53	4554.85
772	558.00	169.00	4892.54	9833.33	152.68	4842.67
773	617.00	181.00	5220.11	8000.00	164.40	5033.45
774	625.00	183.00	5250.49	7666.67	165.96	5149.06
775	648.00	189.00	5327.20	11800.00	170.80	4747.95
776	707.00	199.00	5652.46	6000.00	182.93	4863.21
777	713.00	201.00	5655.92	11800.00	184.37	4180.75
778	772.00	211.00	5947.11			

Apply OK Cancel

Table D.40E *Crwrcvfg'ej gentij qv'xgrqekf 'xcwgu'qhty gmDC/30'*

Checkshot spreadsheet for 'Checkshots'

Well: BA-1 Sonic log: Δt_p DT

Depth in: MD Time in: TWT

	MD	TWT	Average velocity	Interval velocity	Sonic time	Sonic Int. Vel
178	50.00	38.00	2460.00	2815.79	19.00	
179	371.00	266.00	2764.96	2650.00	61.16	7614.10
180	424.00	306.00	2749.93	2692.31	68.31	7412.37
181	529.00	384.00	2738.23	3363.64	107.42	2684.40
182	566.00	406.00	2772.12	2863.64	118.51	3335.97
183	629.00	450.00	2781.07	2800.00	140.52	2863.24
184	1147.00	820.00	2789.61	3235.85	325.79	2795.96
185	1490.00	1032.00	2881.28	3692.31	432.84	3204.00
186	1586.00	1084.00	2920.18	4125.00	458.79	3699.99
187	1751.00	1164.00	3002.99	4607.14	498.14	4193.10
188	1880.00	1220.00	3076.62	4833.33	526.50	4547.67
189	2141.00	1328.00	3219.49	5254.90	580.52	4831.55
190	2409.00	1430.00	3364.67	4666.67	631.75	5231.50
191	2437.00	1442.00	3375.51	5666.67	637.31	5034.87
192	2471.00	1454.00	3394.42	6125.00	643.61	5394.59
193	2520.00	1470.00	3424.14	6000.00	652.14	5748.52
194	2574.00	1488.00	3455.30	4727.27	661.30	5894.90
195	2600.00	1499.00	3464.63	7714.29	666.55	4952.61
196	2627.00	1506.00	3484.38		671.00	6063.49

Apply OK Cancel